Universitat Autònoma de Barcelona

Structural modeling and functional characterization of mammalian cytosolic carboxypeptidases 2 and 3

Doctoral thesis presented by Olívia Tort Regàs for the degree of PhD in Biochemistry, Molecular Biology and Biomedicine from the Universitat Autònoma de Barcelona

Institut de Biotecnologia i Biomedicina
Unitat d'Enginyeria de Proteïnes i Proteòmica

Thesis supervised by
Prof. Francesc Xavier Avilés Puigvert, Dra. Julia Lorenzo Rivera and Dr. Sebastian Tanco

Olívia Tort Regàs

Prof. Francesc Xavier Avilés Puigvert

Dra. Julia Lorenzo Rivera

Dr. Sebastian Tanco

Barcelona, September 2014

Table of contents

TABLE OF CONTENTS

LIST OF FIGURES

LIST OF TABLES

List of abbreviations

LIST OF ABBREVIATIONS

ACE	Angiotensin converting enzyme
ARD1	Arrest-defective 1-amino-terminal, α-amino, acetyltransferase 1
CFEOM3	Congenital fibrosis of the extraocular muscle type 3
CP	Carboxypeptidase
CCP	Cytosolic carboxypeptidase
CCP1	Cytosolic carboxypeptidase 1
CCP2	Cytosolic carboxypeptidase 2
CCP3	Cytosolic carboxypeptidase 3
CCP4	Cytosolic carboxypeptidase 4
CCP5	Cytosolic carboxypeptidase 5
CCP6	Cytosolic carboxypeptidase 6
CRM1	Chromosome region maintenance 1/exportin1/Exp1/Xpo1
EPC	Elongation protein complex
EDTA	Ethylenediaminetetraacetic acid
ER	Endoplasmic reticulum
FCD	Fuchs corneal dystrophy
GTP	Guanoside-triphosphate
HA	Hemagglutinin
HABA	Hydroxi-azophenyl-benzoic acid
IDA	Inner dynein arms
KIF2A	Kinesin heavy chain member 2A
KO	Knockout
LB	Luria Broth
LA	Luria Broth agar

MAPs	Microtubule associated proteins
MCPs	Metallocarboxypeptidases
MCAKs	Mitotic centromere-associated kinesins
MT	Microtubule
MTOC	Microtubule-organizing center
NES	Nuclear export signal
ODA	Outer dynein arms
ON	Over-night
PCR	Polymerase chain reaction
PCD	Primary ciliary dyskinesia
pcd	Purkinje cell degeneration
PDB	Protein Data Bank
PDGFRα	Platelet-derived growth factor receptor A
PTM	Posttranslational modification
RARRES1	Retinoic acid receptor responder 1
Shh	Sonic hedgehog
αTAT	Tubulin acetyltransferase
TCF4	Transcription factor 4
TCP	Tubulin carboxypeptidase
+TIPs	Plus-end-binding proteins
TTL	Tubulin tyrosine ligase

Preface

PREFACE

This thesis is situated in the field of the mammalian cytosolic carboxypeptidases, particularly focusing in members 2 and 3 from this subfamily of metallocarboxypeptidases. This work gives insight for the first time into the role of those enzymes by *in silico*, *in vitro* and *in vivo* approaches. The thesis consists of five chapters as described below.

The first chapter introduces the fields of metallocarboxypeptidases, microtubules and tubulin posttranslational modifications. The second chapter is a compilation of the experimental procedures and materials used for the experimental work.

The third chapter presents the functional characterization of human cytosolic carboxypeptidase 3 and Dr. Sebastian Tanco also participated in this work. The results from this study were the basis for chapter four, where the function of CCP2 is described and both CCP2 and CCP3 mouse isoforms are studied by protein engineering and using CCP2 and CCP3 knock-out mouse models. The experimental work performed in Chapter IV was performed in collaboration with Dr. Carsten Janke's lab (Institut Curie, France). In this work Cecilia Rocha performed the ciliogenesis experiment and Dr. Ivan Bièche performed the RT-qPCR. Chapters III and IV are subdivided into a summary of the chapter, the results describing the findings in detail and a discussion.

The fifth chapter sets a general discussion on CCP2 and CCP3, their role in the cell and in the context of a family, in mammals, of six genes coding deglutamylating enzymes.

Chapter IV together with the modeling experiments form Chapter III is the basis of the following scientific paper:

Tort O, Tanco S, Rocha C, Bièche I, Seixas C, Bosc C, Andrieux A, Moutin MJ, Avilés FX, Lorenzo J, Janke C. The cytosolic carboxypeptidases CCP2 and CCP3 catalyze posttranslational removal of acidic amino acids. *MBoC*.doi:10.1091/mbc.E14-06-1072

Chapter I:

Introduction

CHAPTER I: INTRODUCTION

1 Peptidases

Peptidases are protein enzymes that catalyze the cleavage of peptide bounds of their substrates. Enzymes are large biological molecules that greatly accelerate the rate of the metabolic reactions that sustain life. In enzymatic reactions like hydrolysis of peptide bounds, selective substrates are converted into products.

For mouse, human and all living organisms, breaking down proteins in order to generate amino acid units to synthetize new proteins is a basic function. Processes like food digestion, growth, remodeling and development of cells and tissues require proteolytic activities on existent proteins to synthetize new ones. In the human genome 597 genes have already been identified corresponding to peptidases, which represent the 3 % of the known genes (Mi *et al.*, 2013). The complete repertoire of proteases expressed by an organism is defined as degradome. Strikingly, the mouse genome presents a larger degradome compared to human. The main differences are found in family members associated with reproductive and immune processes (Puente *et al.*, 2005).

1.1 Nomenclature of peptidases

The terms protease, proteinase and peptidase had originally slightly different meanings (Barrett and Mc Donald, 1986). In the present day, proteolytic enzymes is the most generally understood term but peptidase is the term recommended by the Nomenclature Committee of the International Union of Biochemistry and Molecular Biology (NC-IUBMB) to describe enzymes that hydrolyse peptide bonds. Proteolytic enzymes or peptidases differ remarkably in their properties (*i.e.* size, catalytic mechanism, substrate and biological processes). Some are composed of mainly the catalytic domain and as small as 20-30 kDa, such as cysteine cathepsins; whereas

others can be large, multidomain protein complexes, such as the proteasome (Turk *et al.*, 2012).

1.2 Functions of proteolytic enzymes

1.2.1 Proteases in life processes

In tissue remodeling during growth, proteases have a role in the maintenance of epithelial barriers during the epithelial cell junction rearrangement. Interestingly, in pathologic conditions such as cancer and inflammation, increased levels of junction protein fragments are found in the tissue and body fluids as a result of deregulated proteolytic activities (Nava *et al.*, 2013). Related to inflammation, both acute and chronic wounds are examples of misbalanced proteolytic activities, in which therapies based on proteases modulation may support healing (McCarty and Percival, 2013). Also during tissue remodeling in embryogenesis, the tissue expansion and morphogenetic cell movements in the embryo are driven by proteases. The A Disintegrin and Metalloprotease (ADAM) family is responsible for regulating these processes in the embryo through the cleavage of versican, a proteoglycan of the provisional matrix (Nandadasa *et al.*, 2014).

Growing requires peptidases for remodeling tissues but cell death is also dependent of them. Caspases, a family of peptidases that cleaves after aspartic acid residues, are typically activated in response to cell damage during apoptotic cell death and other proteases participate in autophagy (Mariño *et al.*, 2014). In neurological damage such as ischaemia or neurodegenerative disease, hyperactivated ion channels in neurons are known to activate cathepsin and calpain proteases ultimately leading to necrotic death (Driscoll and Gerstbrein, 2003).

Another important function of proteases is the limited proteolysis of biologically inactive polypeptide precursors in order to generate diversity of bioactive molecules. An example of such activity is the cleavage of neuropeptides by carboxypeptidase 4 (CPA4), as well as the activation of the enzyme precursor by endoproteases that remove the propeptide generating the active form of CPA4 (Tanco *et al.*, 2010).

1.2.2 Peptidases as drug targets

The relevance of peptidases in pathological conditions and as biological regulators highlights them as suitable biomedical targets, although their ubiquitous presence and conserved structure require the design of highly selective drugs. The field of peptidase inhibitors has been explored by the pharmaceutical industry leading to the approval of several drugs for clinical uses (Turk, 2006). For instance, Enalapril (Merck) or Qinapril (Novartis) are peptidyl dipeptidase A (ACE) inhibitors used for hypertension treatments. Whereas peptidase inhibitors constitute the main regulators of the enzymes, some peptidases are synthetized as inactive precursors and need to be activated posttranslationally, such as pancreatic carboxypeptidases (García-Sáez *et al.*, 1997). Another regulatory mechanism is the production of inactive homologous peptidases or shed exosite domains. These inactive homologous proteins have been suggested as playing a role in binding and therefore masking sessile bonds *in vivo* reducing substrate cleavage (Tam *et al.*, 2002). Notably, more than 16% of the human proteolytic enzymes (or degradome) seem to be catalytically inactive owing to substitutions in critical residues located in the active site of the peptidases (Puente *et al.*, 2003). Hence, several layers of control are needed to regulate protease function to avoid uncontrolled cleavages.

1.3 Specificity of proteolytic enzymes

1.3.1 Diversity of proteolytic processes

Despite its own activity regulation mechanisms, some proteases are clearly promiscuous, with an indiscriminate degradative activity towards many substrates, whereas others show high fidelity with exquisite specificity in their ability to target a unique substrate (Puente *et al.*, 2005). This last group is the most attractive for drug design. For instance, the carboxypeptidase U, known as thrombin-activatable fibrinolysis inhibitor (TAFI), has been shown to specifically cleave C-terminal Lys residues from partially degraded fibrin in the coagulation cascade (Strömqvist *et al.*, 2004; Willemse and Heylen, 2009). TAFI constitutes an important drug target for

thrombolytic therapies (Foley *et al.*, 2013). A different example of a specific proteolysis is a process named limited proteolysis, consisting of a cleavage that has as a result the activation or activity modification of the substrate. Limited proteolysis is a subtle mean of post-translational regulation performed by proteases (Turk, 2006).

1.3.2 Peptide bound hydrolysis

The hydrolysis catalyzed by peptidases requires a nucleophile attack. This reaction takes place between the nucleophilic side-chain of a residue (or a water molecule) of the peptidase to the scissile peptide bond of the substrate. The reaction requires a water molecule to disrupt the peptide bound. The specificity of the peptidases is determined by the side-chain (R) of the residues implicated in the reaction (**Figure 1.1**).

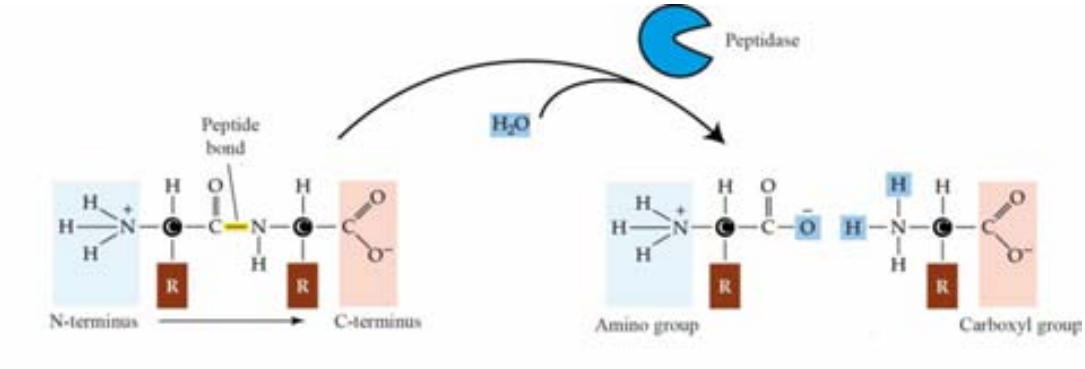

Figure 1.1. Hydrolysis of the peptide bound by a peptidase
Proteases catalyze the hydrolysis of peptide bonds. A water molecule is necessary for cleaving the peptdide bound. R, side-chain of the amino acids forming the peptide bound Adapted from http://www.blc.arizona.edu/

1.3.3 Peptidases substrate specificity

Such as other enzymes, peptidases present substrate specificity and this can be explained by the characteristics of the active site. Schechter & Berger elaborated a conceptual model to explain the specificity of peptidases **(Figure 1.2**). The model considers the presence of specificity subsites in the enzyme, which are able to accommodate the side-chain of a single amino acid residue from the substrate. Accordingly, the binding subsites found in the active site of the peptidase are

described in the model where each subsite of the enzyme is able to accommodate the side-chain of a single aminoacid residue from the substrate. Therefore, substrate residues are indicated as –P3–P2–P1↓P1'–P2'–P3'–, where the peptide bound between P1 and P1' is the substrate for the peptidase to be cleaved. The corresponding binding subsites in the peptidase are named S3, S2, S1 and S1', S2', S3' (Schechter and Berger, 1967).

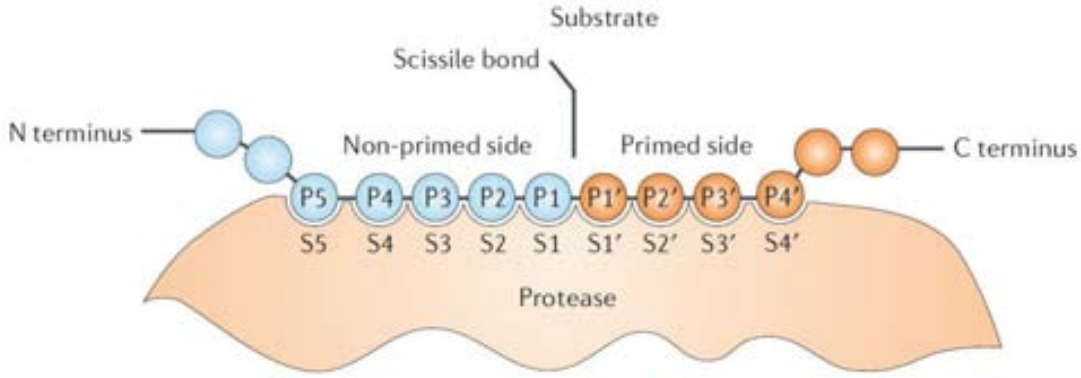

Figure 1.2. Model of peptidase specificity by Schechter&Berger
Diagram of the active site of a peptidase with the specificity pockets denoted as S and the amino acids from the substrate denoted as P. Each S has an affinity for residues (P) in a "lock and Key" mechanism that dictates protease specificity. The primed side represents the corresponding to the C-terminal sequence from the scissile bound. Adapted image (Schechter and Berger, 1967).

As exemplified above, the function of many peptidases, rather than facilitating unspecific degradation, they act very precisely. Peptidases are highly regulated and act in the most diverse pathways. This thesis presents another example of highly specific and regulated proteolytic activity, which is involved in the posttranslational regulation of intracellular proteins.

1.4 Classification of peptidases

Peptidases are classified according to different properties. The classifications that are more commonly used are based on the point of cleavage on the substrate, the catalytic mechanism, or a combination of the hierarchical and structure-based

classification. This last one led to a database of peptidases and inhibitors called MEROPS (Rawlings *et al.*, 2006).

1.4.1 Point of cleavage

A first distinction is made between exopeptidases and endopeptidases. Exopeptidases cleave one or few amino acids either from the N- or C-terminal end of the protein or peptide, while endopeptidases cleave inside the polypeptide chain (**Figure 1.3**). Enzymes that act on the free N-terminus and liberate a single amino acid are called aminopeptidases, while the ones liberating a dipeptide or tripeptide are di- or tripeptidyl-peptidases. Those acting at the free C-terminus are named carboxypeptidases when they liberate a single residue and peptidyl-dipeptidases when cleaving a dipeptide (**Figure 1.3**). This work focuses on a specific subfamily of carboxypeptidases, so that exert their function by cleaving C-terminal tails of other proteins.

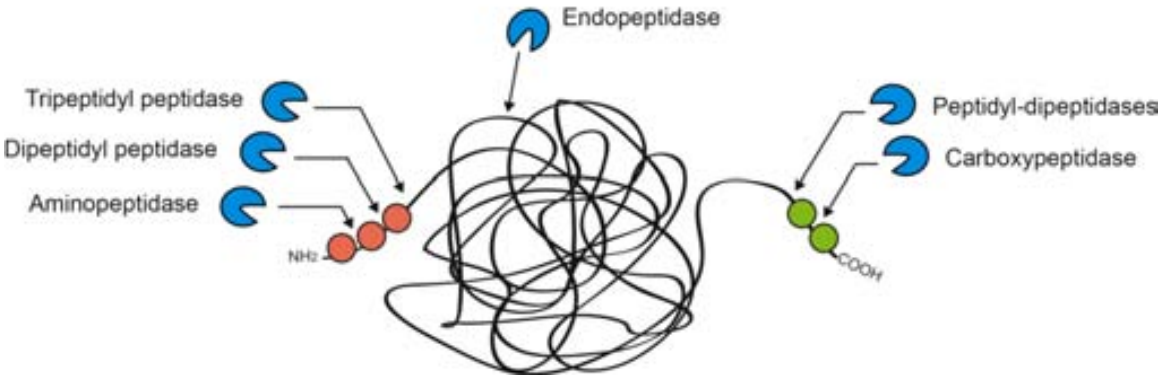

Figure 1.3. Exopeptidases and endopeptidases cleavage sites.
Scheme of peptidases classification based on the site of cleavage in the polypeptide substrate. The N-terminal residues are represented in red and the C-terminal residues in green.

1.4.2 Catalytic mechanism

The hydrolysis catalyzed by peptidases requires a nucleophile attack. In the active site of the peptidase, a nucleophilic side-chain of a residue (or a water molecule) participates in the reaction. Based on the nature of this amino acid participating in the

catalysis, peptidases are classified as serine, threonine, cysteine, aspartic, glutamic and metallopeptidases (**Table 1.1**).

Table 1.1. Catalytic type of proteases and examples

Catalysis	Catalytic type	Example
Covalent-catalysis	Serine	Trypsin, prolyl oligopeptidase
	Cysteine	Papain, cathepsin K
	Threonine	Proteasome
Acid-base catalysis	Aspartic	Pepsin, cathepsin E
	Glutamic	Aspergilloglutamic peptidase
	Metallo	Carboxypeptidase A, Thermolysin
Unknown		gpr endopeptidase, prepilin type IV peptidase

In cysteine peptidases the nucleophile is a -SH group on the side-chain of a Cys present at the active site, whereas in serine and threonine peptidases, the nucleophile is its –OH group. In both cases the reaction is termed covalent catalysis. Differently, aspartic, glutamic and metallopeptidases present the common feature that the nucleophile participating in catalysis is an activated water molecule, process termed water-catalysis (**Figure 1.4**). In the case of aspartic and glutamic peptidases, the water molecule interacts directly with the Asp or Glu residues of the active site, whereas metallopeptidases binds one or two metal ions that in turn bind the activated water molecule (Puente *et al.*, 2003; Rawlings and Salvesen, 2013). In covalent catalysis, histidines (His) normally function as a base, while in non-covalent catalysis Asp or Glu residues and zinc (in metallopeptidases) serve as acids and bases (Turk, 2006).

Cytosolic carboxypeptidases, the focus of this thesis, are proteolytic enzymes classified as metallocarboxypeptidases since they present a single zinc atom coordinated in the active site. However, some peptidases are directed by more complex catalytic mechanisms. There is a significant number of proteases for which the catalytic mechanism remains to be determined (Barrett, 2000). Besides, some of

the mechanisms seem to be represented only in certain species, for instance, glutamic proteases are not found in mammals so far (Turk, 2006).

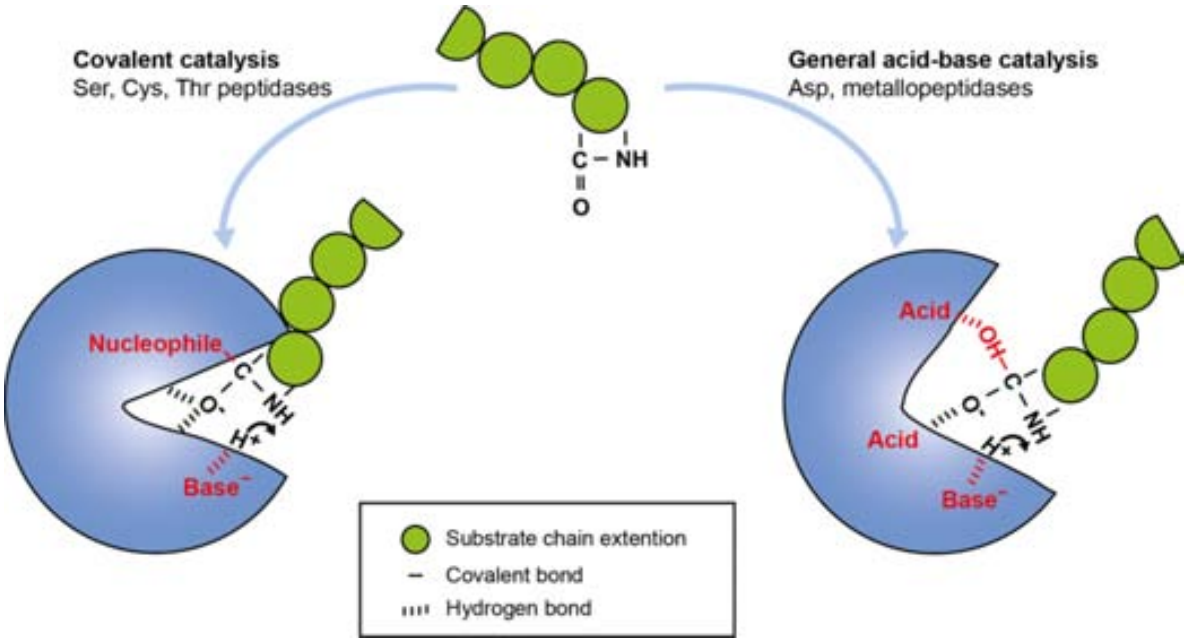

Figure 1.4. Catalytic mechanisms of mammalian proteases.
The five major catalytic classes of peptidases (Ser, Cys, Thr, Asp, Metallo) are divided in the two catalytic groups according to their mechanisms to stabilize the tetrahedral intermediate of the proteolytic reaction. Image adapted from (Turk, 2006).

1.4.3 Structural and evolutionary relationships

Due to increasing numbers of discovered proteases, the need of more complex classifications arose to overcome the limitation of the previous classification strategies, which were not able to account for the ample variability in terms of structure, catalytic mechanism, evolutionary relationships and physiological function.

Taking advantage of the large amount of amino acid sequence data, Rawlings and Barrett described a new form of classification, the MEROPS system (Rawlings and Barrett, 1993; Rawlings *et al.*, 2012). MEROPS system is based on essential structural features that are believed to reflect evolutionary relationships. MEROPS defines families and clans of peptidases. Closely related peptidases are grouped based on similarities in amino acid sequences. Groups of families that show evidence of having a

common origin are then grouped together in a clan. When families contain several distinct groups of proteases that differ greatly in primary structure, they are subdivided into subfamilies.

Following the MEROPS system, metallocarboxypeptidases form the M14 family where "M" denominates the catalytic type (*metallo-)* and the number denominates the family. This thesis focuses on a subfamily of the M14 group that has been proposed as M14D and it is entirely constituted by cytosolic carboxypeptidases of different species. The complete list of families and clans recognized in the MEROPS can be found in the Web version of the MEROPS database (http://www.merops.co.uk).

1.5 Carboxypeptidases

Concerning the site of cleavage, the main focus of this thesis is a subfamily of carboxypeptidases (CPs). More precisely, and referring to its catalytic mechanism, they are metallocarboxypeptidases since they present a zinc atom coordinated at the active site. Three catalytic types of carboxipeptidases have been described: metallocarboxypeptidases (MCPs), serine carboxypeptidases and cysteine carboxypeptidases (**Table 1.2**), from which MCPs is the most numerous subgroup.

The catalytic feature of metallocarboxypeptidases is mainly composed of two histidines and a glutamic acid, except for the M2 family that includes an additional histidine. Serine carboxypeptidases present a triad in the active site (serine/aspartic acid/histidine) while the cysteine group functions with a catalytic dyad (cysteine/histidine).

Table 1.2. Classification of carboxypeptidases.

Catalytic type	Family	Enzymes	Catalytic feature
Metallo	**M2**	ACE2	**HEXXH…H**
	M14 subfamily A	CPA1 CPA2 CPA3 CPA4 CPA5 CPA6 CPB CPU/TAFI CPO	
	M14 subfamily B	CPE CPD CPM CPN CPZ CPX1 CPX2 AEBP1	**HXXE…H**
	M14 subfamily C	gamma-D-glutamyl-(L)-meso-diaminopimelate peptidase I	
	M14 subfamily D (proposed subfamily)	CCP1 CCP2 CCP3 CCP4 CCP5 CCP6	
	M15	zinc D-Ala-D-Ala carboxypeptidase	**HXXXXXXD…H**
	M20 subfamily A	glutamate carboxypeptidase	**HXD…D…EE…E…H**
	M20 subfamily D	carboxypeptidase Ss1	**DXD…D…EE…H**
	M28 subfamily B	glutamate carboxypeptidase II NAALADASE L peptidase	**HXD…D…EE…D…H**
	M32	carboxypeptidase Taq TcCP1 TcCP2	**HEXXH...H**
Serine	**S10**	serine carboxypeptidase A vitellogenic carboxypeptidase-like protein RISC peptidase	**catalytic triad S/D/H**
	S28	lysosomal Pro-X carboxypeptidase	
Cysteine	**C1 subfamily A**	cathepsin X	**catalytic dyad C/H**

Adapted from Vendrell and Avilés, 1999.

1.5.1 Structure and mechanism

The model protein used to elucidate the mechanism of zinc-dependent peptidases was bovine carboxypeptidase A (bCPA). The first high resolution structure in the Protein Data Bank (PDB) dated from 1986 (Christianson and Lipscomb, 1986) and several improvements in resolution (Kilshtain-Vardi *et al.*, 2003) and structures of complexes with natural peptide and organic inhibitors have been obtained since then (Arolas *et al.*, 2005; Fernández *et al.*, 2010). Bovine CPA presents a zinc ion coordinated by three residues forming the active site: His69, Glu72 and His196 (active bovine CPA numbering) (**Figure 1.5**) while the fourth ligand is a water molecule (Kilshtain-Vardi *et al.*, 2003). Arg127 and Glu270 participate directly in the catalysis of the substrate.

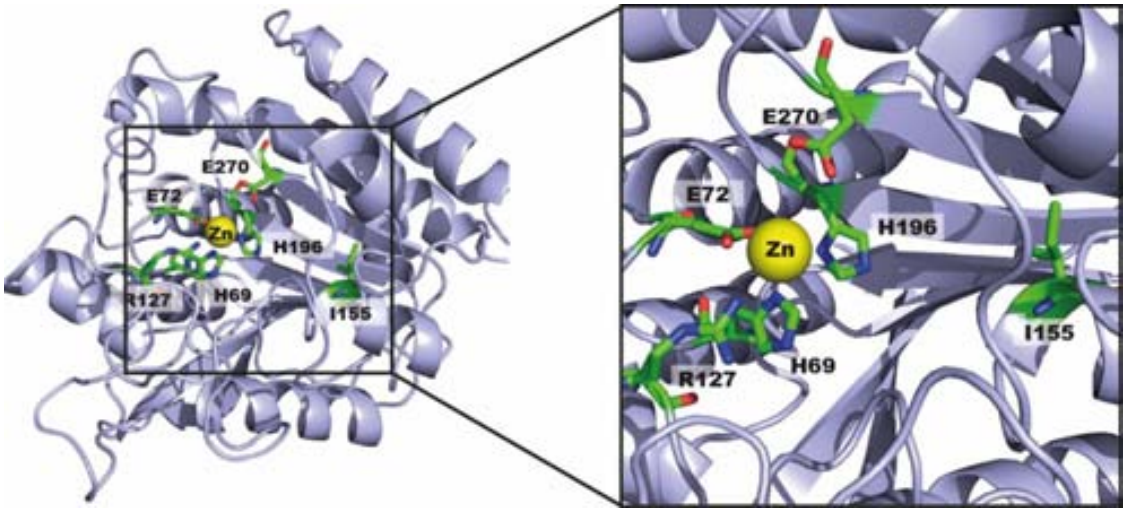

Figure 1.5. Bovine carboxypeptidase A structure and active site residues
Structural representation of native bovine carboxypeptidase A at 1.25 Å resolution (PDB 1M4L) with the main residues involved in catalysis (left) and a detailed representation of the active site (right). The Zn ion is coordinated with His69, Glu72 and His196 and a water molecule. Glu270 is the catalytic residue, Arg127 participates in stabilizing the intermediate and Ile155 is a main determinant of specificity. Images of structures were generated with PyMOL 1.3.

The mechanism of catalysis is still not fully understood. Two major mechanisms have been proposed, both consistent with the experimental data available (Kilshtain-Vardi *et al.*, 2003; Gomis-Rüth, 2008). The anhydride mechanism proposes a

nucleophilic attack to the scissile peptide bound by Glu270 that would result in an intermediate (acyl-enzyme) and it would consequently be disrupted by a water molecule before liberating the product. In the general acid/base mechanism, it is the zinc-bound water molecule that would carry out the nucleophilic attack (previously deprotonated by Glu270), leading to an intermediate (tetrahedral) that would collapse by proton donation to the leaving amine group by Glu270 (Gomis-Rüth, 2008; Fernández *et al.*, 2013).

A key residue participating in the hydrolysis is Glu270. The substitution of the glutamic acid at position 270 in bovine CPA and other metallocarboxypeptidases for alanine (A), valine (V) or glutamine (Q) eliminates the nucleophilic and acid/base properties of residue E270. This substitutions drastically reduce the activity with few perturbation of substrate affinity (Devault and Nault, 1988; Cha and Auld, 1997). These properties were exploited in the thesis to generate inactive mutants while preserving the native folding of the enzyme and its substrate binding sites.

1.5.2 Specificity and the active site

The active site of carboxypeptidases is commonly located in a groove on the surface of the enzyme (Vendrell *et al.*, 2000). Its substrate specificity can be inferred from the properties of binding subsites arranged along the catalytic residues responsible for the hydrolysis of the peptide bound. Accordingly, the binding subsites found in the active site of the peptidase are described in the model where each subsite of the enzyme is able to accommodate the side-chain of a single amino acid residue from the substrate (**Figure 1.1**). Accordingly, substrate residues are indicated as –P3–P2–P1↓P1', where P1' is the C-terminal substrate residue to be cleaved, and the corresponding binding subsites in the carboxypeptidase are named S3, S2, S1 and S1' (Schechter and Berger, 1967).

The residues involved in the catalytic mechanism of MCPs have been extensively studied. We can differentiate four main groups: the catalytic residues (Arg 127 and Glu 270); the zinc-binding residues (His69, Glu72 and His196); the substrate

stabilizers (Asn144 and Arg145); and the S1'-shaping residues. The last group of residues define a dead end pocket which is complementary to the C-terminal side-chain (R in **Figure 1.6**) of the substrate (the amino acid that is cleaved) (Gomis-Rüth, 2008).

In CPA, C-terminal side-chain of the last residue of the substrate (represented as P1' in **Figure 1.6**) is an aromatic residue (tyrosine, Y), that shapes the S1' subsite, which is a hydrophobic pocket in bovine CPA. The properties of S1' pocket are likely to reveal the substrate specificity of the carboxypeptidases as well as it is relevant to improve selectivity drug design (Devel *et al.*, 2010) since most of the natural or synthetic inhibitors for metallocarboxypeptidases bind the active site of the enzyme (Vendrell *et al.*, 2000; Fernández *et al.*, 2010b, 2013).

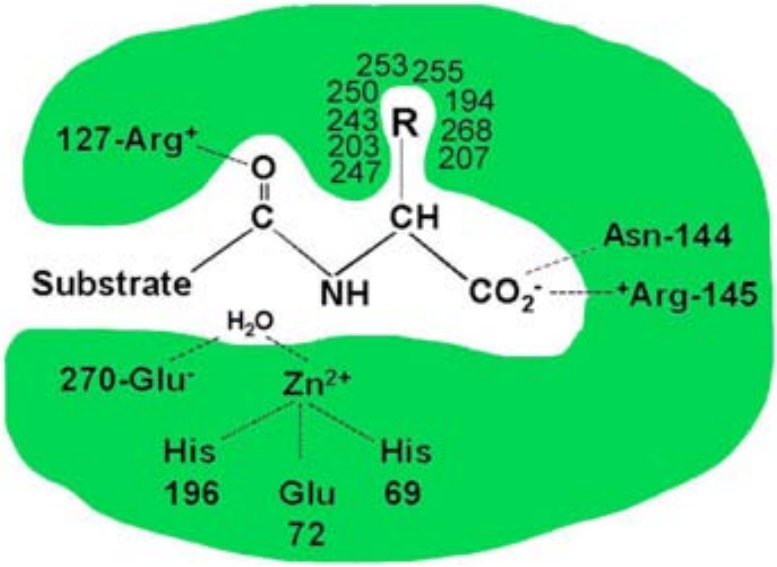

Figure 1.6. Substrate-binding residues in S1' of A-like MCPs.
Scheme of the substrate-binding residues shaping the S1' pocket in the active site of carboxypeptidases from the M14A family. Residues are numbered after active bovine CPA. Adapted from (Tanco *et al.*, 2010).

1.5.3 Functions of carboxypeptidases

Approximately half of all proteases are extracellular. Of the intracellular ones, a minor proportion are intramembrane, located in plasma and organelle membranes

(Turk *et al.*, 2012). When focusing on carboxypeptidases, the extracellular ones are often produced as inactive precursors and later activated (by cleavage of the prodomain hiding the entrance of the active site) in the extracellular media when reaching the correct location (Kassell and Kay, 1973). Other carboxypeptidases are intracellular and must remain in specific compartments or under regulated conditions to avoid non-specific degradation of the cell components.

The C-terminal processing of proteins performed by carboxypeptidases can be part of a degradative process or can take part in protein maturation or regulation. Classical carboxypeptidases involved in protein degradation are also known as the pancreatic members (CPA1, CPA2, and CPB) and they perform C-terminal cleavage of dietary proteins in the digestive tract.

A distinct purpose of C-terminal cleavage is to obtain a maturation or regulation of the polypeptidic substrate. Examples of such a function are CPA4, CPA6 and CPE, that can cleave C-terminal residues of neuropeptides (Lyons and Fricker, 2010; Tanco *et al.*, 2010; Cawley *et al.*, 2012); activated CPU (TAFI), which is a potent attenuator of fibrinolysis through the cleavage of lysins on partially degradated fibrin (Bajzar *et al.*, 1995; Willemse and Heylen, 2009); and in the immunologic response, CPA3, found in the secretory granules of mast cells and has been linked to immunological defense (Pejler *et al.*, 2007). Dysfunction of carboxypeptidases such as CPE, CPA4 or CPA6 results into pathological disorders ranging from obesity to cancer to epilepsy (Ross *et al.*, 2009; Sapio and Fricker, 2014). These examples highlight protein regulation by C-terminal cleavage as a key process in health and disease. Additionally, limited proteolysis forms a whole system for generating posttranslational modifications (PTMs) on proteins or peptides. A set of more than 300 PTMs can modify proteins bun only few consists of posttranslational addition of amino acids to preexistent proteins.

Cleavage of peptides is a well-studied process where carboxypeptidases participate, such as angiotensin converting enzyme (ACE) in the cleavage of angiotensin I to generate angiotensin II (George *et al.*, 2010; Guang *et al.*, 2012) or CPN and CPE in cleaving chemokines and neuropeptides (Keil *et al.*, 2007; Cawley *et al.*, 2012). C-terminal degradation of proteins as a PTM represents a big potential

machinery for increasing the range of protein function. Particularly, C-terminal limited proteolysis is often irreversible, near ubiquitous, and generate new C-termini (Lange and Overall, 2013) with all the responses that this can generate to living organisms.

A protein displaying high C-terminal diversity in eukaryote is tubulin, the essential component of microtubules. This work will focus in this component of the cytoskeleton as a core target of confined C-terminal proteolytic machinery.

2 Microtubules

Microtubules (MTs) are dynamic polarized polymers composed of α/β-tubulin heterodimers. Tubulin heterodimers associate forming a hollow tube composed of mostly 13 protofilaments of α/β-tubulin dimers aligned in parallel. MTs constitute the largest filaments of the cytoskeleton, taking part in a variety of cell structures and functions in eukaryotic cells, ranging from cell shape, polarity or motility to mediators of cellular interactions with the external media and regulators of the internal trafficking.

2.1 Types of microtubules

Tubulin can assemble in filaments with very different architectures: the centrioles in the centrosome that nucleates MTs, the axons and dendrites in neurons, the mitotic spindle that pulls chromosomes apart in dividing cells, the midbody (Steigemann and Gerlich, 2009), cilia and flagella from eukaryotic cells (**Figure 1.7 A-D**). Although it was thought MTs were restricted to eukaryotic cell, the recent discovery of *TubA* and *TubB* genes together with evidence of bacterial microtubules (Pilhofer *et al.*, 2011) opens a new field to study tubulin dynamics and function in the prokaryotic cell.

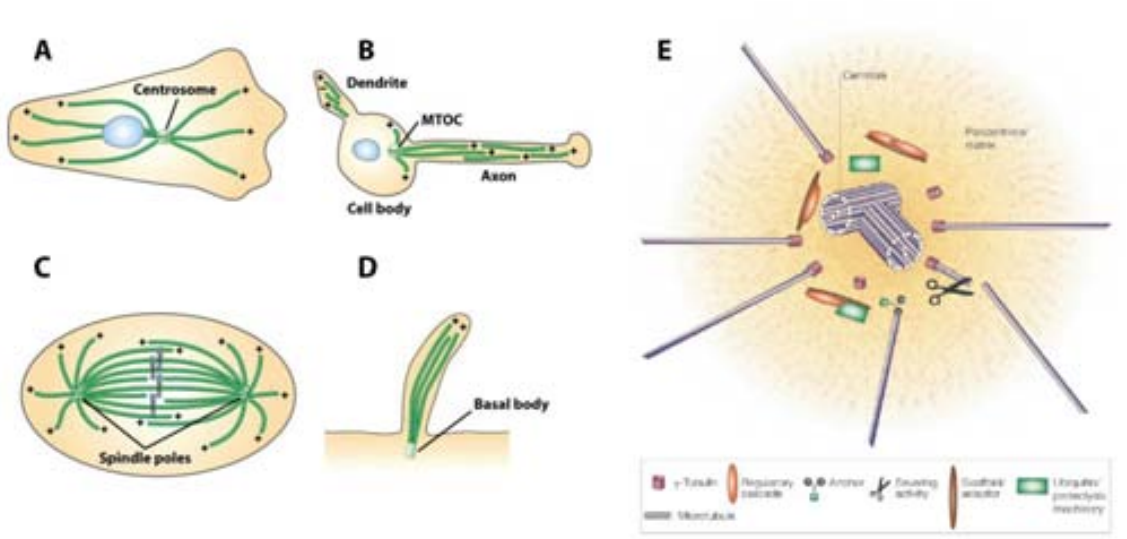

Figure 1.7. Diversity of tubulin-based structures in eukaryotic cells.
A) Microtubules nucleated from the centrosome. B) Axonal and dendritic microtubules in neurons. C) Dividing cell with the mitotic spindle binding to the chromosomes and the aster microtubules towards the cell membrane. D) Cilia or flagella arising from the basal body. E) Structure of the centrosome or microtubule organizing center showing a pair of centrioles in the center; microtubule lattices; the pericentriolar matrix (PCM), in which the minus end of microtubules are embedded, and γ-tubulin. Scaffolding proteins in the PCM and other regulatory proteins organize multiple activities of the centrosome. Source of A,B,C,D: http://www.studyblue.com/notes/note/n/bio-exam-1-inside-the-cell/deck/5467817; Source of E: (Feng and Walsh, 2001).

The exact mechanism that allows microtubules to achieve their function in the cell is not yet completely understood. However, essential function and flexibility of the lattice relies on the properties of the tubulin subunits. Tubulin undergoes cycles of polymerization and depolymerization, rearranges in complex structures such as the axonemes or the centrosomes (**Figure 1.7 E**). The different functionality (interaction with certain proteins) of the final microtubule will depend on the properties of the building blocks that form the array. Furthermore, tubulin is a GTPase. Only β-tubulin but not α-tubulin hydrolyses guanoside-triphosphate (GTP) during the assembly of the heterodimer. The energy input from GTP hydrolysis serves to generate nonequilibrium dynamics that permits the fast adaptation of the microtubules over time and the generation of motility (Valiron *et al.*, 2001).

2.2 Microtubules: structure and dynamics

2.2.1 The tubulin superfamily

The building block of microtubules are α- and β-tubulin, 55 KDa proteins from the tubulin superfamily, which also includes other members: γ-, δ-, ε- and ζ-tubulin (Oakley, 2000; McKean *et al.*, 2001). γ-Tubulin shares 29–35% amino acid identity with α- and β-tubulin and was discovered in *Aspergillus nidulans* (Oakley and Oakley, 1989). Differently from α- and β-tubulins, γ-tubulin does not take part in the microtubule lattices but in the nucleation of microtubules (Joshi *et al.*, 1992). Most fungal and animal cells have discrete microtubule-organizing centers (MTOCs), which are termed spindle pole bodies in fungi, and centrosomes in animal cells. γ-Tubulin is located in the MTOCs (**Figure 1.7 E**) and is associated with the mitotic spindle in several animal cells (Oakley, 2000).

δ-Tubulin was also discovered during a gene screening in *Chlamydomonas reinhardtii*, a unicellular flagellate green algae (Dutcher and Trabuco, 1998). Contrarily to α-, β- and γ-tubulins, δ-tubulin does not present a lethal phenotype when knocked-out and is absent in many sequenced genomes such as *Saccharomyces cerevisiae* (Chang and Stearns, 2000). The gene was neither found in *Caenorhabditis elegans,* which has aflagellate spermatids (Gogonea *et al.*, 1999). δ-Tubulin is found associated with the centrioles (Chang and Stearns, 2000) and particularly highly expressed in mouse testis. In testis, δ-tubulin is associated with the manchette, a specialized microtubule system involve in sperm head reshaping present in elongating spermatids.

Another tubulin subunit, ε-tubulin, localizes to the pericentriolar material. In particular, ε-tubulin is specifically recruited in the older centrosome from a newly duplicated pair and it has been detected in the midbody between dividing cells, where also γ-tubulin can be observed (Chang and Stearns, 2000). ε-Tubulin is required for centriole duplication and organization of the pericentriolar material (Chang *et al.*, 2003). Hence, γ-, δ- and ε-tubulin can be found in centrosomes while displaying different patterns.

ζ-Tubulin discovery was made in basal bodies from *Trypanosoma brucei* and *Leishmania major* (Vaughan *et al.*, 2000) and the tubulin superfamily is likely to

increase, such as with the incorporation of η-tubulin found in *Paramecium tetraurelia* (Ruiz *et al.*, 2000). A punctual mutation in η-tubulin inhibits basal body duplication and it is speculated to participate in tethering γ-tubulin or γ-tubulin complexes to basal bodies.

2.2.2 Tubulin dynamics

Focusing on microtubules, the subunits composing the filaments are α-/β-tubulin heterodimers. Microtubule assembly proceeds in three phases: nucleation, elongation and steady state. *In vitro*, tubulin aggregation or assembly requires heat (30-37 °C), GTP and certain tubulin threshold concentration. Tubulin is not able to assemble into MTs at low temperatures and only GTP-tubulin complexes are incorporated into MTs (Valiron *et al.*, 2001). Under these two conditions MTs dynamics follow the three phases mentioned above. Nucleation is the assembly of the first tubulin dimers. During the next step, tubulin dimers are added at the ends of MTs generating a tubular structure. *In vivo*, tubulin dimers are joined to one of the edges generating a polarized filament. At the third phase, steady-state, a fixed proportion of tubulin is in the filament form, whereas another tubulin pool remains soluble.

At steady-state, MTs remain out of equilibrium since continuous GTP hydrolysis is needed and constant exchange of tubulin subunits form the soluble tubulin pool. Two mechanisms can lead this process and have been observed either *in vitro* and *in vivo*: treadmilling and dynamic instability. Treadmilling is based on the asymmetric behavior of the two poles of the MT filament. The plus end is terminated with the β subunit and polymerize quicker than the slow-growing ends in α-tubulin, termed minus end (Margolis and Wilson, 1978). In animal cells, minus ends are generally anchored at centrosomes (Howard and Hyman, 2003). The dynamic instability model establishes that an individual MT never reaches an equilibrium length but persists in between longer or shorter assembly and disassembly phases (Mitchison and Kirschner, 1984; Koning *et al.*, 2008). When fast disassembly predominates, the process is termed catastrophe and when fast assembly leads, it is called *rescue* (Howard and Hyman, 2009) (**Figure 1.8**).

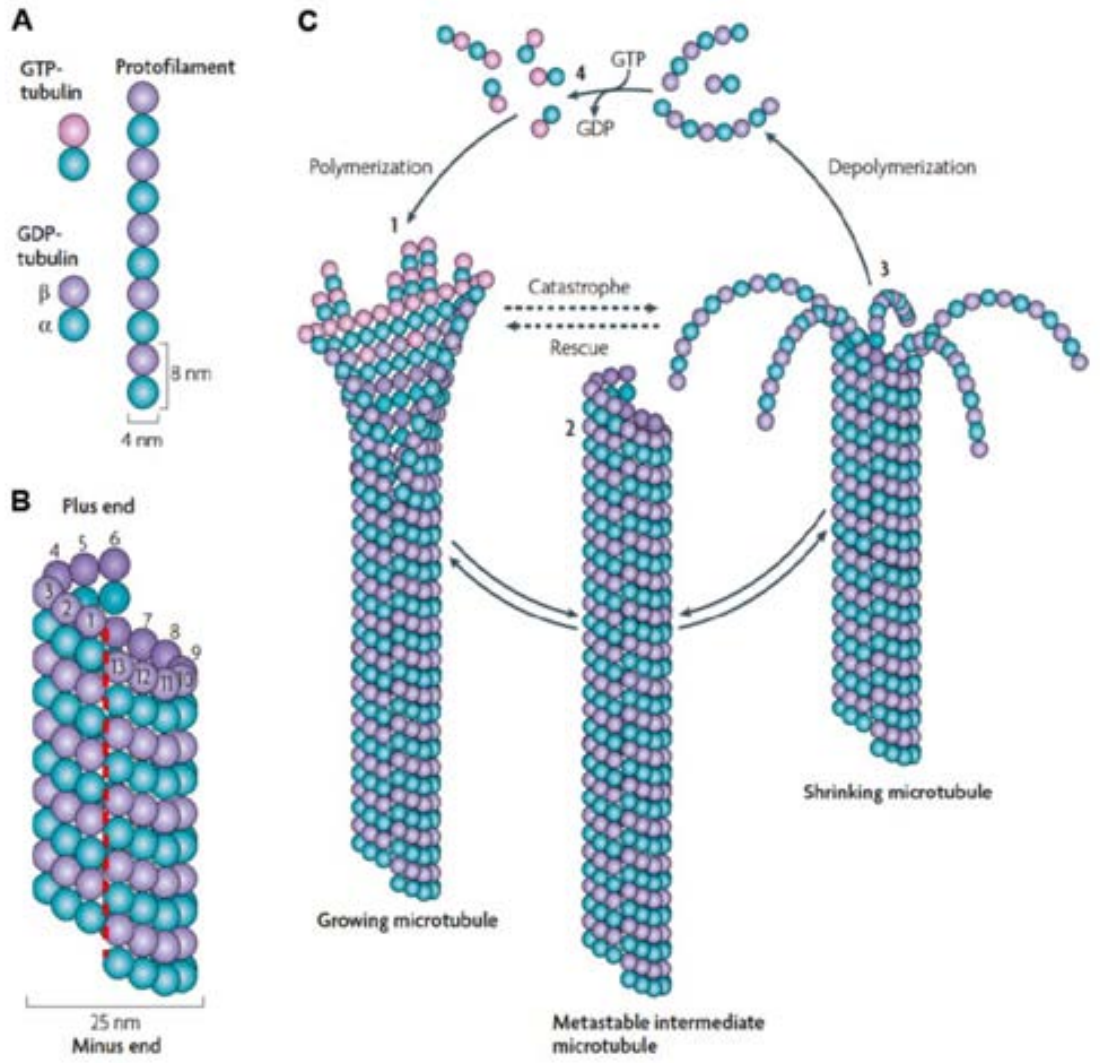

Figure 1.8. Regulation of growth and shrinkage of microtubules.
(A) Microtubules are composed of stable α/β-stable heterodimers. The β-subunit contains a GTP molecule when the dimer is in the soluble conformation and it hydrolyzes to GDP when it is incorporated to the filament. (B) The α/β dimers are disposed in a polar head-to-tail linear fashion along the protofilaments. Lateral association of protofilaments forms a cylindrical and helical MT wall typically comprising 13 parallel protofilaments in vivo and generates the lattice seam (red dashed line). D) A cap of GTP-tubulin at the plus (+) end is thought to promote and stabilize the growth phase (1). Loss of the GTP cap (e.g. by the action of depolymerases: kinesin 8 and 13) results in rapid shrinkage (catastrophe), with the protofilaments bending away from the microtubule axis. Microtubules can be rescued by incorporating new GTP-tubulin dimers. Source: (Akhmanova and Steinmetz, 2008)

In vivo, tubulin dynamics undergo rapid changes and several proteins interfere in this process. MT dynamics change significantly during the differentiation of a cellular lineage (Lacroix *et al.*, 2014). Certain differentiated cells need stable MTs to be

functional (e.g axons in neurons); others need efficient depolymerization such as the mitotic spindle (Mitchison, 2014). This requires the existence of MT stabilizing and destabilizing molecules. Those are end-binding proteins that can be classified into two groups: the MCAKs group (for mitotic centromere-associated kinesins) and plus-end-binding proteins (or +TIPs) (Howard and Hyman, 2003). MCAKs diffuse along MTs instead of walking till reaching both microtubule ends and function destabilizing them. A comparable process is the rapid targeting of DNA restriction enzymes to their restriction site (Helenius *et al.*, 2006). Most of the +TIPs bind to the growing end of the MTs and stabilize the filament during the elongation phase. End-binding proteins (EB), a type of +TIPs, specifically bind between protofilaments at the growing MT ends except at the MT seam (Maurer *et al.*, 2012), where the lateral contact of protofilaments is α-β instead of α-α or β-β. Also, rescue or rapid growth can be actively driven by MT polymerases such as XMAP215, able to recognize the polymerized form of tubulins through the tumor overexpressed gene (TOG) domain and accelerate growth (Ayaz *et al.*, 2012). This shows the high selectivity of proteins associated to MTs.

2.2.3 Microtubules in organization and transport

Microtubule dynamics is highly regulated by multiple factors: tubulin diversity (isoforms and post-translational modifications) and microtubule-associated proteins, among them the plus-tip tracking proteins (de Forges *et al.*, 2012). This regulation is necessary for microtubule functions in the cell, as it is the major intracellular organizer and transport network (**Figure 1.9**). In most interphase cells, microtubule arrays are nucleated and organized by the centrosome from which the polymers radiate into the cell cytoplasm (Valiron *et al.*, 2001). Nevertheless, nucleus and the Golgi apparatus can, in addition to the centrosome, be sites of microtubule nucleation and influence their own organization with a sub-population of specific microtubules (de Forges *et al.*, 2012).

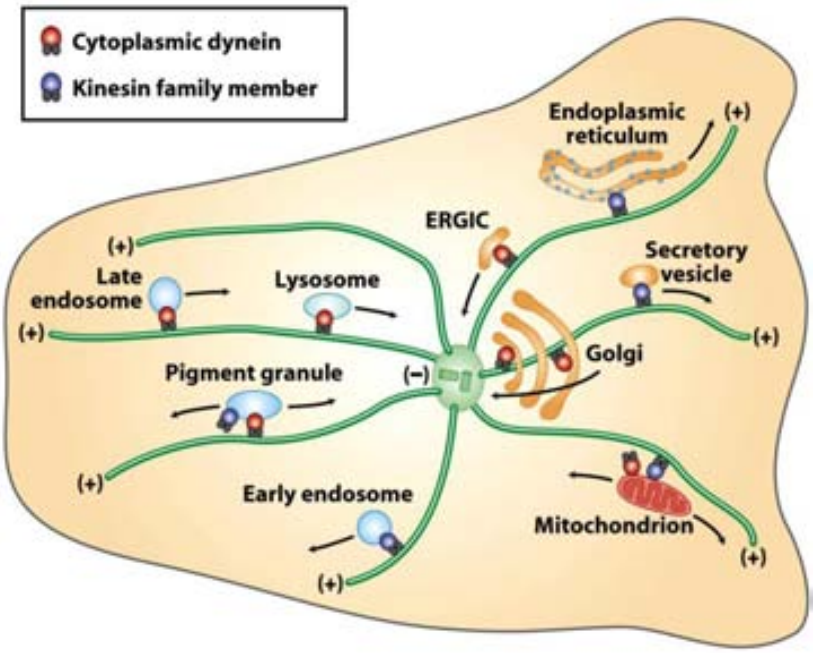

Figure 1.9. Microtubule network in the cell and organelle transport.
Directional transport of vesicles, early endosomes and endoplasmic reticulum towards the cell boundaries (positive end) is driven by kinesin family members. Transport towards the minus end is carried out by the cytoplasmic dynein. Source: (Lodish, 2008).

MTs are involved in cell shape and motility (Etienne-Manneville, 2004) but also in intracellular organization and transport of organelles. The mitotic spindle pulls the two chromatids apart towards the opposite poles by the specific binding of depolymerizing MTs to the kinetochores (Nogales and Ramey, 2009). This process separates one into two new nuclei and is mediated by the interaction of spindle MTs and the kinetochores (Tanaka, 2010). The midbody appears at the end of cytokinesis and physically separates the two daughter cells before the abscission (Elad *et al.*, 2011). Related to nuclear organization, MTs also participate in the nuclear envelope breakdown (Beaudouin *et al.*, 2002).

MTs in animal cells are involved both in shaping the endoplasmic reticulum (ER) and in the formation of ER tubes. KIF5B/kinesin-1 seems to be the major motor protein involved in ER positioning; but other Tip Attachment Complexes (TACs) mediate interactions between MTs and the ER tubes. In most animal cells, the Golgi apparatus is shaped as a ribbon and closely associated with the centrosome. Microtubule-dependent molecular motors are also essential for Golgi organization, particularly the

minus-end directed motor, cytoplasmic dynein (de Forges *et al.*, 2012). However, other plus-end directed motors including actin-based motors (Allan *et al.*, 2002) and non-motor MT-binding proteins also participate in Golgi assembly and dynamics (Rios and Bornens, 2003). In addition, mitochondria (Pilling and Horiuchi, 2006), intracellular vesicles (Kapitein *et al.*, 2010) and mRNA transport (Yoo *et al.*, 2010) is mediated by motor proteins along the MTs.

Another particular MT-based transport takes place in the cilia and flagella. Here they are responsible for essential processes such as sperm motility and signal transduction into the retina or the ear.

2.3 Cilia and flagella

MTs or tubulin complexes are the main structural components of highly specialized organelles such as centrioles (Bornens, 2012) and axonemes, which are the backbones of cilia and flagella (Satir and Christensen, 2007). Two centrioles lie at the core of the centrosome: the mature (mother) and the daughter. Centrioles are composed of nine triplets of microtubule "blades" organized around a central cartwheel. The centrioles play a crucial role in recruiting the proteins composing the pericentriolar material, where MTs nucleate. Specifically the mature centriole has an additional role in nucleating the formation of cilia and flagella in most eukaryotes (Azimzadeh and Marshall, 2010; Bettencourt-Dias *et al.*, 2011). The formation and function of the cilia or flagella requires a transport system called intraflagellar transport (IFT), which is conserved from protists to humans (Scholey, 2008). Those organelles have abundant MT diversity, and are focused in this thesis regarding their functional implications.

2.3.1 Basal body and the axoneme

Cilia are membrane-bound projections derived from the mature centriole. The cilium contains a microtubular structure, named ciliary axoneme, embedded in a specialized ciliary membrane. In mammalian multiciliated cells of the epithelia, the

axoneme presents a structural feature of 9 microtubular doublets surrounding a central pair of singlet MTs (9+2), the axoneme possesses outer and inner dynein arms (ODA and IDA), which are the molecular motors responsible for the sliding of the doublet microtubules and therefore generating movement. The dynein arms produce a helical beat, which is modified by interdoublet links and the radial spoke/central-pair interaction resulting in controlled bending and effective stroke (Okada *et al.*, 2005; Lindemann and Lesich, 2010).

In contrast to the motile multicilia, single, immotile primary cilium has a 9+0 structure without the characteristic dynein arms (Satir and Christensen, 2007; Bettencourt-Dias *et al.*, 2011). The special category of motile monocilium with 9+0 structure was found in the embryonic node during development (**Figure 1.10**). The nodal cilia regulates the left-right body asymmetry by generating a leftward flow in the extraembryonic fluid during organ morphogenesis (Okada *et al.*, 2005; Blum *et al.*, 2014).

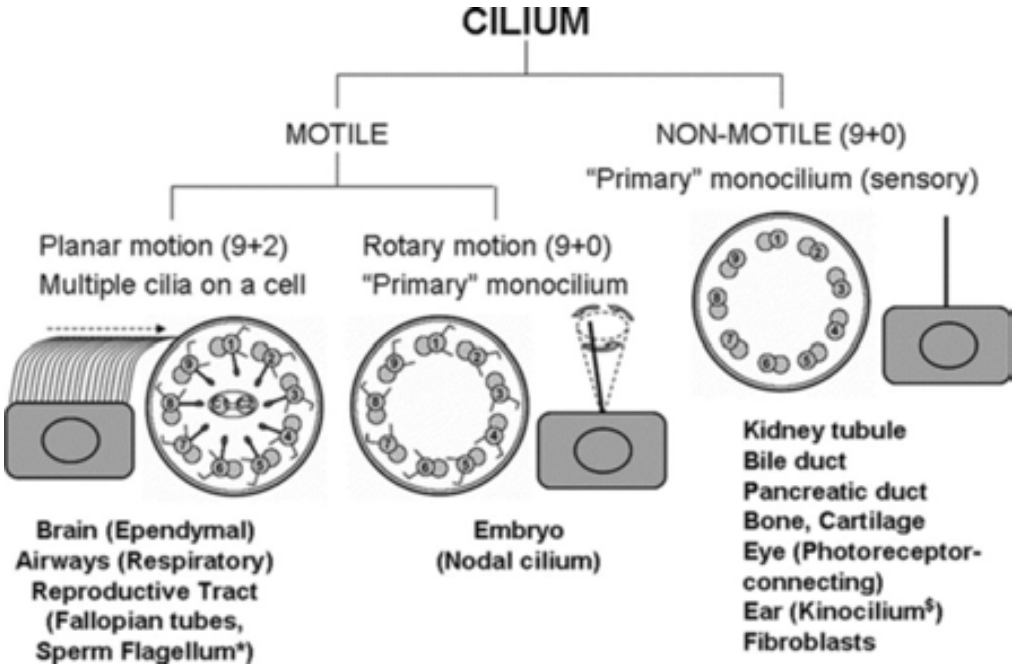

Figure 1.10. Cross-sectional structure and components of motile and primary cilia
*Cilia axoneme cross-sections of non-motile (9+0 arrangement) and motile cilia (9+2 or 9+0 arrangement) are illustrated. The model shows the planar synchronous motion of motile cilia (9+2), the rotatory motion of motile monocilium (9+0), and the immotile cilium. *Solitary axoneme in the sperm mirrors the structure of the cilium. $Subcellular structure of the kinocilium is debatable. Source:* (Leigh *et al.*, 2009).

The ciliary membranes of both motile and immotile cilia enclose specific receptors and ion channels that initiate signaling pathways controlling motility and/or linking mechanical or chemical stimuli (ligands). The cilia is rooted in a ciliary pocket, an invagination from the plasmatic membrane with close contacts to the actin cytoskeleton and that contains clathrin-coated pits for endocytic functions (Molla-Herman *et al.*, 2010).

Remarkably, cilia have a tight connection to pathways initiated by ligands as diverse as Sonic hedgehog, growth factors, cytokines or Ca^{2+}. Pathways occurring in the cilium are later affecting the whole cell through intracellular transduction cascades regulating differentiation, migration, and cell growth during development and adulthood. While the importance of motile cilia and flagella in biology was clear from the early times (*e.g.* in respiratory epithelium, female reproductive tract and male sperm), primary cilia were thought to be a vestigial organelle. Increasing evidences show the importance of primary cilia including severe clinical phenotypes (Satir and Christensen, 2007).

2.3.2 Motile cilia/flagella and ciliopathies

Motile cilia are found in various epithelial surfaces, including respiratory airways, brain ependymal cells lining the ventricles, along the female reproductive tract and in the node of embryos. The function of motile cilia is moving mucus or fluids. These cilia present a motile axoneme with similar structure to the flagella found in the mammalian sperm tail. Before the development of *in vitro* fertilization, the motility of sperm was essential for fertility. And, as a result of the study of male infertility, primary ciliary dyskinesia (PCD) was first diagnosed (Afzelius, 1976).

Abnormal motility is associated with axonemal ultrastructural defects (Satir and Christensen, 2007; Moore *et al.*, 2013), which are grouped under PCD [MIM 244400], a genetically heterogeneous disorder. PCD can either involve single organ disorders or occur as multisystem disorders, with phenotypically variable and overlapping disease manifestations depending on the nature of the ciliopathy. Due to this heterogeneity,

ciliopathies can involve either motile cilia or primary cilia and also appear as diverse clinical manifestations (Ramamurthy and Cayouette, 2009).

PCD affectation leads to symptoms including abnormal sperm motility (subfertility or infertility), cystic kidneys, blindness, hearing impairment (deafness), and sinopulmonary disease in the respiratory tract. This last symptom is due to impaired mucociliary transport in the airways that manifests as perinatal respiratory distress, chronic respiratory infections, rhinosinusitus, otitis media, and bronchiectasis (Barbato *et al.*, 2009). Also the nervous system can be affected by motile cilia deficiency, as dysfunctions of ependymal cilia movement is associated with accumulation of cerebrospinal fluid at the lateral ventricles of the brain, leading to hydrocephalus (Lee, 2013).

Treatments currently applied to ciliopathies (and particularly to PCD), are mainly to prevent exacerbations and to slow the progression of lung disease. Such treatments are based on antibiotics, airway clearance and anti-inflammatory strategies (Lobo *et al.*, 2014; Lucas *et al.*, 2014).

2.3.3 Primary cilia

The primary cilium is a sensory organelle that receives both mechanical and chemical signals from other cells and the environment, and transmits these signals to the nucleus to elicit a cellular response. Primary cilia present a similar structure as motile cilia, differing in the absence of the central pair of microtubules in the axoneme and the dynein arms (hence they are immobile). They are relatively short in size and found on mammalian epithelial cells, such as those of the kidney tubule, bile and pancreatic ducts, but also on non-epithelial cells, such as chondrocytes (Poole *et al.*, 1985), fibroblasts, and neurons (Lee and Gleeson, 2011).

In most cells, the formation of the primary cilia (**Figure 1.11**) is closely related to the cell cycle. In fibroblasts in culture, primary cilium grow when the cells become confluent and enter G_0 (Wheatley, 1971). Therefore, a close regulation exists between the cell cycle and the primary cilia (Kim and Tsiokas, 2011), and some components are shared by cilia and centrosome such as IFT88 (Robert *et al.*, 2007).

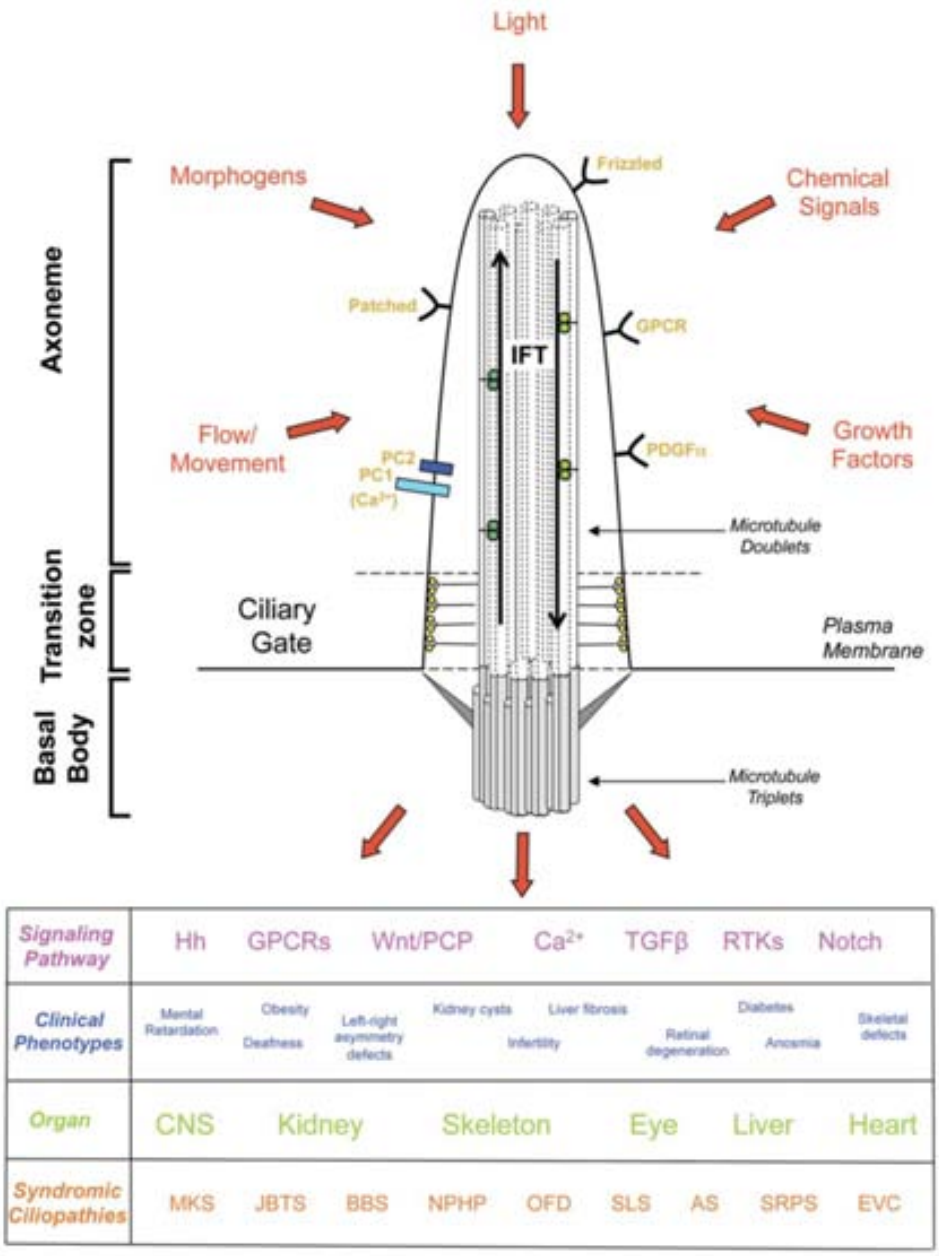

Figure 1.11. Overview of primary cilium structure and signaling pathways

The primary cilium is composed of the basal body inserted into the cell membrane, a transition zone and the axoneme towards the external medium. This organelle presents intraflagellar transport (IFT) and governs diverse signaling pathways: Hh, Hedgehog; GPCRs, G-protein-cupled receptors; Wnt/PCP, Wingless/Planar cell polarity; Ca^{2+}, TGFβ, Transforming Growth Factor beta; RTKs, Receptor tyrosine kinases; and Notch. Dysfunction of the primary cilium results in clinical phenotypes including ciliopathies. MKS, Meckel-Gruber Syndrome; JBTS, Joubert Syndrome: BBS, Bardet Biedl Syndrome; NPHP, nephronophthisis; OFD, Oral-Facial-Digital Syndrome; SLS, Senior-Løken Syndrome; AS, Alstrom Syndrome; SRPS, Short Rib-Polydactyly Syndrome; EVS, Ellis-van Creveld Syndrome. Source: (Fry *et al.*, 2014).

A major function of the primary cilia is the transduction of signaling pathways (**Figure 1.11**) involved in differentiation and development (Pan *et al.*, 2013). Under normal conditions, these signal pathways ensure homeostasis, thus the maintenance of the differentiated tissue state or controlled division and differentiation. However, abnormal signaling in cilia –due to aberrant ciliogenesis or misplacement or mutation of ciliary membrane components- lead to abnormal tissue growth, aberrant cell division and to several human pathologies (Satir and Christensen, 2007). An example of primary cilia disorder is retinitis pigmentosa, characterized by night blindness and progressive loss of peripheral vision due to rod photoreceptors undergoing cell death (Ramamurthy and Cayouette, 2009).

In the retina, the photoreceptor cells have a highly specialized primary cilium named the outer segment, which is essential for photosensation. The outer segment contains the axoneme of the cilium and disk membranes components. The visual pigments (opsins or rhodopsins) need to be constantly transported via intraflagellar transport (IFT) to the disk membranes (Young, 1967). Mutations affecting photoreceptor protein trafficking or ciliogenesis lead to mislocalization or accumulation of the visual pigments that can eventually result in photoreceptor cell death causing retinitis pigmentosa (Ramamurthy and Cayouette, 2009). In the nervous system, primary cilia play critical roles in controlling neuronal development, modulating various signal transduction pathways. Defects in the central nervous system range from cerebellar malformation and oculomotor apraxia (absence of voluntary eye movement control) to mental retardation (Lee and Gleeson, 2011).

Also the link between primary cilia and cell cycle has as an impact in pathological conditions. There is a marked implication of primary cilia malfunction in carcinogenic processes (Shpak *et al.*, 2014). Primary cilium dysfunction blocks signal transduction pathways such as Sonic hedgehog (Shh) (Ruat *et al.*, 2012) and platelet derived growth factor receptor A (PDGFRα) (Schneider *et al.*, 2005). Shh is important during development in left-right body axis, neural tube closure and patterning and formation of the limbs, teeth, pancreas, lungs and hair follicles. PDGFRα is essential in normal embryogenesis, inflammation and wound healing. In addition, both Shh and PDGFRα are involved in carcinogenesis (Michaud and Yoder, 2006). Specifically, the

loss of primary cilia has been observed in a wide range of cancer types (Hassounah *et al.*, 2012; Shpak *et al.*, 2014) and has been shown to be associated with greater cancer/tumor progression and poorer prognosis (Emoto *et al.*, 2014).

3 The tubulin code

3.1 Tubulin isoforms: a first layer of diversity

Tubulin-based structures participate in all kind of processes in living organisms. Each of α, β and γ- tubulins display different physicochemical properties such as net electric charge, dipole moments and dipole vector orientations (Tuszynski *et al.*, 2006) but conserve a core architecture. The structural breakdown of MT lattices often associates with pathological conditions such as neurodegeneration, cancer, infertility or blindness. These varied affectations and diversity of tubulins reflect the diversity of MT structures and the importance to understand the dynamics and the chemistry of its building block: tubulin.

In view of the huge variety of MT functions, the targeting of distinct MTs for precisely defined roles in cells appears primordial. Great advances lead to understand the implication of microtubule-associated proteins (MAPs) and molecular motors in the functional specialization of MT populations such as the mitotic spindle, the kinetochores or the axons in neurons (van der Vaart *et al.*, 2009). However, the signals that confer specificity to individual or groups of MTs, allowing certain MT-MAP interactions but not others to happen, are not yet completely understood.

The conserved structure of the α-tubulin-β-tubulin dimer is essential for MT assembly and architecture in a hollow tube (Nogales *et al.*, 1998; Alushin *et al.*, 2014). Because this structured part of tubulins must remain conserved to construct the hollow tube, the variability allocates to the unstructured C-terminal tails (**Figure 1.12** and **Table 1.3**). Therefore, functionally distinct MT species can be generated by two mechanisms involving chemical changes in the tubulin subunits. This can be either by incorporating selected tubulin isotypes into the MT lattice (Ludueña and Banerjee, 2008), or by generating posttranslational modifications (PTMs) onto selected MTs in

cells (Janke and Bulinski, 2011). The major differences among α- and β-tubulin isoforms –also called isotypes- as well as most of the known PTMs of tubulin take place at the C-terminal tails of tubulins (**Figure 1.12 A**). The C-termini of α and β-tubulin exist in at least two different stable conformations that is either projecting it towards the outer part of the lattice or collapsed onto the microtubule surface (Tuszynski *et al.*, 2006). These C-terminal tails differing in conformation and chemical properties are the key interaction sites for MAPs and motors (Sirajuddin *et al.*, 2014).

Table 1.3. Characteristics of human tubulin isotypes

Tubulin					CNBr C-terminal peptide	
Isotype[a]	Gene	Accession number	pI	Mass (Da)[b]	Mass (Da)[c]	C- Terminal Sequence
α1A	TUBA1A	NP_006000	4.94	50135.6	2860.19	AALEKDYEEVGVDSVEGEGEEEGEEY
α1B	TUBA1B	NP_006073	4.94	50151.6	2860.19`	AALEKDYEEVGVDSVEGEGEEEGEEY
α1C	TUBA1C	NP_116093	4.96	49895.3	2590.04	AALEKDYEEVGADSADGEDEGEEY
α4A	TUBA4A	NP_005991	4.95	49924.4	2633.07	AALEKDYEEVGIDSYEDEDEGEE
α3C	TUBA3C	NP_005992	4.98	49959.6	4150.77	EEGEFSEAREDLAALEKDYEEVGVDSVEAEAEEGEEY
α3D	TUBA3D	NP_525125	4.98	49959.6	4150.77	EEGEFSEAREDLAALEKDYEEVGVDSVEAEAEEGEEY
α3E	TUBA3E	NP_997195	4.97	49916.6	4090.71	EEGEFSEAREDLAALEKDYEEVGVDSVEAEAEEGEEY
α8	TUBA8	NP_061816	4.94	50093.6	4156.72	EEGEFSEAREDLAALEKDYEEVGTDSFEEENEGEEF
α-like 3	TUBAL3	NP_079079	5.68	49908.7	3058.40	EEAEFLEAREDLAALERDYEEVAQSF
βI	TUBB	NP_821133	4.78	49670.8	3366.33	NDLVSEYQQYQDATAEEEEDFGEEAEEEA
βII	TUBB2B	NP_821080	4.78	49953.1	3466.36	NDLVSEYQQYQDATADEQGEFEEEEGEDEA
βIII	TUBB3	NP_006077	4.83	50432.7	1624.64	YEDDEEESEAQGPK
βIVa	TUBB4	NP_006078	4.78	49585.8	3350.38	NDLVSEYQQYQDATAEEGEFEEEAEEEVA
βIVb	TUBB2C	NP_006079	4.79	49831.0	3479.42	NDLVSEYQQYQDATAEEEGEFEEEAEEEVA
βV	TUBB6	NP_115914	4.77	49857.1	3551.41	NDLVSEYQQYQDATANDGEEAFEDEEEEIDG
βVI	TUBB1	NP_110400	5.05	50326.9	810.35	EPEDKGH

[a] α-Tubulin nomenclature reflects the revised nomenclature for the α-tubulin gene family (Khodiyar *et al.*, 2007).
[b] Protein mass is the average mass.
[c] CNBr peptide mass is reported as the monoisotopic neutral mass.
Adapted from (Miller et al., 2010)

3.1.1 α-Tubulin isotypes

In terms of C-terminal differences a set of at least 5 α-tubulin and 8 β-tubulin isotypes are described in humans (**Figure 1.12 B**). One of the α-tubulin isotypes, TUBA4A, represents a constitutive detyrosinated form, missing the C-terminal tyrosine (Tyr), thus its expression would increase the pool of detyrosinated microtubules in the absence of posttranslational modifications. The accumulation of TUBA4A was suggested as a factor responsible for male azoospermia (non-measurable sperm levels)

(Bhagwat *et al.*, 2014). TUBA8 displays a different C-terminal aromatic residue, a phenylalanine (Phe) instead of Tyr. This tubulin isotype conserves the aromatic properties at the C-terminal, probably in a permanent way, since the tubulin carboxypeptidase might not be able to remove C-terminal Phe or do it less efficiently (**Figure 1.12 B,** left and **Table 1.3**).

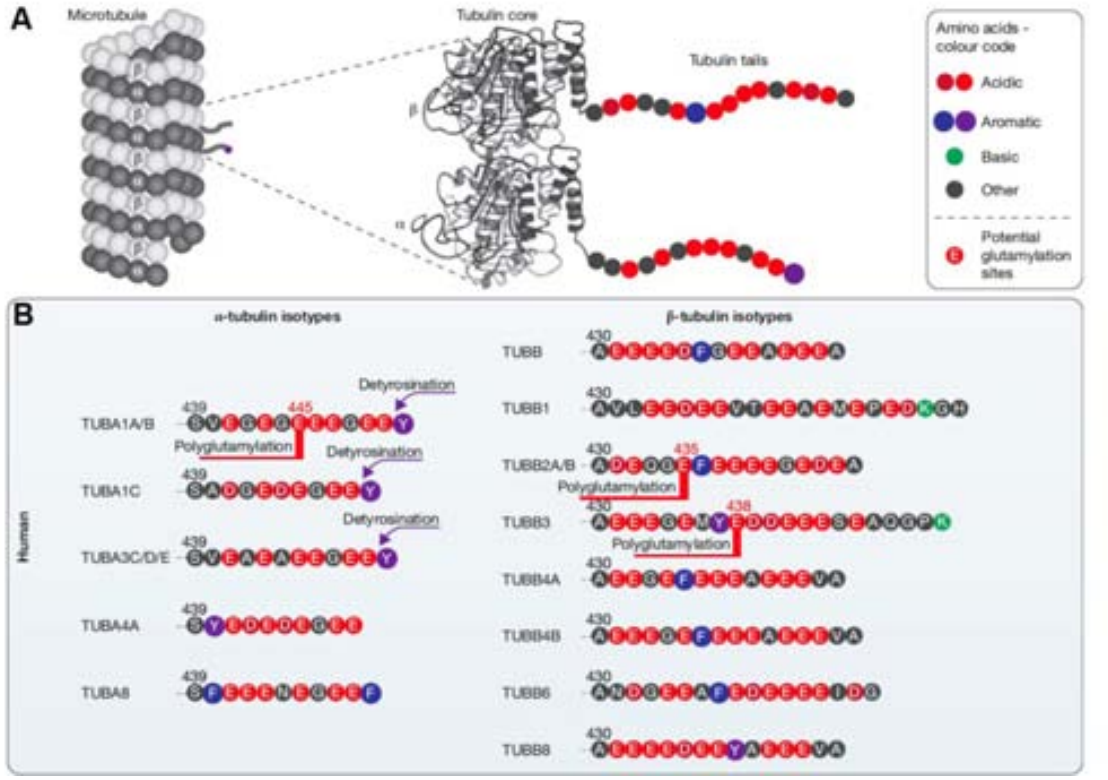

Figure 1.12. Variability of human tubulin isoforms in the C-terminal tails
A) *Schematic representation of the localization of C-terminal tubulin tails on the microtubule lattice. A microtubule lattice with α- and β-tubulins pictured as dark and light grey spheres, respectively (left) and the structure of the α- and β-tubulin dimer, with addition of the C-terminal tails.* ***B)*** *Comparison of C-terminal tails from all human and yeast (S. cerevisiae) tubulin isotypes. All glutamate residues within these tails could serve as potential polyglutamylation sites, but the previous identified are labeled. Source:* (Wehenkel and Janke, 2014).

In addition to the changes in its C-terminal primary sequence, TUBA4A and TUBA8 are non-acetylable at lysine 40. TUBA4A is increased in asthenozoospermia (reduced sperm motility) as compared to normal spermatozoa, while TUBA8 and the testis-specific acetylable α-tubulin isoform TUBA3C are reduced (Bhagwat *et al.*, 2014).

Moreover, mutations in the neuronally expressed TUBA1A and also the β-tubulin isotype TUBB2B are associated with a wide range of overlapping cortical malformations, also similar to patients with mutations in TUBA8 (Cushion *et al.*, 2013).

3.1.2 β-Tubulin isotypes

Similarly to α-tubulin C-terminal tails, β-tubulin isotypes present acidic tails, with stretches of glutamic acids (Glu), but they differ from α-tubulin for the absence of a terminal aromatic residue. β-Tubulin isotypes end with alanine (Ala) except for TUBB1 ending in histidine (His), TUBB3 with lysine (Lys) and TUBB6 with glycine (Gly) (**Figure 1.12B,** right and **Table 1.3**). Differential implications have been associated to distinct β-tubulin isotypes in neurons: TUBB is required for cell viability, TUBB2 for neurite outgrowth and TUBB3 for protection against free radicals and reactive oxygen species (Guo *et al.*, 2010). Besides, TUBB3 mutations are known to impair axonal guidance, microtubule dynamics and MT-kinesin interaction (Tischfield *et al.*, 2010). These mutations are associated with various neurological syndromes such as ocular motility disorder, a congenital fibrosis of the extraocular muscle type 3 (CFEOM3), and malformations of cortical development (Poirier *et al.*, 2010; Tischfield *et al.*, 2010).

Tubulin isoforms are often tissue and differential-stage specific (*e.g.* TUBA8 is mostly expressed in non-mitotic tissues such as heart, skeletal muscle and brain) (Stanchi *et al.*, 2000). Different α- and β-tubulin isotypes are required for processes like positioning, differentiation and survival of neurons and male fertility (Tischfield and Engle, 2010; Bhagwat *et al.*, 2014). The aberrant expression of specific β-tubulin isotypes, in particular βIII-tubulin, or of microtubule-regulating proteins is important clinically in tumour aggressiveness and resistance to chemotherapy (Kavallaris, 2010). Mutations in tubulin isotypes, particularly in neuronal disorders, are referred as tubulinopathies and are associated with an increasing spectrum of clinical severity (Bahi-Buisson *et al.*, 2014; Romaniello *et al.*, 2014).

Importantly, patients with C-terminal mutations in TUBB3 presents a more severe CFEOM3 phenotype and these C-terminal mutations impairs kinesin advances towards the MT +end (Tischfield *et al.*, 2010). Mutations in the C-terminal tail of

TUBB3, which markedly differs from the rest of isotypes, cause particularly severe dysfunctions. Abundance of this tubulin isotype could also have prognostic value for carcinomas of unknown primary site, as high levels of TUBB3 correlate with resistance to chemotherapy and shorter overall survival (Sève *et al.*, 2008).

3.2 Tubulin posttranslational modifications increase microtubule diversity

Tubulin isotypes permit a wide spectrum of heterodimers to build different MT identities. However, faster mechanisms than *de novo* synthesis of tubulin subunits and proteosomal degradation are required for rapidly targeting and de-targeting MT for specific functions (*e.g* in metaphase, anaphase or telophase). In this context, PTMs rapidly modulate MT functional properties (Verhey and Gaertig, 2007).

The most studied PTMs of tubulin include acetylation (L'Hernault and Rosenbaum, 1985; Piperno and Fuller, 1985), phosphorylation, palmitoylation, the recently described polyamination (Song *et al.*, 2013) that would participate into axonal stability, and PTMs involving addition or removal of amino acids either at the gene-encoded C-terminus or as lateral amino acid tails (Janke and Bulinski, 2011) (**Figure 1.13**). These last PTMs include the addition/removal of the C-terminal tyrosine from α-tubulin (tyrosination/detyrosination) (Thompson, 1977; Gundersen *et al.*, 1984); the generation of Δ2-tubulin by the hydrolysis of the glutamate at the penultimate position of α-tubulin (Paturle-Lafanechère et al., 1991; Lafanechère and Job, 2000); a further glutamic acid removal to generate Δ3-tubulin (Berezniuk *et al.*, 2012); and the tubulin polymodifications concerning branching stretches of amino acids.

Tubulin polymodifications consist of the addition/removal of a variable number of glutamates (polyglutamylation) (Eddé *et al.*, 1990) or glycines (polyglycylation) (Redeker *et al.*, 1994) as side-chains. These amino acidic chains lay on specific glutamates near the C-terminal tails of both α- and β-tubulin. These C-terminal modifications cause structural and chemical changes in regions of the outer surface of MT fibers and centrioles (Wloga and Gaertig, 2010), which are interaction sites for MAPs (Bonnet *et al.*, 2001; Ikegami *et al.*, 2006) and motor proteins (Wang and Sheetz, 2000; Ikegami *et al.*, 2007). MAPs and motors are sensitive to C-terminal changes in

tubulins, preferring either certain isotypes or PTMs (Sirajuddin *et al.*, 2014). Additionally, changes in the expression levels of enzymes catalyzing tubulin PTMs have been described in cancer (Lafanechère *et al.*, 1998; Kashiwaya *et al.*, 2010; Das *et al.*, 2014).

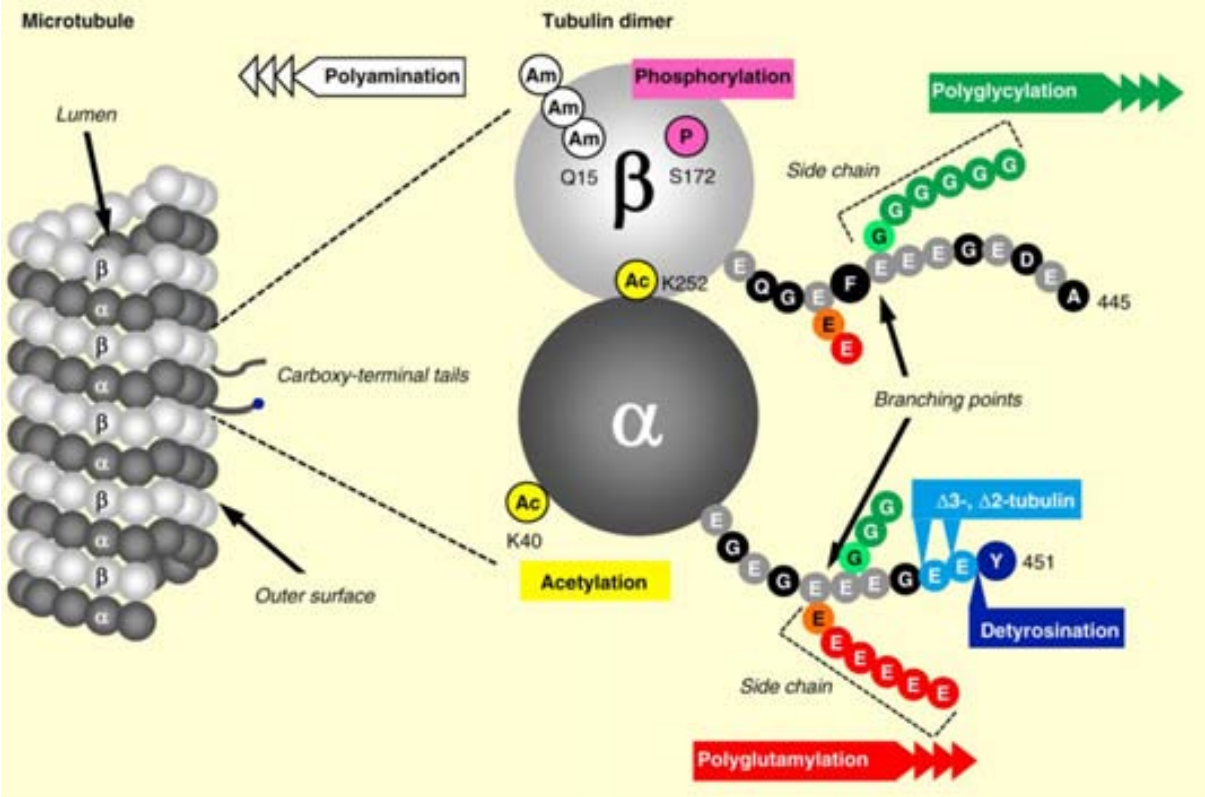

Figure 1.13. Tubulin posttranslational modifications
Microtubules are assembled to hollow tubes composed of 13 protofilaments. The globular parts of the tubulins form the microtubule walls and the luminal surface, while the C-terminal tails decorate the outer surface of microtubules. While most PTMs are found on the C-terminal tail, K40 acetylation of α-tubulin is present in the lumen; K252 acetylation site of β-tubulin is present at the α/β-tubulin interface; polyamination at Q15 and phosphorylation at S172 localize in the globular, folded part of β-tubulin. Detyrosination/tyrosination, Δ2- and Δ3-tubulins modulate the C-terminal tails of α-tubulin, and polyglutamylation and polyglycylation are found within the C-terminal tails of both α- and β-tubulin. Source: (Magiera and Janke, 2014).

Two known enzyme families participate in tubulin polymodifications: tubulin tyrosine ligase like proteins (TTLLs) and cytosolic carboxypeptidases (CCPs). The TTLL protein family contains glutamylases and glycylases (Janke *et al.*, 2005a; van Dijk *et al.*,

2007). So far, only deglutamylases have been identified in the family of cytosolic carboxypeptidases (CCPs), a subfamily of M14 MCPs (Kalinina *et al.*, 2007; Rodriguez de la Vega *et al.*, 2007; Rogowski *et al.*, 2010). This thesis focuses on two members of the CCP subfamily.

3.2.1 Acetylation

Two acetylation sites were described on tubulins, Lys40 of α-tubulin, a residue located in the lumen, and Lys252 residue of β-tubulin, which is present at the α-/β-tubulin interface. Acetylation of Lys40 takes place in the polymerized MT while β-tubulin acetylation happens preferentially on the soluble heterodimer (Chu *et al.*, 2011).

The only known acetyltransferase responsible for Lys40 acetylation in mammals is α-tubulin acetyltransferase (αTAT), while two deacetylases have been reported: HDAC6 (Hubbert *et al.*, 2002) and SIRT2 (North *et al.*, 2003). Other acetyltransferases have been demonstrated to interfere with Lys40 acetylation, such as ARD1-NAT1 complex (ARD1 named after arrest-defective 1-amino-terminal, α-amino, acetyltransferase 1) involved in dendritic arborization during neuronal development (Ohkawa *et al.*, 2008); the elongation protein complex (EPC) (Creppe *et al.*, 2009); and GCN5 (Conacci-Sorrell *et al.*, 2010). αTAT activity on Lys40 occurs at a low rate, in a stochastic manner along the microtubules, and requires lateral interface contacts between protofilaments (Szyk *et al.*, 2014). The low rate activity of αTAT ensures that only long-lived MTs are acetylated. Anti-Lys40-acetylation antibody stains discrete MT populations in the interphase cell and reveals that ciliary, flagellar, centrioles, mitotic spindle, midbody and neuronal MTs are strongly acetylated at Lys40. This particular modification is described as required in touch receptor neurons, and it could be part of a mechanism that orients cells during three-dimensional migration (Wynshaw-Boris, 2009).

Acetylation of β-tubulin happens at Lys252 by the acetyltransferase SAN, in non-polymerized tubulin (Chu *et al.*, 2011). The acetyl group interacts with the phosphate group of the α-tubulin-bound GTP located at the interface of α-/β-tubulins.

It has been proposed that the acetylation slows down tubulin incorporation into MTs by neutralizing the positive charge on Lys252 and allowing tubulin heterodimers to adopt a conformation that disfavors tubulin incorporation.

3.2.2 Tyrosination/detyrosination

The α-tubulin subunit of microtubules undergoes a cycle of tyrosination and detyrosination. The enzyme responsible for the removal of this gene-encoded tyrosine (tubulin carboxypeptidase, TCP) is yet unknown, while the enzyme responsible for the religation of the end-terminal tyrosine when this has been clipped-off is the tubulin tyrosine ligase (TTL). TTL was the first tubulin-modifying enzyme to be identified and purified from brain tubulin (Raybin and Flavin, 1977; Schröder *et al.*, 1985). Both forms of tubulin, with and without the tyrosine, are present in most cells. Tyrosinated tubulin is often enriched in more dynamic MTs, whereas detyrosination by TTL is associated with more stable MTs (Wehland and Weber, 1987) (**Figure 1.14**).

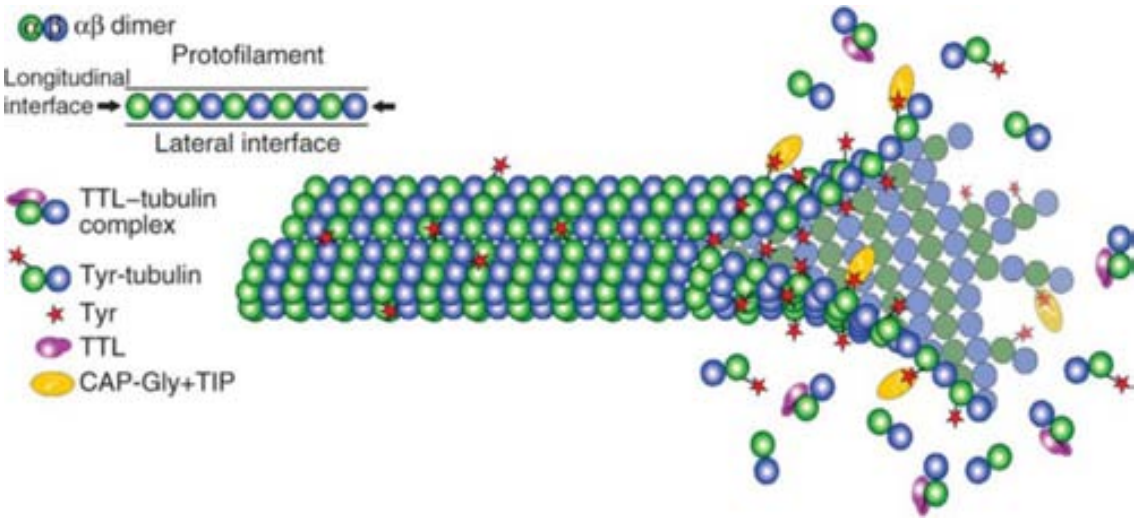

Figure 1.14. Model of action of the TTL on microtubules
TTL acts preferentially on the soluble tubulin pool, whereas detyrosination takes place on the microtubules. For the re-tyrosination process, TTL binds to the α/β-tubulin heterodimer. The TTL-tubulin complex is not favorably incorporated to the microtubule lattice. TTL tyrosinates α/β-tubulin subunits in the soluble form. The newly tyrosinated tubulin is then incorporated at the plus end tip of the microtubule lattice (right), generating an asymmetry that leads to recruit specific proteins sensitive to tyrosinated tubulin (e.g CAP-Gly+TIPs). Source: (Szyk *et al.*, 2011).

TTL works exclusively on soluble α-tubulin-β-tubulin dimers (Raybin and Flavin, 1977) (**Figure 1.14**) while TCP is believed to prefer tubulin in the polymerized state (Kumar and Flavin, 1981). The crystal structure of TTL in complex with tubulin demonstrated that TTL binds to α- and β-tubulin in a so-called curved conformation, acting specifically on the C-terminal tail of α-tubulin, in the tyrosination reaction (Prota *et al.*, 2013).

Posttranslational removal of tyrosine from α-tubulin was first observed in 1977 (Hallak *et al.*, 1977). TCP is known to bind microtubules in living cells and *in vitro* (where the enzyme remains bound throughout several cycles of assembly and disassembly) (Arce and Barra, 1983; Contín *et al.*, 1999), and its activity on MTs is regulated by phosphatase 1 and 2A (Contín *et al.*, 2003). Despite the efforts, the identity of the enzyme is not yet identified, but some of its properties were determined. When compared with pancreatic CPA, TCP seems to be insensitive to inhibition by EDTA (Webster *et al.*, 1992), suggesting that TCP is not a MCP. Further TCP seems to be specific for tubulin, as it barely removes the C-terminal tyrosine from EB1, which contains the C-terminal motif EEY like α-tubulin (Bosson *et al.*, 2012).. Recently, a member of the cytosolic carboxypeptidase family (CCP), agbl2/CCP2 was suggested to display TCP activity based on indirect tests (Sahab *et al.*, 2011). This thesis rules this possibility out and suggests that the hunt for TCP is still open.

The presence of a C-terminal tyrosine has a positive effect on microtubules by recruiting stabilizing factors and affecting the binding of destabilizing MAPs. Consistent with this, tubulin tyrosination is necessary for the binding of MT plus end tracking proteins such as cytoplasmic linker proteins (CLIP) 170 and 115 or $p150^{Glued}$ at the plus-tip of microtubules (Peris *et al.*, 2006) (**Figure 1.14**). On the other hand, the removal of the C-terminal tyrosine in fibroblasts inhibits MT disassembly by reducing the affinity of depolymerizing motors such as the kinesin-13 family motors MCAK (mitotic centromere-associated kinesin) or KIF2A (kinesin heavy chain member 2A) (Peris *et al.*, 2009) and promotes the accumulation of a stable subpopulation of MT, a process that is consistent with cytoskeletal/cell differentiation. A higher depolymerizing activity of kinesin-13 on tyrosinated microtubules was confirmed recently by *in vitro* studies (Sirajuddin *et al.*, 2014). In the same line, in rat hippocampal neurons, tyrosinated

tubulins that are abundant in somatodendrites prevent the wild-type kinesin-1 from binding to MTs (Konishi and Setou, 2009). Moreover, TTL activity is suppressed during tumor growth pointing out that this enzyme may have a role in tumor cell regulation (Lafanechère *et al.*, 1998).

The composition and distribution of modified MTs change along morphogenesis associated with polarization. Two-dimensionally spread cells contain more detyrosinated MTs located towards the leading edge, while three dimensionally polarized cells have more acetylated MTs towards the apical region (Quinones *et al.*, 2011). Detyrosinated tubulin has been reported in MT-based protrusions that would promote reattachment in suspended mammary epithelial cells. Hence, detyrosination could have a role in spreading breast cancer metastasis (Whipple *et al.*, 2007). While each PTM is separately associated with a function and may cause a moderate effect, the combination of PTMs can increase the response, such as such as detyrosination and acetylation on kinesin-1 motility (Kaul *et al.*, 2014). In summary, tubulin tyrosination arises a key player in morphogenesis, axonal function and tumor growth.

3.2.3 Δ2- and Δ3-tubulin

α-Tubulin can display two other PTMs at its C-terminus. The C-terminus of detyrosinated α-tubulin (-GEE) can suffer the removal of the penultimate glutamic acid, generating a form of tubulin known as Δ2-tubulin (-GE) (Paturle-Lafanechère et al., 1991; Lafanechère and Job, 2000). Δ2-tubulin is regarded as a non retyrosinable form of α-tubulin that is found in extremely stable MTs (Paturle-Lafanechère *et al.*, 1994). TTL shows no activity towards Δ2-tubulin *in vitro* (Rüdiger *et al.*, 1994) and the *Ttl* knockout (KO) mice has no compensatory activity to avoid the accumulation of Δ2-tubulin (Erck *et al.*, 2005).

The responsible enzymes described to generate Δ2-tubulin are members of the cytosolic carboxypeptidases subfamily, namely, CCP1, CCP4, CCP5 and CCP6 in human and mouse (Rogowski *et al.*, 2010; Berezniuk *et al.*, 2013a). In *C. elegans*, a small population of axonal MTs is maintained in an unstable state by MT-depolymerizing kinesins. Axonal injury triggers downregulation of those kinesins and upregulation of

growing MTs locally to the axon tip. In a second phase of regrowth, *C. elegans* cytosolic carboxypeptidase 6 (CCPP-6) is required for stabilizing MTs growth through Δ2-tubulin generation (Ghosh-Roy *et al.*, 2012).

Recently, the removal of an additional glutamic acid was shown to generate another form of tubulin named Δ3-tubulin (-G), identified in assays with tubulin and purified CCP1 and CCP5 (Berezniuk *et al.*, 2012, 2013a). Whether Δ3-tubulin is an artifact or has biological implications remains to be elucidated.

3.2.4 Polyglutamylation

Polyglutamylation is a reversible PTM, consisting of the addition of several lateral glutamic acid residues as a linear side-chain, using a glutamic acid in the primary sequence as the insertion point (Eddé *et al.*, 1990; Janke *et al.*, 2008). Therefore, the addition of the branching point consists in a ligation reaction of a Glu to the γ-carboxyl of an internal Glu in the protein (in tubulin this site is close to the C-terminus). Both, the branching point Glu and the Glu residues that elongate the side-chain are added by enzymes from the TTL-like (TTLL) family, that share a core domain with TTL (Janke *et al.*, 2005a; van Dijk *et al.*, 2007) (**Figure 1.15**).

In mammals, there are seven confirmed polyglutamylases: TTLL1, TTLL4, TTLL5, TTLL6, TTLL7, TTLL11 and TTLL13. Some TTLLs (TTLL4, TTLL5 and TTLL7) are specific initiators, adding the initial branching point, while others (TTLL1, TTLL6, TTLL11 and TTLL13) preferentially elongate the chain (van Dijk *et al.*, 2007). Similarly, the reverse reaction is performed by members of the cytosolic carboxypeptidase family, where CCP5 is specific for the removal of the branching point, and CCP1, CCP4, and CCP6 shorten the acidic side-chain (**Figure 1.15**), in addition to the previously described role in the generation of Δ2-tubulin (Rogowski *et al.*, 2010).

Besides tubulin, other substrates of glutamylases and deglutamylases have been described. TTLL4 glutamylase can add glutamic acid side-chains to nucleosome assembly proteins 1 and 2 (NAP1 and NAP2) (Janke *et al.*, 2005a; Van Dijk *et al.*, 2008). Likewise, deglutamylases can cleave the Glu from the acidic C-terminal of myosin light chain kinase and telokin (Rogowski *et al.*, 2010).

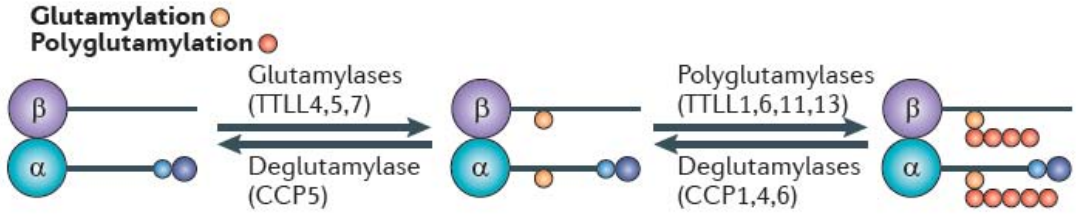

Figure 1.15. Enzymatic machinery involved in glutamylation and deglutamylation
The generation of polyglutamylation in mouse and human starts with the addition of a branching glutamate on both α- and β-tubulin by the initiation enzymes (TTLL4, 5 and 7). The elongation of the chain is carried out by TTLL1, 6, 11 and 13. The reverse reaction involves deglutamylases that remove chains of glutamic acids linked by peptide bonds (CCP1, 4 and 6) while CCP5 is the only deglutamylase able to cleave the γ-linked glutamate. CCP, cytosolic carboxypeptidase; TTLL, tubulin Tyr ligase-like. Source: (Janke and Bulinski, 2011).

PTM patterns together with tubulin isotypes have been suggested to form the tubulin code (Verhey and Gaertig, 2007; Janke, 2014). Polymodifications like polyglutamylation or polyglycylation can encode a gradual set of signals based on different specific patterns. The parameters that would define these patterns are distinct: (i) the density of polyglutamylated tubulin heterodimers within a single microtubule, (ii) the choice between α- and β-tubulin subunits and between isotypes, (iii) the length of the glutamate chains, and (iv) the specific sites of the C-terminal tail that allocate the modifications. Combinations of these parameters (*e.g* density and length of polyglutamylation, tubulin subunit and isotypes) can lead to different MT tracks. Accordingly, TTLL enzymes discriminate between α- and β-tubulin showing different preferences (Regnard *et al.*, 1999; van Dijk *et al.*, 2007).

In most proliferating mammalian cells, interphasic MTs are glutamylated at a low level, and it is only during mitosis, that spindle MTs show an increased level of β-tubulin-specific polyglutamylation (Regnard *et al.*, 1999; Verhey and Gaertig, 2007). And while the mitotic spindle and midbody contain short glutamylated lateral chains, polyglutamylated long chains are found in the centrioles and basal bodies. Also, the axoneme of cilia and flagella are polyglutamylated. In neurons, most MTs are typically modified with side-chains of 1 to 6 glutamate residues (Janke and Bulinski, 2011). Experimental data suggest that several neuronal MAPs and kinesins bind preferentially

to polyglutamylated tubulin (Bonnet *et al.*, 2001), which has been further confirmed by recent *in vitro* studies (Sirajuddin *et al.*, 2014), that showed that kinesin-2 processivity on MTs is significantly enhanced by polyglutamylation. This modification also induces microtubule severing by recruitment of spastin (Lacroix *et al.*, 2010). In the mouse model of *Purkinje cell degeneration* (*pcd*) caused by a mutation in *Nna1* gene (coding for the CCP1 deglutamylase), neuronal degeneration has been linked to microtubule hyperglutamylation (Rogowski *et al.*, 2010).

Localization studies of recombinant GFP-tagged TTLLs in cilia have shown preference of TTLL1, TTLL9 and TTLL11 to basal bodies whereas TTLL5, TTLL6 and TTLL7 localize along the ciliary axoneme (Janke *et al.*, 2005a; van Dijk *et al.*, 2007). In several organisms, polyglutamylases are necessary for coordinating the beating behavior of cilia.

In *Ttll1* KO mice, the axonemal intrinsic curvature (necessary for effective strokes) and beating asymmetry are lost in tracheal cilia, causing mucus accumulation and coughing (Ikegami and Sato, 2010; Vogel *et al.*, 2010). Studies in neuronal PC12 cells has shown that TTLL7 could have a specific role in the growing of MAP2-positive neuritis in the nervous system (Ikegami *et al.*, 2006). Similarly, TTLL6, an α-tubulin-specific polyglutamylase, has been shown to be an important regulator of the beating of brain ependymal cilia. Notably, TTLL6 cannot be replaced by any of the other glutamylases expressed in these cells (Bosch Grau *et al.*, 2013). On the other hand, hyperglutamylation can lead to impairment of MT-based structures. In *Tetrahymena*, overexpression of the side-chain elongating enzyme Ttll6Ap caused contrary effects in different MT populaitons of the same cell: stabilization of cytoplasmic MTs and destabilization of axonemal MTs of the cilia (Wloga *et al.*, 2010).

As for the enzymatic machinery, certain members of the TTLL-family and certain carboxypeptidases of the CCP subfamily would respectively generate and reverse polyglutamylation. While few is known about the remaining CCP2 and CCP3, the rest of the TTLLs are dedicated to the addition of Gly residues, generating another PTM named polyglycylation.

3.2.5 Polyglycylation

Glycylation and polyglycylation is a PTM consisting of the addition of glycine residue(s) on proteins as a lateral chain that is inserted into a gene-encoded Glu residue. This modification was first identified by mass spectrometry in *Paramecium* axonemal α- and β-tubulin (Redeker *et al.*, 1994). While glutamylation is found in several microtubule populations, glycylation is mainly restricted to the axoneme of motile cilia and flagella. However, cytoplasmic tubulin of *Paramecium* show low levels of polyglycylation and shorter chains (1-5 Gly units for α- tubulin and 2-9 for β-tubulin) compared to up to 34 Gly residues-length in axonemal MTs (Redeker *et al.*, 1994; Bré *et al.*, 1998; Vinh *et al.*, 1999).

Tubulin glycylases are also members of the TTLL family. Three enzymes have been identified in mammals, less numerous than the glutamylases (Rogowski *et al.*, 2009). Two initializing ligases, TTLL3 and TTLL8, catalyse the ligation of the first Gly to a Glu of the modified protein (**Figure 1.16**). Only one polyglycylase is known, TTLL10, which can elongate the side-chain by adding Gly residues (Ikegami *et al.*, 2008; Ikegami and Setou, 2009). In tubulin, four different Glu sites can allocate polyglycylation near the C-terminus (Vinh *et al.*, 1999).

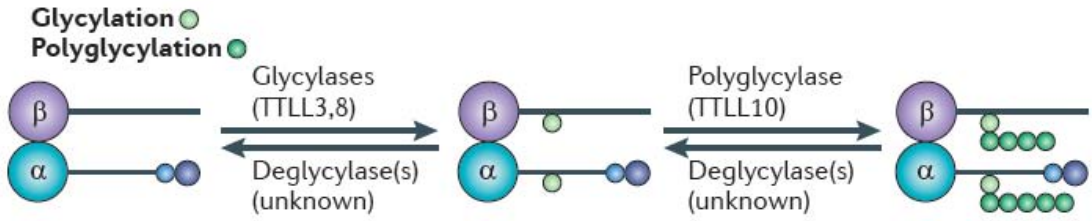

Figure 1.16. Enzymatic machinery participating in glycylation and deglycylation
The generation of polyglycylation in mouse and human is initiated by the addition of branching glycine chain on both α- and β-tubulin by the initiation enzymes TTLL3 and TTLL8. The elongation of the chain is carried out by TTLL10. The enzymes responsible for the reverse reaction remain to be discovered. Source: (Janke and Bulinski, 2011).

Studies in different organisms indicate the importance of glycylation in ciliary assembly and the potential of this PTM in modifying other substrates. Mouse TTLL3 displays a strict tubulin preference whereas TTLL8, the other initiator, is able to

additionally modify other substrates: ANP32A, ANP32B, SET, RanGAP, and nucleolin. In contrast, in *Drosophila* the two TTLL3/8 group gene products can act bifunctionally as initiating and elongating enzymes. Relatedly, polyglycylation was lost in human sperm by the introduction of mutations in TTLL10, therefore the same function has to be held only by monoglycylation (Rogowski *et al.*, 2009). Those two examples illustrates that those enzymes changed or lost function through evolution.

The importance of glycylation in cilia assembly was assessed in zebrafish, where the loss of TTLL6 function displayed only mild defects on motility and ciliary ultrastructure. However, the co-depletion of *Ttll6* and *Ttll3* caused near complete loss of cilia motility and induced a variety of axonemal ultrastructural defects (Pathak *et al.*, 2011). Recent studies on mouse brain ependymal cilia showed that TTLL3 and TTLL8 are required for the stability and maintenance of these motile cilia, as depletion of *Ttll8* in *Ttll3* KO mice led to complete loss of motile ependymal cilia (Bosch Grau *et al.*, 2013).

Two deglycylating enzymes from the metallopeptidase M20C subfamily were discovered in *Giardia duodenalis,* termed gDIP1 and gDIP2 (giardial dipeptidase 1 and 2) (Lalle *et al.*, 2011). gDIP1 and gDIP2 are able to deglycylate tubulin *in vitro* and *in vivo*. Genes encoding for M20C peptidases have been identified so far in the genome of Bacteria, Archaea and in the protozoans *G. duodenalis*, *Trichomonas vaginalis*, and *Entamoeba dispar* (Rawlings and Salvesen, 2013). No member of this subfamily of carboxypeptidases has been identified in mammals so far.

4 Cytosolic carboxypeptidases

This thesis describes the study of the specificity and function of two new tubulin modifying enzymes, belonging the most recently discovered subfamily of MCPs (Kalinina *et al.*, 2007; Rodriguez de la Vega *et al.*, 2007). These are CCP2 and CCP3, poorly studied members of the cytosolic carboxypeptidase subfamily.

CCPs were first described to localize in the cytosol, based on localization studies using recombinant enzymes (Kalinina *et al.*, 2007), and for this reason they were called cytosolic carboxypeptidases. However, the study of the endogenous enzymes in

mammalian cell lines indicate that they also display a nuclear/nucleolar localization and that CCPs are present at the Golgi apparatus, at the axoneme of primary cilia and mitotic spindle in cell division (Rodríguez de la Vega Otazo *et al.*, 2013). These enzymes present a wide taxonomic distribution, as CCPs can be found in Bacteria, Protista, Animalia, Fungi or Plantae, but are absent in Archaea (Rodríguez de la Vega Otazo *et al.*, 2013). The number of paralogs is variable among species, ranging from 1 gene in Fungi (chytrids) or 1-2 genes in Proteobacteria to 6 genes in frogs, birds and mammals. Remarkably, in ciliated protozoan like *Paramecium tetraurelia* up to 32 CCP genes can be found.

CCPs constitute the proposed MCP subfamily M14D according to MEROPS classification system. The six CCP genes/proteins in human and mouse genomes are named *Agtpbp1*/CCP1 to *Agbl4*/CCP6 as detailed in **Table 1.4** (Kalinina *et al.*, 2007; Rodriguez de la Vega *et al.*, 2007).

Table 1.4. Gene and protein symbols of mouse and human CCPs

M14D clusters	Mouse gene symbols	Human gene symbols	Protein symbols
M14D3 CCP1/CCP4	*Agtpbp1, Nna1*	AGTPBP1, NNA1	CCP1, AGTPBP1, NNA1
	Agbl1	AGBL1	CCP4, AGBL1
M14D4 CCP2/CCP3	*Agbl2*	AGBL2	CCP2, AGBL2
	Agbl3	AGBL3	CCP3, AGBL3
M14D2 (CCP6)	*Agbl4*	AGBL4	CCP6, AGBL4
M14D2 (CCP5)	*Agbl5*	AGBL5	CCP5, AGBL5

4.1 Structural domains of CCPs

Reflected in CCP6 as model CCP, all CCPs share two common features, the carboxypeptidase catalytic domain (homologous to bCPA) and its adjacent N-terminal conserved domain (N-domain) (**Figure 1.17**). Additionally to the core N- and

carboxypeptidase domains, CCPs display variability in terms of protein length and domain composition that reflects their evolutionary relationship (**Figure 1.17**). CCP1 and CCP4 cluster together and share an armadillo-like (Arm) domain at the N-terminus that could be implicated in protein/protein or protein/nucleic acid interaction. CCP1 and CCP4 also share a second domain (previous to the N-domain) and a short sequence at the protein C-terminus. Similarly, CCP2 and CCP3 cluster together and they are similar in sequence and domain composition, with extra C-terminal and N-terminal domains. CCP5 differs from other CCPs by a long extension at its C-terminus and two insertions (of 20 and 80 resudues in length) in the carboxypeptidase domain, just before the zinc-anchoring motifs (Rodriguez de la Vega *et al.*, 2007). CCP6 represents the basic core of a CCP, being the shorter CCP in size and only exceeding both the N- and carboxypeptidase domains with short sequence extensions at the edges (**Figure 1.17**).

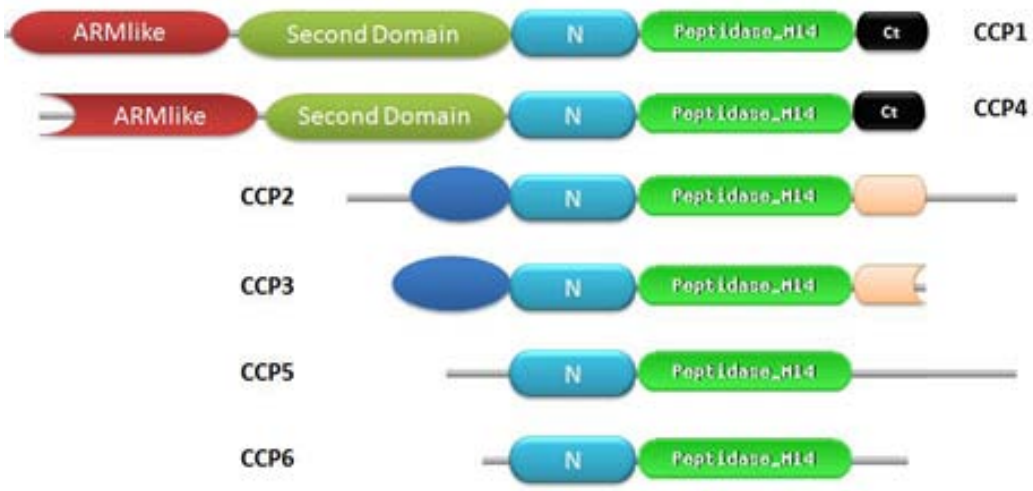

Figure 1.17. Schematic representation of the domain composition of mouse and human CCPs
The core domains of CCPs are the carboxypeptidase catalytic domain (peptidase_M14, green) and the characteristic conserved N-domain (light blue). Arm represents an armadillo-like domain (red) and the other represented domains are poorly defined, displaying no homology with known domains.

The carboxypeptidase catalytic domain exhibits a similar topology of secondary structure elements with M14A and M14B members (*e.g.* bCPA and CPN, respectively), despite the low sequence identity. Contrarily, the N-domain of 150 residues is

characteristic of CCPs and differs from extra domains present in other M14 subfamilies; *i.e.* the transthyretin-like C-terminal domain of M14B MCPs (*e.g.* CPE, CPD) and the N-terminal activation region or prodomain in M14A members (*e.g.* CPA1, CPA4), which needs to be cleaved to generate the active form of the enzyme.

4.1.1 Crystal structure of CCPs

Recently, the structure of a CCP from *Pseudomonas aeruginosa* (PaCCP) was solved (PDB 4a37) (Otero *et al.*, 2012), showing that the N-domain comprises a novel β-sandwich fold and that the carboxypeptidase catalytic domain is shorter and more compact, when compared to similar domains in classic MCPs (**Figure 1.18**).

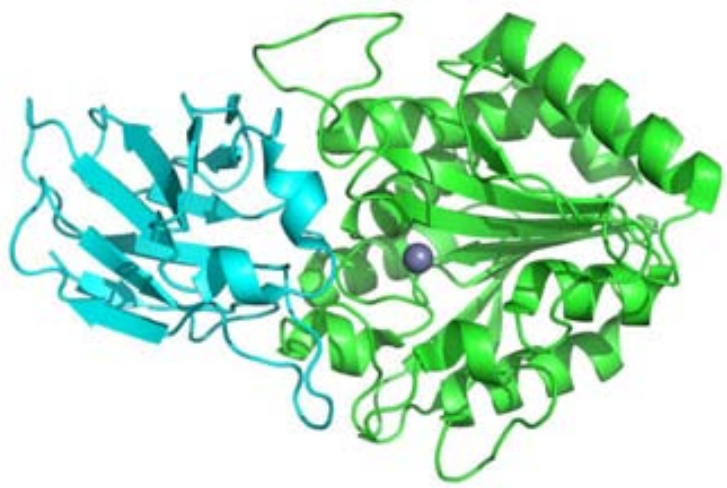

Figure 1.18. Structural representation of *Pseudomonas aeruginosa* CCP
Structural representation of Pseudomonas aeruginosa at 1.6 Å resolution (PDB 4a37). The N-domain folds in a β-sandwich structure (light blue) and the carboxypeptidase catalytic domain display the classical α/β-hydrolase structure (green). Image of structures were generated with PyMOL 1.3.

Two additional structures of CCPs from bacterial origin are currently available the PDB: *Burkholderia mallei* (PDB 3k2k) and *Shewanella denitrificans* (PDB 3l2n). Despite only minor changes in the entrance of the active site were observed in all cases, no hydrolytic function has been assessed for these enzymes so far. PaCCP lacks activity against small carboxypeptidase synthetic substrates or purified brain tubulin (Otero *et al.*, 2012).

4.2 CCP1 and the *pcd* mouse model

The most studied member of this subfamily is CCP1, also named NNA1 (from Nervous system nuclear protein induced by axotomy) or AGTPBP1 (from ATP/GTP-binding protein 1) from the name of the genes coding for CCP1, which are *Nna1* or *Agtpbp1*. The transcript coding for CCP1 is highly expressed after damage at spinal motor neurons, during axogenesis and axon reinervation (Harris *et al.*, 2000). Moreover, in recessive *Nna1* mutant mice –known as *pcd* (Purkinje cell degeneration) mouse– Purkinje cells, selected thalamic neurons, retina photoreceptors and mitral neurons in the olfactory bulb degenerate, and the mouse display defective spermatogenesis (Landis and Mullen, 1978; Fernandez-Gonzalez *et al.*, 2002). As a consequence, *pcd* mouse is characterized by an ataxic phenotype that appears at postnatal day 21, with de-coordinated movement showing awkwardness when ambulation. By 4 weeks of age *pcd* mouse presents pronounced gait ataxia that becomes severe at 6 weeks and remains without further progression. At a cellular level, Purkinje cell degeneration in *pcd* mice is characterized by dendrite retraction and shrinkage (Chakrabarti *et al.*, 2009). Recently, hierarchical clustering of microarray data analysis has shown that *Nna1* could be associated with Alzheimer's disease (Guttula *et al.*, 2012).

4.2.1 Hyperglutamylation

Recently CCP1 has been linked to deglutamylating function and the lack of this enzyme has been associated with hyperglutamylation (Rogowski *et al.*, 2010). Genetic targeting of CCP1 can rescue Purkinje cells in *pcd* mice, whereas a punctual mutation in the catalytic Glu1094 of CCP1 (residue equivalent to the Glu270 of bCPA) prevent CCP1 to process the polyglutamylated side-chains of tubulin (Wu *et al.*, 2012). In this line, the lack of the neuronal specific TTLL1 counteracts the hyperglutamylation in *pcd* mouse brain, as the double mutant mice for *Nna1* and *Ttll1* rescues the phenotype (Berezniuk *et al.*, 2012). Loss of CCP1 homolog, CCPP-1, in *C. elegans* ciliated sensory

neurons also causes degeneration by increasing the levels of polyglutamylation of sensory cilia (Kimura *et al.*, 2010). CCPP-1 activity evidences to be required for ciliary maintenance but not ciliogenesis and the affected cilia exhibit defective MT structure in the B-tubules of the axoneme.

4.2.2 Neuronal death of the Purkinje cells

Prior to neuronal death, Purkinje cells of *pcd* mice do not activate apoptosis but undergo autophagy and mitophagy (*i.e.* autophagy of mitochondria). Altered mitochondria morphology, endoplasmic reticulum histopathology and autophagosome engulfment of mitochondria were observed by ultrastructural analysis of Purkinje cell soma. This increase of aberrant mitophagy could contribute to Purkinje cell degeneration in *pcd* mice (Chakrabarti *et al.*, 2009). Accordingly, proteomic and localization analysis in the CCP1 ortholog mutant flies and *pcd* mice have revealed a role of CCPs in bioenergetics and mitochondrial functions (Chakrabarti and Zahra, 2010).

A fraction of CCP1 localizes to the nucleus, as observed by Rodriguez *et al.* in human HeLa cells (Rodríguez de la Vega Otazo *et al.*, 2013). CCP1 shuttles between the nucleus and the cytoplasm, mediated by a functional nuclear export signal (NES) in CCP1 that directly binds to the nuclear export receptor CRM1 (Thakar *et al.*, 2013). Consistent with a role of CCP1 in the nucleus, the *pcd* mutation has been shown to induce the formation of DNA damage/repair foci in mitral cells of the olfactory bulb. These DNA alterations associate with transcriptional inhibition, heterochromatinization, nucleolar segregation and the reorganization of nuclear speckles and Cajal bodies. In nuclear speckles, pre-mRNA splicing factors are assembled and stored, while Cajal bodies are nuclear organelles involved in biogenesis of small ribonucleoproteins (Valero *et al.*, 2006). Analyses of histones of the *pcd* mouse have identified epigenetic hallmarks of chromatin reorganization in degenerating Purkinje cells genome and gene silencing linked to defective DNA repair (Baltanas *et al.*, 2011).

4.3 Deglutamylases in the CCP family

The functions of four of the six cytosolic carboxypeptidases (CCPs) have been recently studied in detail. CCP1, CCP4 and CCP6 not only remove glutamate residues from the C-terminus of posttranslationally added polyglutamate side-chains, but also from the gene-encoded tubulin C-terminus to generate Δ2-tubulin (Rogowski *et al.*, 2010; Berezniuk *et al.*, 2012). CCP5 is also a deglutamylase and it is the only CCP described to efficiently remove the γ-linked glutamate residue that acts as branching point of the polyglutamate side-chains. Purified CCP5 assays demonstrate its ability to cleave α-linked glutamic acids but it presents higher preference for the γ-linked (Berezniuk *et al.*, 2013a). Distinctively, CCP2 has been suggested to act as tubulin tyrosine carboxypeptidase, removing the C-terminal tyrosine from α-tubulin (Sahab *et al.*, 2011) but other groups failed in reproducing this result. Thus, further studies are needed on CCP2. Besides, the only member of the CCP subfamily that remains uncharacterized is CCP3.

4.3.1 CCPs in pathologies

To date, no mutations within the human CCP1-CCP6 protein orthologs were correlated with specific ataxic syndrome reminiscent of the *pcd* mouse (Baird and Bennett, 2013). However, two different missense mutation alleles of *AGBL1* (CCP4), leading to a premature termination of CCP4, have been associated with Fuchs corneal dystrophy (FCD), a genetically heterogeneous disorder of the corneal endothelium, where CCP4 is expressed. Recombinant expression of the pathogenic form of truncated CCP4 in HEK293T cells show nuclear localization instead of the wild-type cytoplasmic setting (Riazuddin *et al.*, 2013). Moreover, several human deficiencies have been genetically mapped to the regions comprising CCPs (**Table 1.5**). In sheep, a mutation in AGTPBP1 catalytic domain has been identified, displaying a lower motor neuron disease that correlates with the *pcd* mouse phenotype. These sheep are born normal and develop weakness and quadriplegia after the first week of life (Zhao *et al.*, 2012).

Table 1.5. Human conditions of unknown cause that map to defined genetic regions encompassing CCPs

Condition	OMIM	Band Interval	Encoding gene	Alternative name
Spastic Paraplegia-19	607152	9q33-q34	*AGTPBP1, NNA1*	CCP1
Spastic Paraplegia-41	613364	11p14.1-p11.2	*AGBL2*	CCP2
Spinocerebellar ataxia-32	613909	7q32-q33	*AGBL3*	CCP3
Primary ciliary dyskinesia-8	612274	15q24-q25	*AGBL1*	CCP4
Essential hereditary tremor-2	602134	2p25-p22	*AGBL5*	CCP5
Dystonia-9: episodic ataxia & spasticity	601042	1p33	*AGBL4*	CCP6

Adapted from (Baird and Bennett, 2013)

4.3.2 CCPs regulation and interaction partners

Many proteases require activation by cleavage of its prodomain, by a change in the pH, by liberation or exposure to the right cellular compartment; and may be inactivated by proteolytic degradation or by specific inhibitors. CCPs are synthesized as active proteases and found in the cytosol or nucleus of the cells (Kalinina *et al.*, 2007; Rodríguez de la Vega Otazo *et al.*, 2013). The presence of free proteases in the cytosol must require highly regulated mechanisms to avoid degradation of non-desired substrates.

Little is known about the regulation or the protein complexes allocating CCPs other than the likely interaction with tubulin given the function of CCPs in cleaving tubulin PTMs, but other potential substrates are emerging showing a putative role of CCPs in the nucleus (Tanco *et al.*). Not only different substrates and novel compartment allocation, but also interacting partners of CCPs might give insight in how these proteases are regulated. Biochemical interaction has been shown for CCP4/AGBL1 with a protein involved in Fuchs corneal dystrophy (FCD), the FCD-

associated protein transcription factor 4 (TCF4). In FCD, a mutated form of CCP4 has been found to diminish this interaction, possibly contributing to the disease pathogenesis (Riazuddin *et al.*, 2013). Similarly CCP2/AGBL2 was detected by interactomic techniques as interacting partner for the retinoic acid receptor responder 1 (RARRES1), a membrane protein downregulated in cancer that is homologous of the carboxypeptidase inhibitor latexin (Sahab *et al.*, 2011). While TCF4 was hypothesized being a substrate of CCP4 (Riazuddin *et al.*, 2013), RARRES1 (or latexin) might rather be an inhibitor of CCPs (although no consistent data has been published so far) (Sahab *et al.*, 2011; Zhang *et al.*, 2014). Upregulation of *CcnB3*, a meiosis-related cyclin, was found in *pcd* mice. This upregulation and the similarities between the testicular phenotype of *Ccnb3* KO mice and that of *pcd* mice has led to suggest that CCNB3 could interact with CCP1 (Kim *et al.*, 2011). In brief, RARRES1 and CCNB3 are two putative interactors/regulators of CCPs but little is known about interactomics in the field of CCPs so far.

4.4 CCPs and axoneme of cilia and flagella

Some CCPs are described to function as tubulin deglutamylases (*i.e.*, shorten the length of glutamate side-chains) (Rogowski *et al.*, 2010). Besides, CCPs have been phylogenetically inferred to present a remarkable correlation with cilia and basal bodies, which are microtubular organelles that perform critical physiological and developmental processes (Rodríguez de la Vega Otazo *et al.*, 2013). CCP5 -but not CCP2 or CCP6- knock-down perturbs cilia motility in zebrafish and induces typical ciliopathy phenotypes, including hydrocephalus, pronephric cysts and axis curvature (Pathak *et al.*, 2014).

Whether CCP1 could display a mild but similar phenotype as CCP5 remains controversial (Lyons *et al.*, 2013; Pathak *et al.*, 2014). Quantitative peptidomics of adult brain of the *pcd* mice revealed altered peptides derived from secretory pathway proteins, being the pattern of peptides comparable to the ones found in mice lacking primary cilia (Berezniuk *et al.*, 2013b).

4.4.1 Male infertility and CCP disfunctions

Several mutations in *Nna1* gene have been described leading to similar reduction of Nna1 expression and equivalent *pcd* phenotypes. Severe alleles of *pcd* mice exhibit abnormal sperm development and male infertility. Sperm is abnormal in shape, with defects including abnormal and vacuolated heads, no heads, and abnormal midpieces and tails (Mullen *et al.*, 1976). Contrarily to the other Nna1 mutations, pcd^{2J} males are fertile. The reduced level of *Nna1* mRNA may be sufficient to support spermatogenesis in pcd^{2J}, but not in other *pcd* alleles (approximately 20-fold reduction) (Fernandez-Gonzalez *et al.*, 2002).

The pcd mouse is one of the few 21 mouse models of flagellum abnormalities (Escalier, 2006). Immunohistological and gene expression analysis of the pcd mouse have revealed the importance of CCP1 in spermatogenesis and for survival of germ cells at spermatocytes stage onward. Spermatocytes and spermatids from the *pcd* mouse undergo apoptotic death (Kim *et al.*, 2011).

OBJECTIVES

The research group of Prof. Francesc Xavier Avilés at the Institut de Biotecnologia i Biomedicina at the Universitat Autònoma de Barcelona, has for many years focused on structural and functional studies of metallocarboxypeptidases and its inhibitors. One of the latest carboxypeptidase subfamily where the group participated in the discovery and first description is cytosolic carboxypeptidases.

The general objective of this thesis was to elucidate the function of cytosolic carboxypeptidases 2 and 3 (CCP2 and CCP3), the two members of the CCP subfamily poorly characterized. For this purpose, a complete study ranging from *in silico* to *in vivo* approaches was performed.

Specific objectives are outlined in each chapter:

CHAPTER 1

- To structurally model the carboxypeptidase domain of human CCP3 in order to identify the active site amino acid residues that participate in the catalysis.
- To explore the predicted substrate specificity of human CCP3 experimentally and in the context of tubulin posttranslational modifications.
- Evaluation of the activity of the human CCP3 compared to a protein engineered dead version of the enzyme displaying a punctual mutation at the catalytic Glu270.
- To study the interaction between CCPs and microtubules through subcellular distribution along the cell cycle and by copurification approaches.
- To determine the *in vitro* activity of human CCP3 using purified tubulin as substrate and the evaluation of other potential C-terminal acidic protein substrates.

CHAPTER 2

- To predict the substrate specificity of CCP2 through structural modelling and analysis of the active site residues in comparison to CCP3.
- To evaluate the protein domain sequences of the active short 72.6-kDa human CCP3 isoform to settle a strategy to determine the core of CCPs and generate active mouse CCP2 and CCP3
- To generate truncated forms of mouse CCP2 and CCP3 in order to obtain forms of the enzyme with increased and detectable activity.
- To investigate detyrosinating and deglycylating putative activities and determine CCP2 and CCP3 stringency and preference towards acidic substrates.
- To determine the expression profile of the six CCP genes in tissues of wild type mice by qRT-PCR (named *Agtpbp1* and *Agbl1* to *Agbl5* at the gene level).
- To generate CCP2 and CCP3 knockout mice and realize a screen of mouse tissues for polyglutamylation levels compared to wild type mice.
- To generate the CCP2/CCP3 double knockout mouse and examine the polyglutamylated levels in selected tissues.

Chapter II:
Experimental procedures

CHAPTER II: EXPERIMENTAL PROCEDURES

1 Cloning and DNA methods

1.1 Polymerase chain reaction (PCR)

The constructs corresponding to human CCP1 and CCP3 genes were designed for protein production and purification purposes, whereas mouse CCPs and its truncated forms were design for functional studies in mammalian cell lines.

For the protein production strategy, the cDNA of the 72.6 kDa isoform of human CCP3 (Q8NEM8-2, Uniprot) and the cDNA of the human 138.4 kDa CCP1 (Q9UPW5-1, Uniprot) were cloned into pOPINFS expression vector (Berrow *et al.*, 2007). For CCP3, a *Strep*-tag II was introduced at the N-terminus and a hemagglutinin (HA) epitope, at the C-terminus. For CCP1, *Strep*-tag II and HA-tag were both introduced at the C-terminus. In addition, the cDNA of human TRAD1 was cloned in pTriEx-6 expression vector (Novagen) with *Strep*-tag II and HA-tag, both at the N-terminus.

As for the constructs aiming functional studies of the enzymes, the cDNAs encoding for full-length murine cytosolic carboxypeptidase (CCP) and a set of truncated forms were C-terminally fused to Green/Yellow fluorescent protein (GFP/YFP). The primers used to generate each construct and the vectors where the PCR products were inserted are listed in **Table 2.1**.

The PCR reactions were performed with Pwo Master (Roche), using Pwo SuperYield DNA Polymerase following the manufacturer's instructions. Standard cycling conditions were used in the thermocylcer (Mastercycler Pro S, Eppendorf) for each pair of primers. PCR products were checked in an agarose gel for quantity and size. The product of the DNA amplification was purified with a Gel-Extraction Kit (Qiagen) before proceeding to digestion with restriction enzymes.

Table 2.1. Primers used for the cloning of cytosolic carboxypeptidases and their truncated forms

Gene	Vector	Primers Fw/Rev
mCCP1	pcDNA3.1-EYFP	Fw: cgcggagtcgacACCATGAGCAAGCTAAAAGTGGTGGGAGAG Rev: cgccgctgatcaAATCAGGTGTGTTCTTGATACCTCAG
mCCP2	pEYFP	Fw: cgcggactcgagACCATGAATGTCCTGCTTGAGATGGCTTTTC Rev: cgccgcagatctTGGGTATGTGTATATATGCAAGGATGGG
mCCP3	pEYFP	Fw: cgcggactcgagACC ATGTCAGAAGATTCAGAGGAGGAAGAC Rev: cgccgcggatccCTGATGCTGTTGCAAGTTGGCTATC
mCCP3_opt	pEYFP	Synthetic gene optimized for bacterial codon usage (GeneCust).
hCCP3	pOPINFS	Fw: aggagatataccatggctagctggagccacccgcagttcgaaaaa ATGTCAGAAGATTCAGAAAAGGAAGAC Rev: ctagagaactgacatttttattgagaTAAAGCTTTCTAGACCAT
mCCP4	pEGFP	Fw: cgaattctagccATGGCTGAACAAGAAGGCAGT Rev: ctggatccgggagacacagagatgtcac (non coding region)
mCCP5	pEYFPr	Fw: ccgcgactgcagACCATGGAGCTGCGCTGTGGGGGATTGC Rev: ccgcgaggtaccTCCCTCTGCGAGTCGGCGGTGAGC
mCCP6	pEYFP	Fw: cgcggactcgagACCATGGCGGAGCGGAGCCAGACAGCGCC Rev: ccgcagaTCTAAAGGGGGTTGATGGGTCTTTG
mCCP2_N2190	pEYFP	Fw: cgcggactcgagACCATGAATGTCCTGCTTGAGATGGCTTTTC Rev: ccgcggatccGCTCTTCTGGTACTGCTCATTCCG
mCCP2_N1992	pEYFP	Fw: cgcggactcgagACCATGAATGTCCTGCTTGAGATGGCTTTTC Rev: ccgcggatccTAAATCCATATCTTGTCCAAAGTTATTC
mCCP2_Z1703	pEYFP	Fw: cggactcgagACCatgGACTCACTTCTGCTGAGCTCGCC Rev: ccgcggatccTAAATCCATATCTTGTCCAAAGTTATTC
mCCP2_Z1334	pEYFP	Fw: cggactcgagACCatgACACTGCAAGGGCCGGACGAC Rev: ccgcggatccTAAATCCATATCTTGTCCAAAGTTATTC
mCCP2_Z1607	pEYFP	Fw: cggactcgagACCatgGACTCACTTCTGCTGAGCTCGCC Rev: ccgcggatccGTCAGGATCACAGAAATCCAG
mCCP3_N1998	pEYFP	Fw: cggactcgagACCATGAGCGAGGACTCTGAAGAAG Rev: ccgcggatccGTAAACTTCCTGCATATTGTTCTGG
mCCP3_N1809	pEYFP	Fw: cggactcgagACCATGAGCGAGGACTCTGAAGAAG Rev: ccgcggatccGGTATCCGTGTTATCGGAGACGC
mCCP3_Z1670	pEYFP	Fw: cggactcgagACCatgGACCCGTTTTTCCCACGCACCAC Rev: ccgcggatccGGTATCCGTGTTATCGGAGACGC
mCCP3_Z1325	pEYFP	Fw: cggactcgagACCatgGTGGATAACTGCGACAACACCC Rev: ccgcggatccGGTATCCGTGTTATCGGAGACGC
mCCP3_Z1583	pEYFP	Fw: cggactcgagACCatgGACCCGTTTTTCCCACGCACCAC Rev: ccgcggatccGTCCGGGTCGCAGTAGTCCAG

1.2 Digestion with restriction enzymes

The PCR products and cloning vectors were incubated for 2-3h with the appropriate restriction enzymes (Roche and New England Biolabs). In addition, vectors

were dephosphorylated to avoid plasmid recircularization by adding bovine alkaline phosphatase (Roche) to the digestion mix and incubating for additional 30 min. After the incubation, all the reaction mix was loaded on an agarose gel and the digestion bands were cut out on a long wavelength type UV transilluminator and DNA was extracted with the Gel Extraction Kit (Qiagen).

1.3 Ligation and transformation

Digested PCR product and vector are mixed in an approximate molar ratio of 3:1, in a total volume of 10 µl. Thus, 1× ligation buffer and 0.5 µl of T4-ligase (Roche) are added. The reaction is carried out at 16 °C for 1 h and 5 µl of the mixture is directly transformed into competent *Escherichia coli* cells (either XL1Blue or DH5α strains). Heat-shock of 40 s at 42 °C is applied, with previous and posterior incubation on ice. After 30 min recovery in Luria Broth (LB) medium at 37 °C, cells are plated onto LB agar (LA) plates complemented with the appropriate antibiotics.

1.4 Site-directed mutagenesis

Inactive/dead forms of murine CCP2, murine CCP3 and the 72.6 kDa isoform of human CCP3 (Q8NEM8-2, Uniprot) were generated by mutating the catalytic glutamic acid (E) at the active site to a glutamine (Q), using the QuikChange mutagenesis method. The primers used for this purpose are listed in **Table 2.2**.

Table 2.2. Mutagenic primers for mouse cytosolic carboxypeptidases

Gene (mutated amino acid)	Vector	Primers Fw/Rev
mCCP2_E593Q	pEYFP	Fw: GCTACACCATGcAGTCTACCTTTGGC Rev: CAAAGGTAGACTgCATGGTGTAGCTG
mCCP3_E540Q	pEYFP	Fw: CTTTCACCCTGcAAGCAACTTTCTGCG Rev: GAAAGTTGCTTgCAGGGTGAAAGAATTGC
hCCP3_E534Q	pOPINFS	Fw: TACCATGcAGGCCACCTTCTGTGGATCTAC Rev: AGGTGGCCTgCATGGTAAAGCTGTTCCTGA

Briefly, mutagenic primers were mixed at 100 µM with 20 ng of the plasmid template, dNTPs (0.4 mM each) and 0.7 µl of Pfu polymerase (Promega) in the recommended buffer conditions for the DNA amplification step. After 16 rounds of amplification and a final elongation step of 30 min, the product was digested with DpnI for 2 h at 37 °C to remove the template plasmid. The resultant mixture was transformed as described previously and plated in LA plates with the appropriate antibiotics. After plasmid isolation of the selected colonies, the mutation was confirmed by DNA sequencing analysis.

1.5 DNA purification and sequencing

Antibiotic-resistant colonies were grown in LB under antibiotic pressure over-night (ON). Plasmid DNA mini-preparations were performed using standard protocols (home-made solutions or GeneJET Plasmid Miniprep Kit, Thermo Scientific) and clones were evaluated by sequencing analysis (VWR or Macrogen). Midi-preparations of plasmid DNA for transfection into mammalian cells were obtained from 50 ml bacterial culture grown over-night in LB with antibiotic, using the Plasmid Midi-Kit (Qiagen). DNA concentration and purity was assessed using the Nanodrop spectrophotometer (Thermo Scientific).

2 Cell culture

2.1 Cell lines and maintenance

Adherent HEK293T cells, from American Type Culture Collection (ATCC, Rockville), were maintained in Dulbecco's modified Eagle's medium (DMEM, Gibco) supplemented with 10% fetal bovine serum (FBS) and 2 mM Glutamax (Gibco) and incubated at 37 °C with 10% CO_2. The HEK293F cell line (Invitrogen) was grown with FreeStyle 293 Expression Medium (Gibco) at 37 °C with 8% CO_2 under agitation (120 rpm). HepG2 and HeLa cells, from ATCC, were subcultured with Minimum Essential Medium (MEM, Gibco) supplemented with 10% FBS, 2 mM Glutamax and maintained with 5% CO_2 at 37 °C.

2.2 Transfection

HEK293T cultures were transfected or cotransfected after 24 h plating. The transfection reagent used was a 1 μg/ml solution of polyethylenimine, linear (PEI, Polysciences) in a 1:3 DNA:PEI ratio. For cotransfection of CCPs with telokins, a ratio of DNAs CCP:telokin of 5:1 was applied corresponding to 2.5:0.5 μg per 30-mm dish plate. Cultures were collected 48 h after transfection by pipetting up and down with phosphate buffered saline (PBS). HEK293F cell cultures were transfected with 1 μg/ml of pOPINFS-CCP3 DNA with a 1:3 DNA:PEI ratio, after 24 h of being seeded at a density of $0.5x10^6$ cells/ml.

2.3 shRNA analysis

HuSH 29-mer commercial shRNA constructs against CCP3 in PGFP-V-RS vector (OriGene) were used for knock-down assays. A construct codifying a specific CCP3 shRNA (sh72: accaagtattatcggtgcctgaaagaatt) was tested for knock-down effectiveness on CCP3, by co-transfecting 50% confluent HEK293T cultures with CCP3 and the shRNA vectors in a 1:3 ratio of DNA:PEI.

For shRNA clone selection, cultures were trypsinized when plates reached 70-80% confluence and 1 μg/ml puromycin (Invivogen) was applied to the cell cultures every 2-3 days. Transfection efficiency and clone stability were followed by in-vivo fluorescence with an inverted fluorescence microscopy Eclipse (Nikon) and by Western-blotting.

2.4 Cell lysis

Cultures of HEK293F were recovered 72 h after transfection by centrifugation at 400 g for 10 min. HEK293T cell cultures were obtained by pipetting up and down with PBS followed by centrifugation at 400 g for 7 min. Cultures of HepG2 were recovered by scrapping in lysis buffer after a wash in PBS.

Cells were disrupted in repeated freeze/thaw cycles and lysed in 100 mM Tris-HCl, pH 8, 150 mM NaCl and 0.1% NP-40 supplemented with EDTA-free protease inhibitor cocktail Set III (Calbiochem®) and centrifuged for 10 min at 15,000 g at 4 °C. Supernatants were quantified by Bradford assay (Pierce) in a 96-well plate or by absorbance at 280 nm using a Nanodrop spectrophotometer.

3 Protein purification

3.1 Affinity purification with *Strep*-tag

Protein production with purification purposes was performed in HEK293F cells. CCP3 and CCP1 transfected cells were lysed as previously described. The lysate was incubated on ice for 30 min and passed through a 25 G needle (Terumo). Two consecutive centrifugations at 3,000 g for 15 min followed by a final 40 min centrifugation at 40,000 g were performed to clear the lysate. This pre-cleared lysate was filtered through a 0.22 µm filter and applied to an affinity *Strep*-Tactin MacroPrep pre-filled cartridge H-PR column (IBA GmbH) for affinity purification. Unbound proteins were washed with 100 mM Tris-HCl, pH 8, 150 mM NaCl, and CCP3, CCP1 and TRAD1 were eluted with the buffer containing 2.5 mM d-Desthiobiotin. Eluted fractions were analyzed by SDS-PAGE and the purest fractions containing the enzyme were pooled for proteomic studies and *in vitro* activity/inhibition assays.

3.2 Size exclusion chromatography

HepG2 cells were lysed with buffer A (50 mM Tris-HCl, pH 7.5, 150 mM NaCl, 0.1 mM EGTA and 0.1% β-mercaptoethanol complemented with 1 mM sodium orthovanadate (Sigma) and EDTA-free protease inhibitor cocktail Set III. The supernatant was recovered and 2 mg of HepG2 lysate was fractionated on a Sephadex 200 10/300 GL (GE Healthcare) column in buffer A. Fractions were collected, monitored at 280 nm and analyzed by SDS-PAGE electrophoresis followed by immunoblotting.

4 Protein analysis

4.1 1D SDS-PAGE

Conventional SDS-PAGE was performed using standard protocols (*i.e.* for standard and NAP gels) and a specific protocol to resolve tubulin subunits was applied for this purpose (TUB gels). The buffer conditions are detailed in **Table 2.3**. Samples were loaded with previous incubation in 5X Laemmli sample buffer (450 mM DTT, 10% SDS, 400 mM Tris-HCl pH 6.8) for 5 min at 95 °C. In standard gels, DTT was replaced with beta-mercaptoethanol (Sigma).

Table 2.3. Polyacrylamide gels composition

Chemical	Standard		NAP gels		TUB gels	
	Lower	Upper	Lower	Upper	Lower	Upper
Tris-HCl	375 mM (pH 8.8)	125 mM (pH 6.8)	375 mM (pH 8.8)	125mM (pH 6.8)	375mM (pH 9.0)	125 mM (pH 6.8)
SDS	0.1% (pure BDH)				0.1% SDS (Sigma)	
ammonium persulfate (APS, Sigma)	0.05%		0.08%		0.08%	
40% Acrylamide solution (Biorad)	Variable		Supplemented with 1.04% of bisacrylamide		Supplemented with 0.54% of bisacrylamide	

Protein samples were run in an electrophoresis chamber with 1x running buffer. For NAP and standard gels, the running buffer was composed of 25 mM Tris, 192 mM glycine, 0.1% SDS (pure BDH) and deionized water. For TUB gels electrophoresis, the running buffer composition was 50 mM Tris, 384 mM glycine, 0.1% SDS (Sigma) and deionized water.

After the electrophoresis, gels were stained with colloidal Coomassie solution or transferred into membranes by Western blotting.

4.2 2D SDS-PAGE

Two-dimensional electrophoresis consisted of an isoelectric focusing step (IPGphor Isoelectric Focusing System; GE Healthcare) and an SDS-PAGE. For the resolution of CCP3 interactors, the sample was loaded on previously hydrated 7 cm pH 3–10 Immobiline strips (GE Healthcare). Samples were first precipitated (2-D Clean-up kit, GE Healthcare) and then resuspended in the loading buffer (20 mM DTT, 1.4% DeStreak, and 0.5% [v/v] IPG buffer [GE Healthcare]).

4.3 Western-blot

After SDS-PAGE electrophoresis, proteins were transferred onto PVDF membranes (Immobilon-P, Millipore) or nitrocellulose membranes (EMD Millipore) and detected using primary antibodies described in **Table 2.4**.

Table 2.4. Primary antibodies

Antibody name	*Antigen*	*Type*	*Dilutions*			*Provider*
			WB cell lines	***WB tissue extracts***	***immuno cytochemistry***	
12G10	*α-tubulin*	*mouse monoclonal*	*1:1,000*	*1:400*	-	*from J. Frankel, E. M. Nelson, University of Iowa, USA*
anti-β-tubulin	β-tubulin	*mouse monoclonal*	-	-	*1:200*	*Sigma #*T5201
anti-Δ2-tubulin	CEGEEEGE-COOH	*rabbit polyclonal*	*1:5,000*	*1:5,000*	1:1,000	*produced in-house*
anti-deTyr-tubulin	-CGEEEGEE-COOH	*rabbit polyclonal*	*1:2,000*	-	-	*Millipore #*AB3201
polyE	*-CEEEEEEEEE-COOH*	*rabbit polyclonal*	*1:4,000*	*1:10,000*	-	*produced in-house*
polyG	*-CGGGGGGGGG-COOH*	*rabbit polyclonal*	*1:6,000*	-	-	*produced in-house*
anti-GFP	*GFP, YFP, CFP*	*rabbit polyclonal*	*1:5,000*	-	-	Torrey Pines Biolabs, #TP401

Protein bands were visualized with HRP-labeled donkey anti-rabbit (1:10,000; GE Healthcare) or goat anti-mouse (1:10,000; GE Healthcare) followed by detection with chemiluminescence (ECL Western blot detection kit from GE Healthcare or Immobilon Western Chemiluminiscent HRP substrate from Millipore).

5 Confocal microscopy

5.1 Cell fixation with preservation of microtubule structure

For immunofluorescence, HEK293T or HeLa cells were seeded onto culture dishes and transfected after 24 h plating as described before. After 12 h, cells were trypsinized and plated onto sterile glass coverslips in 6-well plates (Nunc) and incubated for 24 h before fixation. A fixation method to preserve microtubule structure was applied (Bell and Safiejko-Mroczka, 1995). In brief, cells were incubated 10 min at room temperature in 1 mM DSP (dithiobis[succinimidyl propionate]) in Hank's balanced salt solution (HBSS) followed by incubation for 10 min with 1 mM DSP in microtubule-stabilizing buffer (MTSB). Cells were washed in PBS for 5 min with 0.5% Triton X-100 in MTSB before fixation with 4% paraformaldehyde (PFA) in MTBS. This step was followed by 5 min wash in PBS, 5 min wash in PBS containing 100 mM glycine and a final wash in PBS.

5.2 Immunocytochemistry

Following fixation, cells were washed for 5 min in PBS containing 0.1% Triton X-100 and then incubated with primary antibodies with 0.1% Triton X-100 and 2% bovine serum albumin (BSA; Sigma) in PBS for 1 h at room temperature. Next, cells were washed 4 times with PBS 0.1% Triton X-100 followed by 1 h incubation with anti–rabbit Alexa Fluor 568 and anti–mouse Alexa Fluor 350 (Invitrogen) in PBS containing 0.1% Triton X-100. Washes were performed before coverslips were mounted with ProLong Gold (Life Technologies).

Immunofluorescence images were collected on an inverted confocal microscope (Leica SP5) and a 63X objective at 25 °C. Images were analyzed using LAF AS Lite 1.8.1 (Leica) and composed in Illustrator 15.0.2.

6 RNA extraction and qPCR

6.1 RNA extraction with Trizol

Mouse organs were dissected and immediately frozen in liquid nitrogen. Tissue crushing and homogenization was done using mortar and pestles under liquid nitrogen. Tissue powders were directly transferred to an appropriate amount of TRIzol reagent (Life Technologies) for RNA extraction. Chloroform (0.2 ml for each 1 ml of initial TRIzol) was added to the homogenized suspension and samples were vigorously shaken for 15 s. After 3 min incubation at room temperature, samples were centrifuged for 15 min at 12,000 g using a microfuge. Aqueous phase was transferred to new tubes containing isopropanol. After 15 min incubation at room temperature, samples were centrifuged for 10 min at 12,000 g and the pellet was washed with 1 ml of 70% ethanol. The RNA was dissolved in 30 µl of sterile, RNAase-free water and stored at -80°C.

Concentration of RNA was determined by absorbance at 260 nm using a Nanodrop Spectrophotometer. The quality of the RNA samples was determined by comparing the quality and relative quantities of the 18S and 28S rRNA bands after agarose-gel electrophoresis, staining with ethidium bromide, and visualization with UV light.

6.2 Quantitative RT-PCR

Quantitative RT-PCR was applied under standard conditions using the SYBR Green Master Mix kit on the ABI Prism 7900 Sequence Detection System (Perkin-Elmer) and specific primers (**Table 2.5**). The relative mRNA expression levels of each

gene are expressed as the N-fold difference in target gene expression relative to the *Tata-binding protein* (*Tbp)* gene. Graphics were performed with GraphPad PRISM 5.

Table 2.5. Primers for quantitative RT-PCR on mouse CCPs

Gene	Primer name	Sequence (5'-3')
Agtpbp1	AGTPBP1-U1	TTCCACAGAGTCAGATACTGCCAGAT
	AGTPBP1-L1	CAGAACTTCCATGCCTGTAGAACCT
Agbl2	AGBL2-U2	AATCTGCAGAAAGCCGTCAGAGT
	AGBL2-L2	AGTGTGTTTGTCCGTGTAGAGGTCA
Agbl3	AGBL3-U1	CTGTTTACCCAAACTCCAAGGAAGAT
	AGBL3-L1	GGATGTTCGGTTACCCCCAACT
Agbl1	AGBL1-U2	GAGCTGTCCTGTAGCTTTGAGGAACT
	AGBL1-L2	AAGCAACACTTGGAATGTGGTGGT
Agbl5	AGBL5-U2	GCACCCAAAAGGTCAGCCAT
	AGBL5-L2	GCCGCCTTCTGTCTGAGCA
Agbl4	AGBL4-U2	CCAAGAGTCTTTACCGAGATGGGAT
	AGBL4-L2	CTGTGGTCTGGGCAGCGATAGT

7 Animal experiments

7.1 Generation of *Agbl2* KO, *Agbl3* KO and *Agbl2/Agbl3* double KO mice

The conditional mutant mouse lines for *Agbl2* (on exon 9) and *Agbl3* (on exons 7 + 8) were established at the Mouse Clinical Institute (MCI, Illkirch, France). The targeting vector was constructed as follows. The 5' (4.5 kb for *Agbl2*; 3.5 kb for *Agbl3*), 3' (3.5 kb for *Agbl2*; 4.7 kb for *Agbl3*) and inter-loxP (1.1 kb for *Agbl2*; 3.0 kb for *Agbl3*) fragments were PCR amplified and sequentially subcloned into an MCI proprietary vector containing the LoxP sites and a Neo cassette flanked by Flippase Recognition Target (FRT) sites (**Figure 2.1**).

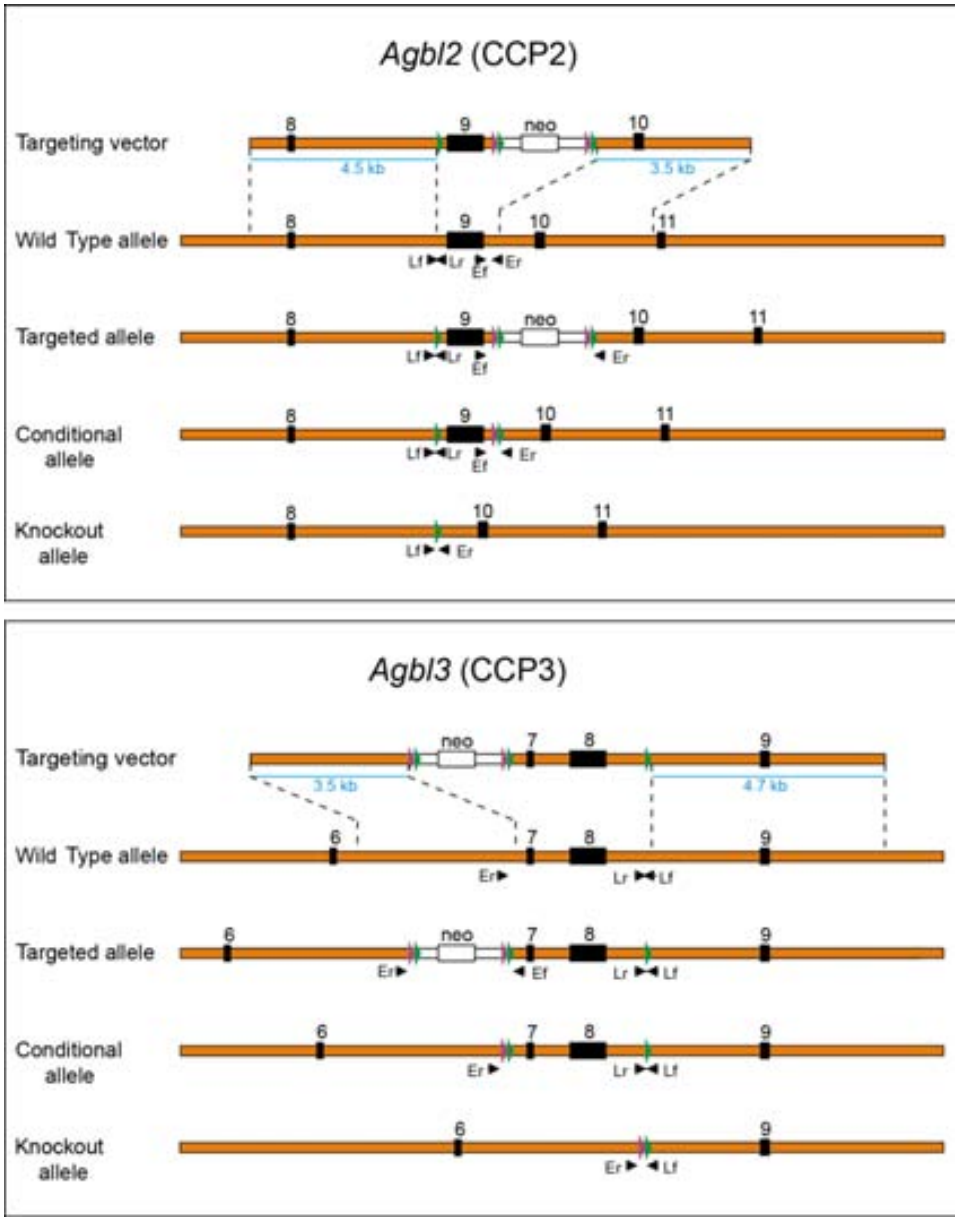

Figure 2.1. Strategy for the generation of the knockout mice

Schematic representation in scale of the targeting vector used and all the possible alleles for Agbl2 and Agbl3 genes. Orange bar: genomic DNA. Black boxes: exons with their corresponding number. Green and purple arrowheads: LoxP and Flp sequences, respectively. White bar: neo cassette, with the neomycin resistance gene (white box). Blue lines: zone of sequence homology for homologous recombination, with the corresponding size in kb. Black arrowheads: primers used for the PCR genotyping.

The linearized construct was electroporated in 129S2/SvPas mouse embryonic stem (ES) cells. After selection, targeted clones were identified by PCR using external primers and further confirmed by Southern blot with 5' and 3' external probes. Two positive ES clones were injected into blastocysts, and derived male chimaeras gave

germline transmission. The excision of the neomycin-resistance cassette was performed *in vivo* by breeding the chimeras with a *Flp* deleter line (C57BL/6N genetic background FLP under ACTB promoter). The *Flp* transgene was segregated by breeding the first germ line mice with a wild type C57BL/6N animal. For generation *Agbl2* KO and *Agbl3* KO mice, *Agbl2* and *Agbl3* floxed mice were crossed with transgenic mice expressing Cre recombinase under the control of a CMV promoter.

The *Agbl2/Agbl3* double KO mice were then generated by crossing the single KO mice. Genomic DNA isolated from mouse tail snip was analyzed by PCR.

Genotyping

Mice were genotyped by polymerase chain reaction (PCR) according to MCI protocols using GoTag polymerase (Promega) and 33 amplification cycles. The three primer pairs listed below were used to define the genotypes.

For CCP2:

(1) CCP2_Ef: CATCCTTAGCAACTCTCCCGATGCCC
CCP2_Er: GGTGGGGGTGTGTGTGAAATGGCTG

(2) CCP2_Lf: CCACGAGCGACCTTCCAAACCTACC
CCP2_Lr: AGCTGCCTGCTACAGCAAACGGG

(3) CCP2_Lf: CCACGAGCGACCTTCCAAACCTACC
CCP2_Er: GGTGGGGGTGTGTGTGAAATGGCTG

For CCP3:

(1) CCP3_Ef: CCTCAAAACCACTGACCATCTAGACAGCC
CCP3_Er: GGGCTGGAGTAGACACTGTACATAAGAAAGC

(2) CCP3_Lf: CTGGAGTGGGACTAGTATCTTGAAGATGGG
CCP3_Lr: CCCCAGGAACTTTGACCCTTTGTGTGC

(3) CCP3_Lf: CTGGAGTGGGACTAGTATCTTGAAGATGGG
CCP3_Er: GGGCTGGAGTAGACACTGTACATAAGAAAGC

7.2 Animal experimentation

Wild type C57BL/6N, *Agbl2* KO, *Agbl3* KO, and *Agbl2/Agbl3* double KO mice were housed under Specific Pathogen Free (SPF) conditions in the animal facility of the Institut Curie. Animals were maintained with access to food and water *ad libitum* in a colony room kept at constant temperature (19-22 °C) and humidity (40-50%) at 12 h light/dark cycles. All experimental procedures were performed in strict accordance with the guidelines of the European Community (86/609/EEC) and the French National Committee (87/848) for care and use of laboratory animals.

8 Structural modeling and bioinformatics

8.1 Structural alignment

The catalytic domain of CCP3 was modeled with the help of the RaptorX server (Källberg *et al.*, 2012) and using as templates the available structures of three CCPs from *Pseudomonas aeruginosa* (PDB 4a37) (Otero *et al.*, 2012), *Burkholderia mallei* (PDB 3k2k) and *Shewanella denitrificans* (PDB 3l2n). While Ramachandran plots were derived for the proposed models to verify proper stereochemistry of the residues, local and overall model quality was verified using Verify3D (Bowie *et al.*, 1990; Luthy *et al.*, 1992) and Prosa-web (Sippl, 1993; Wiederstein and Sippl, 2007). Arg at position 255 was supported by the structure-based sequence alignment performed by RaptorX, I-TASSER (Zhang, 2008; Roy *et al.*, 2010), GalaxyWEB (Ko *et al.*, 2012) and PDBsum (Laskowski, 2001).

8.2 Search for proteins ending with acidic amino acidic stretches in the database

A bioinformatic search for proteins susceptible to be substrates of CCPs was performed using ScanProsite tool (de Castro *et al.*, 2006). The search for total acidic proteins was performed using the pattern [ED](n)>, where **n** represents the number of

consecutive acidic residues at the protein's C-terminus. We searched for C-terminal stretches from two residues and longer. The total number of proteins with a given number of acidic amino acids at the C-terminus was determined from the *Homo sapiens*, *Mus musculus*, *Drosophila melanogaster* and *Caenorhabditis elegans* taxons of the 2014_05 UniProtKB/Swiss-Prot database, using the default settings. Splice variants were not allowed. The same search was repeated for C-terminal tails containing only glutamate residues.

Chapter III:
Characterization of human CCP3

CHAPTER III: CHARACTERIZATION OF HUMAN CCP3

SUMMARY

Six cytosolic carboxypeptidase (CCP) genes have been described in mice and humans and the enzymatic function of four of them was recently elucidated, as CCP1, CCP4, CCP5 and CCP6 were shown to act as deglutamylating enzymes. Here, we characterize a new member of this subfamily and provide new insights into the emerging field of tubulin modifying enzymes. In the present study, we show that human CCP3 is associated with MTs and generates Δ2-tubulin, pointing to a role as deglutamylating enzyme. In immunolocalization experiments we found that CCP3 is associated with midbody MTs during cell division. Finally, the observed specificity of CCPs for acidic amino acids is justified by a structural model of CCP3 catalytic domain. Taken together, these results suggest that CCP3 acts as a deglutamylase associated with MTs, with a possible role in cytokinesis. Finally, these results suggest that the entire CCP family could be formed by deglutamylating enzymes.

RESULTS

9 hCCP3 is a deglutamylating enzyme involved in the generation of Δ2-tubulin

9.1 Overexpression of hCCP3 generateΔ2-tubulin in HEK293T cells

After the discovery that four (CCP1, CCP4, CCP5, CCP6) among the six murine CCPs are deglutamylases (Rogowski *et al.*, 2010), the attention turned to the potential functions of CCP2 and CCP3. Considering that the enzymes responsible for tubulin deglycylation and detyrosination have not been identified so far, it was hypothesized that CCP2 and CCP3 could be involved in these PTMs. This hypothesis was further supported by the fact that the enzymes responsible for the reverse reactions (*i.e.*

polyglutamylation, polyglycylation and tyrosination) are members of the same enzyme family; tubulin tyrosine ligase-like protein or TTLLs. Indeed, an initial report (Sahab *et al.*, 2011) attributed a detyrosinating activity to CCP2, however unambiguous evidence for this activity was not provided. Considering that CCP2 and CCP3 are close paralogs (Rodríguez de la Vega Otazo *et al.*, 2013), we might expect them to have similar substrate specificity and function. In this context, we decided to test whether CCP3 could detyrosinate tubulin, by transfecting a 72.6-kDa human isoform of CCP3 (Q8NEM8-2 Uniprot) in HEK293T cells and analysis by immunoblot of the tyrosination state of α-tubulin. No reduction in tyrosinated tubulin (Tyr-tubulin) or increase in deTyr-tubulin were observed as a result of hCCP3 overexpression (**Figure 3.1 A**).

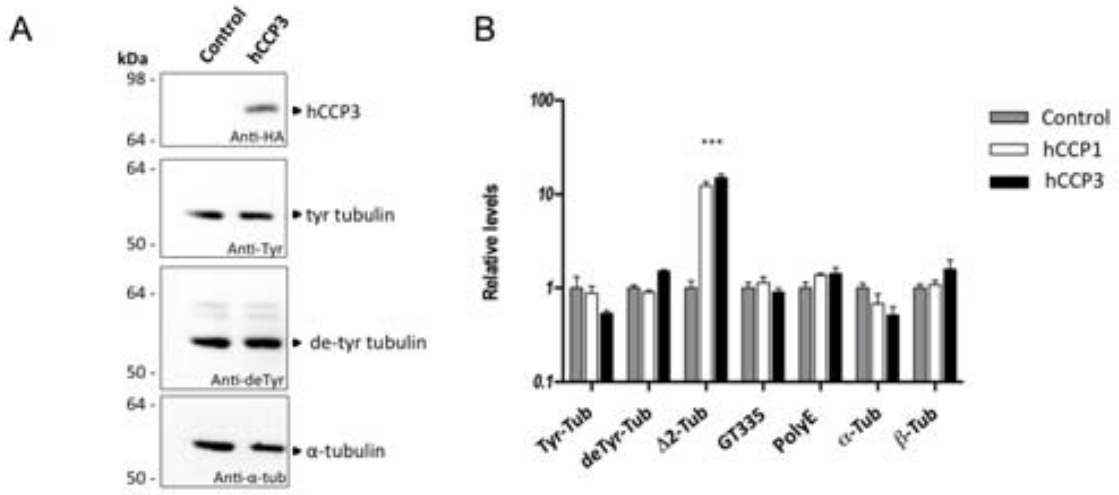

Figure 3.1. Evaluation of tubulin PTMs in HEK293T overexpressing CCP3

A) *Immunoblot analysis of α-tubulin tyrosination levels in HEK293T control cells and cells overexpressing CCP3. Recombinant CCP3 was detected using the anti-HA antibody.* ***B)*** *Immunoblot quantification of the levels of different tubulin PTM for HEK293T cells overexpressing CCP3 and CCP1 compared to control cells. Samples were analyzed for α- and β-tubulins and diverse tubulin PTMs levels. An increase in Δ2-tubulin levels was detected for upon CCP3 and CCP1 overexpression as shown in Annex I. Relative Immunoblot quantification was performed with the Quantity One software. β-actin levels were used to normalize loading variability. Δ2-tubulin levels were significantly increased for both CCP3 and CCP1 overexpressions (***p<0.001 vs control using two-way ANOVA statistic analysis). Error bars represent standard deviation of the mean (n=3). Abbreviation: Tub, tubulin.*

As no detyrosinating activity was observed for CCP3, we wondered if this enzyme could posttranslationally modify tubulin similarly to other CCPs. To test this possibility, CCP3 was transfected in HEK293T cells and the levels of different tubulin PTMs were analyzed by Immunoblot, using non-transfected cells as a negative control and cells overexpressing CCP1 as a positive control for deglutamylase activity (**Figure 3.1 B**). Concerning tubulin polymodifications, we analyzed tubulin polyglutamylation using two different antibodies: the polyE antibody that detects polyglutamate chains of at least three residues long (Shang, 2002), and the GT335 antibody that interacts with the branching point of the lateral polyglutamate chain. No differences in polyE and GT335 signals were detected upon CCP1 or CCP3 overexpression.

Regarding PTMs on the gene-encoded C-terminus of α-tubulin (Tyr-, deTyr-, and Δ2-tubulins), we observed a significant increase of Δ2-tubulin when CCP3 is overexpressed (**Figure 3.1 B, Annex I**), reaching similar levels to those generated by CCP1. CCP1 was previously described as a deglutamylating enzyme that can process the penultimate glutamate residue of α-tubulin (Rogowski *et al.*, 2010), and CCP3 seems to perform a similar role on the primary sequence of α-tubulin. Again, neither Tyr-tubulin (–EEY) nor deTyr-tubulin (-EE) levels were significantly altered by CCP3 overexpression. Taken together, these results suggest that CCP3 is not involved in α-tubulin detyrosination but removes the penultimate glutamate residue from detyrosinated α-tubulin.

9.2 Mutation at the catalytic residue Glu270 inactivates CCP3

To further demonstrate that CCP3 enzymatic activity is responsible of Δ2-tubulin generation, we mutated the equivalent of the catalytic residue Glu270 (using the numbering system on bovine CPA; Glu534 on CCP3 sequence) to a glutamine to generate an inactive mutant of CCP3. While our study was in progress, another report appeared demonstrating that the equivalent residue in CCP1 (E1094) is essential for its deglutamylating activity (Wu *et al.*, 2012). While increased levels of Δ2-tubulin were detected upon CCP3 overexpression, no Δ2-tubulin generation was observed for CCP3-E534Q inactive mutant (**Figure 3.2 A)**, corroborating that Glu534 is required for the

enzyme activity of CCP3 and that the observed Δ2-tubulin generation is linked to CCP3 enzymatic activity.

9.3 CCP3 knock-down shows decreased Δ2-tubulin levels in HEK293T cell extracts

To test whether a CCP3 knock-down presents the opposite effect on Δ2-tubulin levels, a CCP3 specific shRNA sequence (sh72) targeting the carboxypeptidase domain of the enzyme was used. The effectiveness of sh72 knock-down was evaluated in HEK293T cells by cotransfection of CCP3 with sh72, with a scrambled sequence control shRNA (sh13) or with an empty vector (sh07) also as a control. Cultures transfected with sh72 showed a substantial decrease in CCP3 protein expression level and Δ2-tubulin signal when compared to the controls (**Figure 3.2 B**).

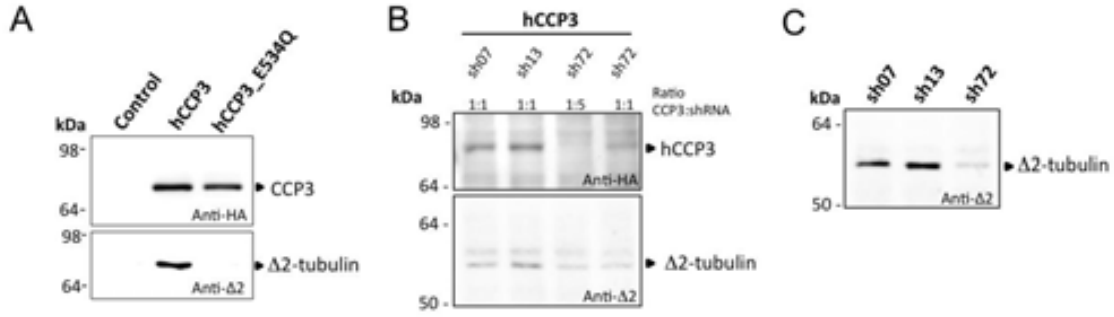

Figure 3.2. Overexpression and knock-down of CCP3

A) *Immunoblot of HEK293T cells overexpressing human CCP3 or CCP3-E534Q mutant. The hCCP3 is detected using the anti-HA-tag antibody and the α-tubulin with the last two residues processed is distinguished from total α-tubulin with the anti-Δ2-tubulin antibody. The point mutation in the catalytic residue Glu270 (E534Q) results in an inactive enzyme unable to generate the increase in Δ2-tubulin observed for native hCCP3.* ***B)*** *Effectiveness of CCP3 shRNAs knock-down on HEK293T cells. Immunoblot using anti-HA and anti-Δ2-tubulin in cells cotransfected with CCP3 and CCP3-shRNAs for 72 h. The shRNAs used were an empty shRNA control vector (sh07), a scramble control shRNA (sh13), and a specific CCP3 shRNAs (sh72), in this case using two different DNA ratios in relation to CCP3 construct.* ***C)*** *CCP3 knock-down on HEK293T cells. Immunoblot analysis of anti-Δ2-tubulin levels on antibiotic selected cell clones at 20 days after transfection and selection with the empty vector (sh07), a scramble shRNA (sh13) and a specific CCP3 shRNA (sh72).*

To investigate the role of endogenous CCP3 in the generation of Δ2-tubulin, we transfected HEK293T cells with sh72 and proceeded with puromycin selection for three weeks. As a result, selected clones showed remarkably lower Δ2-tubulin levels compared to the controls (**Figure 3.2 C**). Consequently, Δ2-tubulin levels in cells are altered either upon CCP3 overexpression or suppression.

10 Binding of CCPs to microtubules

10.1 CCP3 localize to the midbody in dividing cells

Taking into consideration that tubulin is a CCP3 substrate, both proteins are expected to associate along the cell cycle. In order to test this hypothesis, the intracellular localization of endogenous human CCP3 was analyzed in HeLa cells using confocal immunofluorescence laser scanning microscopy. In interphase cells we found a punctuate staining of CCP3 in the cytosol and in the nucleus with a higher accumulation at the perinuclear region (**Figure 3.3**, first row). Nuclear staining was also described for CCP1, which was suggested to participate into nuclear functions related to chromatin remodeling and DNA repair processes (Valero *et al.*, 2006; Baltanas *et al.*, 2011; Rodríguez de la Vega Otazo *et al.*, 2013).

In dividing cells at metaphase we observed a change in CCP3 localization with respect to interphase, with CCP3 showing a granular pattern around the mitotic spindle (**Figure 3.3**, second row). This implies redistribution from the granular random homogeneity to a more regular but still granular pattern. The distribution of CCP3 shows a clearly organized pattern at cytokinesis, where CCP3 colocalizes with α-tubulin at the midbody MTs, at intercellular bridges (**Figure 3.3**, third row). The association of CCP3 with MTs during cytokinesis suggests a putative role of CCP3 in cell division. Interestingly, our group similarly described such localization for CCP5 (Rodríguez de la Vega Otazo *et al.*, 2013).

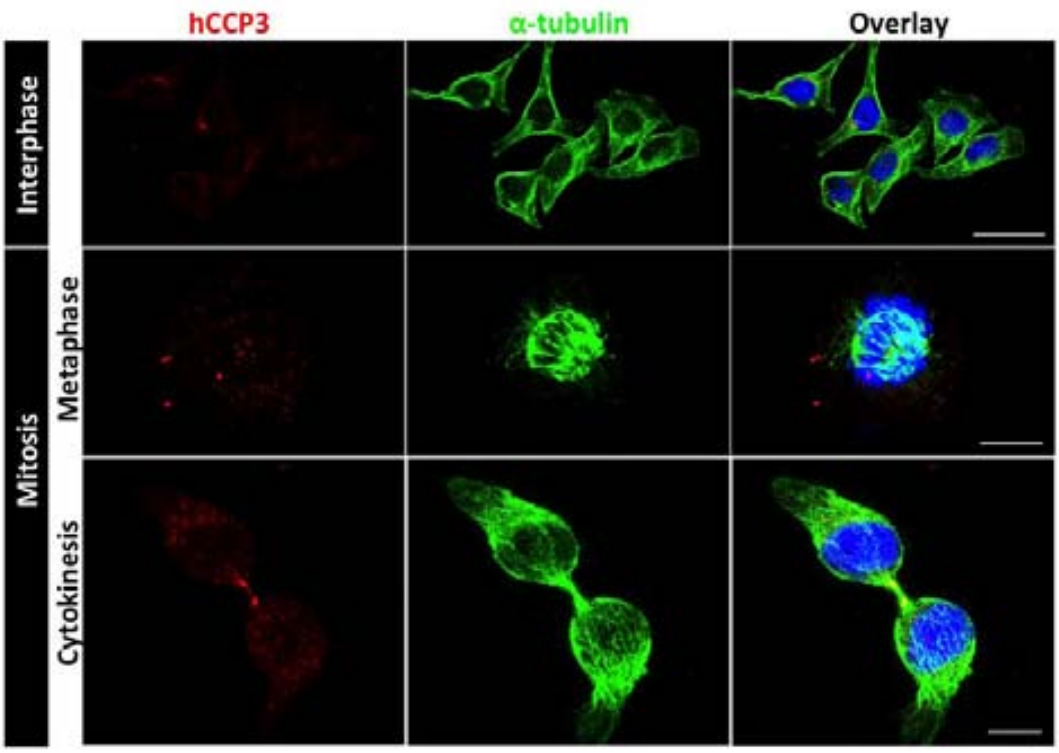

Figure 3.3. Association of hCCP3 with the midbody in dividing cells
Confocal micrographs of HeLa cells immunostained with anti-CCP3 antibody (red) and α-tubulin antibody (green). The Z-projections of a stack of images were obtained with the Easy 3D tool (IMARIS 7.2.1) for interphase cells (first row) and dividing cells (second and third rows). Scale bars, 40 µm (interphase); 10 µm (mitosis).

10.2 CCP1 and CCP3 copurify with microtubules

To further study the association of CCP3 with MTs, we partially purified tubulin from HEK293F control cells and HEK293F cells overexpressing CCP3 (**Figure 3.4).** Recombinant CCP3 is present in the MT fractions along the purification process, as well as in the final semi-purified tubulin fraction named HTub (**Figure 3.4 C)**. In parallel, we analyzed the co-purification behavior of endogenous CCP1, which was also found to partially co-purify with MTs (**Figure 3.4 A-B and D).** Although many proteins might indirectly co-purify with MTs (through a protein that binds to them) at the first steps, those indirectly bound-proteins should decrease after the *in vitro* depolymerization and repolymerization steps (Fourest-Lieuvin, 2006). In conclusion, a fraction of CCP1 and CCP3 seem to be associated with MTs and follow tubulin through successive *in vitro* depolymerization/polymerization cycles.

It is noteworthy that the anti-CCP1 antibody recognizes two clear immunoreactive bands; besides a major band at 140-150 kDa corresponding to full-length CCP1, an immunoreactive band of approximately 80-90 kDa (CCP1 short) can be observed (**Figure 3.4 B and D)**. Similarly, Wu *et al.* reported the presence of lower molecular weight immunoreactive bands for mouse CCP1, both in recombinant protein preparations and in mouse protein extracts (in this case using a made in-house mouse CCP1-specific polyclonal antiserum)(Wu *et al.*, 2012). They may correspond to either alternative splicing forms or be the result of a proteolytic processing of the full-length protein. Interestingly, when CCP3 is overexpressed, the shortCCP1 form appears greatly reduced when compared to the respective control tubulin extracts (**Figure 3.4 B and D)**.

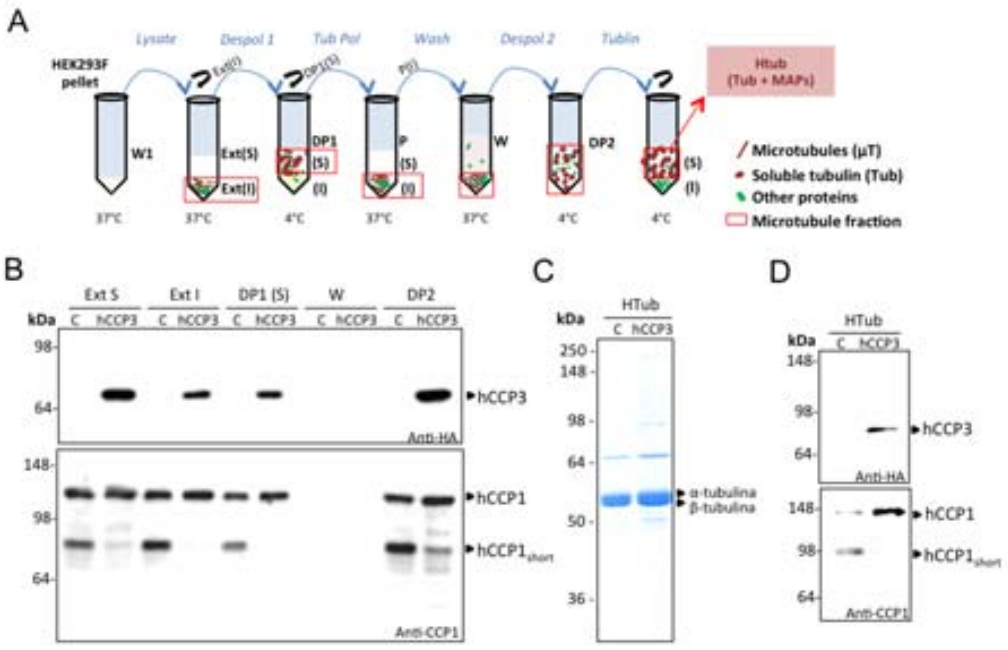

Figure 3.4. Tubulin purification from HEK293F cells and CCPs copurification

A) *Scheme of tubulin purification from HEK293F control (C) cells and HEK293F cells overexpressing hCCP3 for 72h (hCCP3), based on the Fourest-Lieuvin method that consists of extracting MTs from the insoluble cellular fraction (Ext I), which are then subjected to depolymerization (DP) and polymerization (P) steps to obtain human tubulin (Htub) with its associated MAPs.* ***B)*** *Immunoblot analysis of samples from different steps of tubulin purification. The samples analyzed were: Ext (S), initial soluble extract; Ext (I), initial insoluble extract containing MTs; DP1 (S), tubulin resultant from a first MT depolymerization step; W2, wash of the MT pellet after tubulin depolymerization; DP2, soluble fraction after a second depolymerization step. Recombinant hCCP3 was detected with anti-HA antibody and*

endogenous CCP1 was detected with anti-CCP1 antibody. ***C)*** *SDS-PAGE of the semi-purified human HEK293F tubulin (HTub).* ***D)*** *Immunoblot analysis of purified human HEK293F tubulin (HTub) fractions showing the presence of endogenous CCP1 and recombinant CCP3.*

We wanted then to analyze if the hCCP3 fraction non-associated with MTs behaves as a monomeric enzyme, oligomerizes, or can be found in complex with tubulin dimers or other proteins. For this purpose, an extract of HepG2 cells was fractionated through Sephadex 200 10/300 GL size exclusion column chromatography (SEC). This cell line was chosen for the assay because it endogenously expresses immune-detectable levels of the 72.6-kDa hCCP3 isoform. We found that soluble endogenous hCCP3 behaves as a monomer on SEC (**Figure 3.5**), similarly to what was previously observed for mCCP1 (Wu *et al.*, 2012).

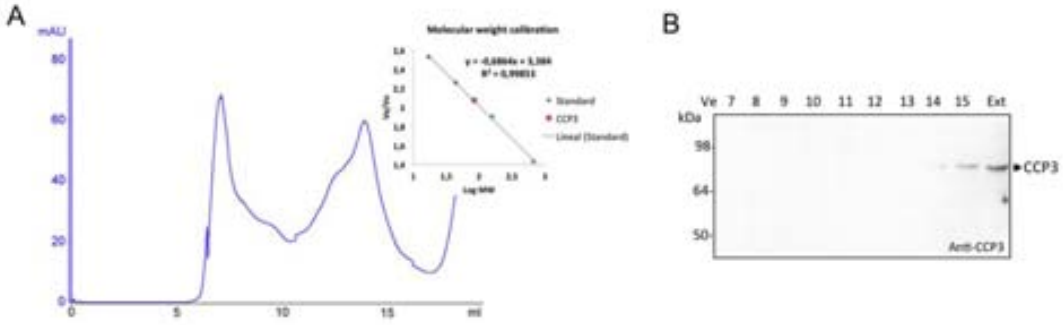

Figure 3.5. Determination of the molecular weight of native CCP3.
A) *Absorbance profile of the FPLC protein separation of a HepG2 cells lysate on a Sephadex 200 10/300 column. As an inset we show a calibration curve using standard proteins: thyroglobulin (670 kDa), γ-globulin (158 kDa), ovalbumin (44 kDa) and myoglobin (17 kDa).* ***B)*** *Immunoblot showing CCP3 immunoreactivity at the eluted fractions. CCP3 elutes at Ve between 14-15 ml, and the calculated molecular weight is between 82 ± 20 kDa. Abbreviations: Ve, elution volume; Vo, void volume.*

10.3 Tubulin is pulled-down by hCCP3

hCCP3 was detected in semi-purified tubulin after two cycles of microtubules polymerization/depolymerization, indicating that part of hCCP3 can associate with microtubules. By gel-filtration we were not able to detect hCCP3 oligomerization and, unexpectedly, we had no evidence of hCCP3-α/β-tubulin complexes (≅182 kDa). In

order to determine if hCCP3 could interact with soluble tubulin heterodimers, we overexpressed Strep-HA-tagged hCCP3 in HEK293F cells, lyse the cells in physiologic buffer and performed a Strep-tag affinity purification keeping the physiologic conditions. The same procedure was applied to non-transfected cells.

hCCP3 complexes were isolated and proteins were separated by 1-D and 2-D SDS PAGE electrophoresis (**Figure 3.6**).The different gel bands were excised and processed for mass spectrometry (MS) analysis. MALDI-TOF was performed followed by identification using the MASCOT search engine (**Table 3.1**). Among the 10 interacting candidates identified, the presence of α- and β-tubulins at a similar level to CCP3 is remarkable and consistent with the proposed hCCP3-α/β-tubulin interaction.

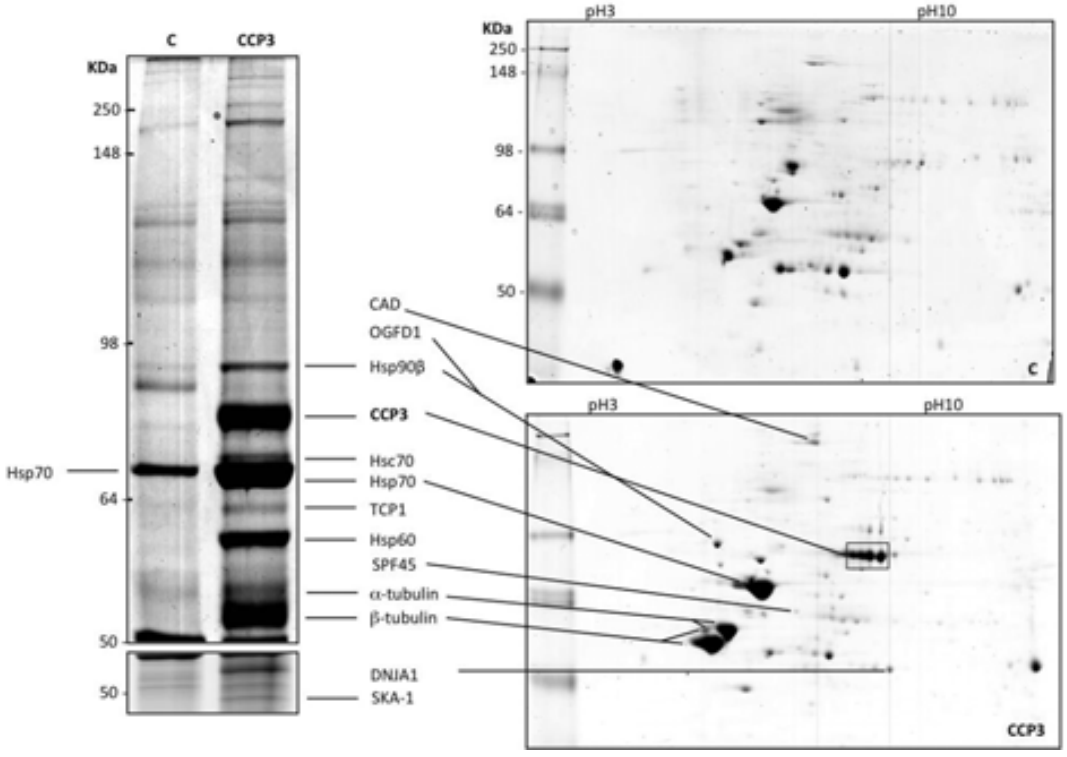

Figure 3.6: Proteomic analysis of CCP3 protein complexes by 1-D and 2-D SDS-PAGE
Protein analysis of CCP3 complex isolated by affinity Strep-tag purification and a control extract purified in the same conditions. Monodimensional 10% polyacrylamide gel (left) and bidimensional gel electrophoresis (2-DE) using a pH range between 3 and 10 and 12.5% polyacrylamide and stained with colloidal Coomassie G-250. Proteins indicated in the figure were identified by peptide mass fingerprinting.

Table 3.1. Protein identifications by peptide mass fingerprinting

Protein	Biological function	MW	Score	Peptides	% seq	Predicted IP
α-tubulin	Microtubules. Cytoskeleton.	50120	170	18	41	4.94
β-tubulin	Microtubules. Cytoskeleton.	49639	168	21	62	4.78
Hsp90β Heat shock protein 90β	Folding. It binds tubulin. Polymerizes tubulin IV isoform.	83212	93	15	14	4.97
Hsc70 Heat shock cognate 71 kDa protein	Folding. As ATPase, clathrin-coated vesicles disassembly	77448	49	5	17	6.64
Hsp60 Heat shock protein 60	Folding (mitochondria/cytoplasma).	25138	90	6	30	9.52
TCP1 T-complex protein 1	Cytosolic chaperon: tubulin and actin folding BBSome assembly / cilia transport vesicles regulation	60550	100	10	24	6.38
DNAJA1 DnaJ homolog subfamily A member 1	Hsc70 co-chaperone. Import of proteins into the mitochondria	44839	83	9	27	6.65
Hsp70 Heat shock protein 70	Folding (inducible in cell stress)	70009	258	32	51	5.48
CAD CAD protein	Fusion protein codifying for GATase, CPSase, ATCase and DHOase enzymatic activities of the pyrimidine pathway	242829	76	12	6	6.02
OGFD1 2-oxoglutarate and iron dependent oxygenase domain containing 1	Regulator of protein translation termination efficiency. Involved in stress granule formation. Found in protrusions of pseudopodia in tumoral cells.	63206	63	9	12	5.03
SKA-1 Spindle and kinetochore-associated protein 1	Microtubule-binding subcomplex of the outer kinetochore, essential for proper chromosome segregation	29465	62	6	26	6.68

Also a group of chaperons (Hsp90β, Hsc70, Hsp60, TCP1 and Hsp70) and a co-chaperone (DNAJA1) were identified from the hCCP3 affinity purified complex. From those, Hsp70 was also identified in the control sample, but it appeared increased when hCCP3 is overexpressed. Some of the interacting candidates could be associated with tubulin instead of CCP3, such as TCP1, a tubulin and actin chaperone. Three non-chaperone proteins were identified besides tubulin: CAD protein, 2-oxoglutarate and

iron dependent oxygenase domain containing 1 (OGFD1) and Spindle and kinetochore-associated protein 1 (SKA-1). CAD is involved in the pyrimidine pathway; OGFD1 regulates protein translation termination and stress granule formation; and SKA-1 is a kinetochore binding protein required for chromosome segregation.

From the proteomic study, we identify again tubulin as hCCP3 interactor. This is consistent with the increase in Δ2-tubulin observed in cell lysates upon hCCP3 overexpression. To further determinate the direct catalytic effect of CCP3 as tubulin deglutamylase, we performed *in vitro* studies with affinity-purified hCCP3.

11 CCP3 activity in vitro

11.1 CCP3 generates Δ2-tubulin on HEK293F purified tubulin

To confirm that the increase in Δ2-tubulin levels is not an indirect effect of hCCP3 overexpression or activity, we performed *in vitro* activity tests with affinity-purified hCCP3 and purified tubulin. hCCP3 eluted from the *Strep*-Tactin affinity column (**Figure 3.7 A**) was incubated for 3 h with either tubulin purified from HEK293F cells or from porcine brain, in the presence or absence of the carboxypeptidase inhibitor ortho-phenanthroline (OP) (Rogowski *et al.*, 2010). HEK293F tubulin contains low levels of Δ2-tubulin and therefore is suitable to test Δ2-tubulin generation. As a result, only active hCCP3 is able to generate Δ2-tubulin *in vitro* (**Figure 3.7 B**). The appearance of a 40 kDa band is observed in the anti-Δ2-tubulin blot for the samples incubated with active hCCP3 enzyme (**Figure 3.7 B**). This protein could not be identified and constitutes a potential hCCP3 substrate, similarly to what was observed for hCCP1 and MLCK or telokin in *pcd* mouse (Rogowski *et al.*, 2010).

Brain tubulin is known to be highly polyglutamylated with long lateral glutamate chains, and thus appropriate to assay the action of hCCP3 over polyglutamylation. Equivalent amounts of *Strep*-tag purified hCCP1 and hCCP3 were incubated with brain tubulin for 3 h, and the levels of polyglutamylated tubulin analyzed using the polyE antibody. In the assayed conditions, no decrease in polyglutamylated tubulin signal was detected in samples treated with active hCCP3, but could be observed for active hCCP1 (**Figure 3.7 C**). This data suggests that, under

the experimental conditions here assayed, the recombinant 72.6-kDa hCCP3 is not able to substantially modify the length of lateral polyglutamylation chains *in vitro*.

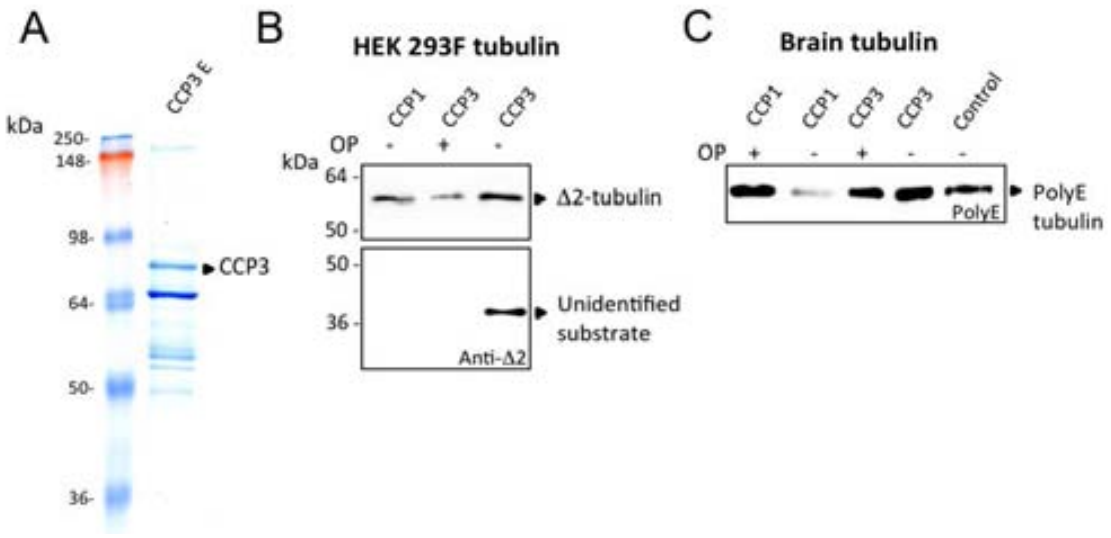

***Figure 3.7. In vitro* activity assay of affinity-purified hCCP3 and hCCP1 on tubulin.**
A) *SDS-PAGE analysis of Strep-tag affinity purified CCP3.* ***B)*** *Anti-Δ2-tubulin immunoblot analysis of tubulin purified from HEK293F cells that was incubated 3 h at 37°C with affinity-purified CCP3 or CCP1 in the presence or absence of 10 mM OP.* ***C)*** *Immunoblot using the polyE antibody on brain tubulin incubated with CCP1 or CCP3 for 3h at 37°C in the presence or absence of 10 mM OP.*

11.2 CCP3 activity on TRAD1

A plausible explanation for CCP3 behavior with polyglutamylated tubulin is that long polyglutamate tails disfavor CCP3 action. Taking this into account, we further look into the action of CCP3 on long polyglutamate chains, in this case located in the protein main-chain, as gene-encoded C-terminal glutamate stretches. For this purpose we selected TRAD1, a protein with 6 consecutive glutamic acid residues at its C-terminus, which has been recently found to be a CCP1 substrate (Tanco *et. al.,* manuscript submitted to MCP). *Strep*-tagged versions of CCP3 and TRAD1 were cotransfected in HEK293T cells and purified. Immunoblot of the affinity purified eluates with anti-HA and Anti-CCP3 show that both TRAD1 and CCP3 were expressed and purified. PolyE immunoblot showed non-significant differences between native

TRAD1 and TRAD1 coexpressed with CCP3 (**Figure 3.8 A**). Taking in consideration that the polyE antibody cannot differentiate C-terminal tails that differ in their length on more than 3 glutamic acid residues, we decided to analyze TRAD1 by mass spectrometry. While two different C-terminal peptides were identified for control TRAD1 (intact C-terminus and a C-terminus lacking one residue), for CCP3-treated TRAD1 we were able to identify in addition to the intact C-terminus a C-terminus where two glutamates were removed, which is consistent with the ability of CCP3 to process TRAD1 C-terminus (**Figure 3.8 B**). In summary, recombinant hCCP3 is not able to completely process long polyglutamate chains as demonstrated by WB analyses. Mass-spectrometry studies suggest that hCCP3 is able to process TRAD1 with an intrinsic low activity/processivity.

A

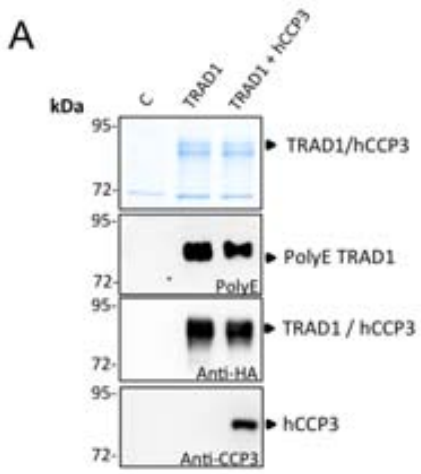

B

	C-terminal sequence	q-Value	PEP
TRAD1	QQGAGDAEEEEEE	0	0.0057
	QQGAGDAEEEEE	0.0027	0.0454
TRAD1 + hCCP3	QQGAGDAEEEEEE	0	0.1534
	QQGAGDAEEEE	0.0041	0.1843

***Figure 3.8. In vitro* activity assay of affinity-purified CCP3 and CCP1 on tubulin**
A) *Coomassie-stained SDS-PAGE gel and immunoblots of Strep-tag affinity purified TRAD1 and CCP3 + TRAD1. Both CCP3 and TRAD1 are HA and Strep double tagged for affinity purification and immunodetection.* ***B)*** *Mass spectrometry analysis of the C-terminal tryptic peptide proceeding from purified TRAD1 and TRAD1 coexpressed with CCP3.*

12 Determination of hCCP3 substrate specificity

12.1 Structural modeling of hCCP3

To gain more insight into the substrate preferences of hCCP3, we structurally align the catalytic domain of the enzyme with the crystal structures of three bacterial

CCPs *Pseudomonas aeruginosa* (PDB 4a37) (Otero *et al.*, 2012), *Burkholderia mallei* (PDB 3k2k) and *Shewanella denitrificans* (PDB 3l2n) (**Figures 3.9 A**). Based on this multiple alignment, we modeled the carboxypeptidase catalytic domain of hCCP3 and identified the main residues participating in catalysis and specificity (**Figures 3.9 B**).

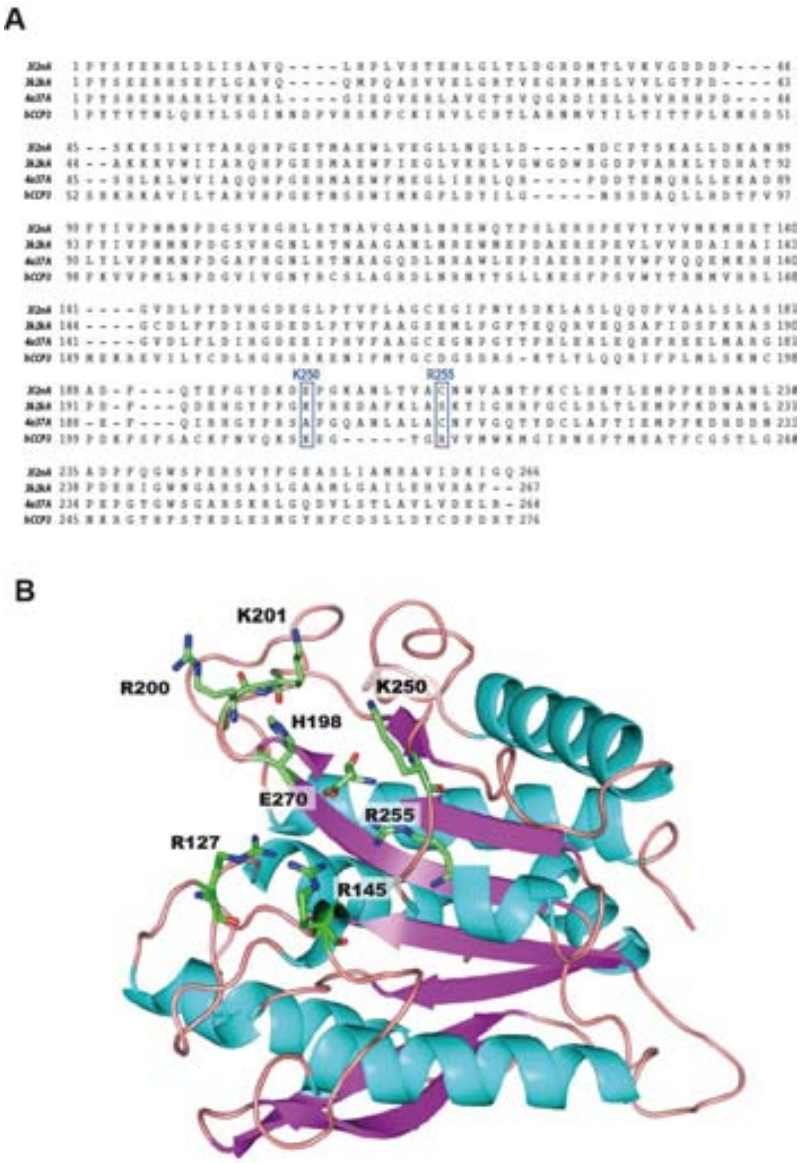

***Figure 3.9*. Structural modeling of the carboxypeptidase domain hCCP3**

A) *Structural alignment of the catalytic domain of hCCP3 with the CCP crystal structures of Pseudomonas aeruginosa (PDB 4a37)* (Otero *et al.*, 2012)*, Burkholderia mallei (PDB 3k2k) and Shewanella denitrificans (PDB 3l2n) obtained with the RaptorX server.* ***B)*** *Modeled structure of human CCP3 (as a convention in the field, all residues are numbered according to the corresponding active-site residues in bovine carboxypeptidase A1 after propeptide cleavage). The catalytic E270, the main substrate-specificity determining R255, and putative secondary binding-site residues are indicated.*

12.2 Analysis of the active site residues

The pockets or subsites of carboxypeptidases, which are the binding sites of their substrates, are usually designated using a standard nomenclature (Schechter and Berger, 1967). Accordingly, substrate residues are indicated as –P3–P2–P1↓P1', where P1' is the C-terminal residue of the substrate to be cleaved, and the corresponding binding subsites in the carboxypeptidase are named S3, S2, S1 and S1' (**Figure 3.10 A**). In the structural model of hCCP3, an arginine (Arg) at position 255 (numbering according to active bovine carboxypeptidase A1 (CPA1; PDB 3hlp), at the base of the S1' subsite or specificity pocket, appears to be critical in determining the substrate preference of these enzymes (**Figures 3.9 B** and **3.10 B**). In metallocarboxypeptidases, the residue at position 255 directly interacts with the C-terminal side chain of the substrates (Arolas *et al.*, 2007; Fernández *et al.*, 2010a). A basic amino acid in this position suggest that hCCP3 should have a preference for acidic amino acids similar to carboxypeptidase O (Wei *et al.*, 2002; Lyons and Fricker, 2011). Sequence alignment of human and murine CCPs predicts that Arg255 is conserved in all six CCPs (**Figure 3.10 C**). Moreover, a lysine or arginine (Lys/Arg250) close to Arg255 is also conserved in the specificity pocket of CCPs, and may contribute to their preference for acidic amino acids (**Figures 3.9 B** and **3.10 C**).

In the hCCP3 model, the entrance to the active site presents an extended positively charged area, which is similarly formed by conserved residues throughout all CCPs, and can be associated to different binding subsites of these enzymes (**Figures 3.10 B** and **3.10 D**). The positively charged area around the active site of CCPs is consistent with their preference for substrates with multiple glutamic acids, like polyglutamylated tubulin (Rogowski *et al.*, 2010; Berezniuk *et al.*, 2012; Wu *et al.*, 2012). Particularly, positively charged amino acids in the S1 subsite are consistent with binding the glutamic acids present at the P1 position of deTyr-tubulin. Additionally, the hCCP3 model show positively charged S2 and S3 subsites, which can explain the ability of this enzyme to accommodate long acidic chains such as lateral polyglutamylation (**Figures 3.10 B**).

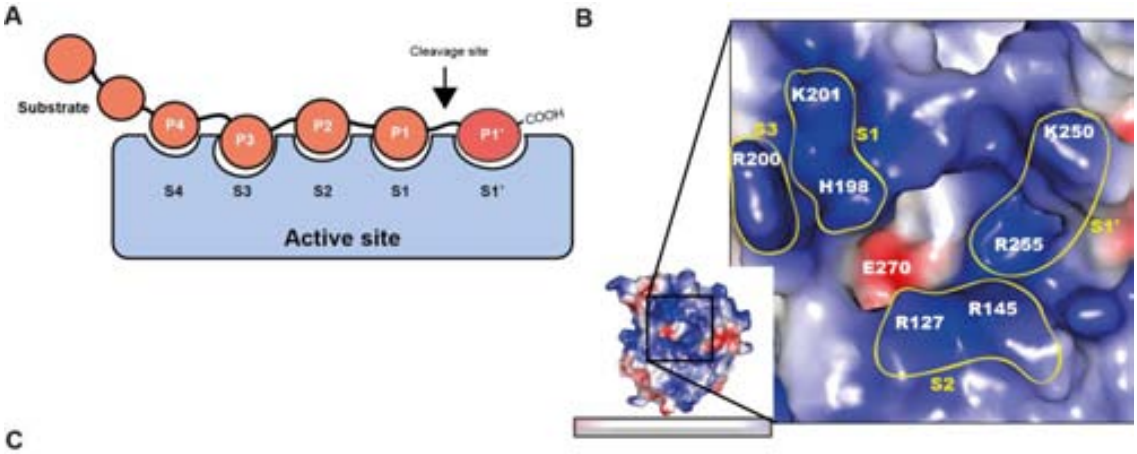

C

Position in bovine CPA (active form)	Homologous amino acid residues forming S1' subsite									Substrate specificity	MEROPS classification
	194	203	207[a]	243	247	250	253	255[b]	268		
Bovine CPA	Ser	Leu	Gly	Ile	Ile	Ala	Gly	Ile	Thr	Hydrophobic	M14A
Human CPA1	Ser	Met	Gly	Ile	Ile	Ala	Ser	Ile	Thr	Hydrophobic	
Human CPA2	Thr	Met	Gly	Ile	Ile	Ala	Gly	Ile	Ala	Hydrophobic	
Human CPA4	Asp	Met	Gly	Thr	Val	Ala	Ser	Ile	Thr	Hydrophobic	
CPT[c]	Thr	Leu	Gly	Gln	Leu	Thr	Asp	Thr	Thr	Broad	
Human CPB	Thr	Ile	Ser	Gly	Ile	Ala	Gly	Asp	Thr	Basic	
TAFI (CPU)	Ser	Val	Ser	Gly	Leu	Ala	Gly	Asp	Thr	Basic	
Human CPE	Asn	Asn	Asp	Gly	Trp	Val	Gly	Gln	Thr	Basic (Arg)	M14B
Human CPD	Asn	Asn	Asp	Asn	Phe	Val	Gly	Gln	Thr	Basic (Lys)	
Human CPO	Thr	Leu	Gly	Asn	Leu	Ser	Ser	Arg	Thr	Acidic	M14A
Human/ mouse CCP1	Asp	Val	Gly	Met	Ser	Lys	Thr	Arg	Thr	Acidic	M14D[d]
Human/ mouse CCP2	Asp	Val	Gly	Met	Ser	Arg	Thr	Arg	Thr	Acidic	
Human/ mouse CCP3	Asp	Ile	Gly	Phe	Asn	Lys	Thr	Arg	Thr	Acidic	
Human/ mouse CCP4	Asp	Ile	Gly	Phe	Lys	Lys	Thr	Arg	Thr	Acidic	
Human/ mouse CCP5	Asp	Cys	Gly	Phe	Asn	Lys	Ser	Arg	Thr	Acidic	
Human/ mouse CCP6	Asp	Gly	Gly	Tyr	Ser	Lys	Thr	Arg	Thr	Acidic	

D

Figure 3.10. Determination of amino acids of the active site of hCCP3 by structural modelling and comparison with other carboxypeptidases

A) *Scheme of the substrate-binding subsites in the active site of carboxypeptidases* (Schechter and Berger, 1967). ***B)*** *Vacuum electrostatics surface representation of the active site of hCCP3. Basic residues are indicated in blue and acidic residues in red. Positions 198 and 201 (corresponding to H462 and K465 in hCCP3) shape the S1 binding site in the hCCP3 model. Positions 127 and 145 (R414 and R424 in hCCP3) define the S2 subsite. Position 200 (R464 in hCCP3) is oriented towards the outer part of the active site, possibly defining an additional, positively charged S3 subsite. Note that although S1' is defined by different residues (**Figure 3.10 C**), we here only depicted positions 250 and 255 since they appear as the major determinants of substrate specificity for CCPs. Structure image was generated using PyMOL 1.3.* ***C)*** *Comparison of the amino acids shaping the S1' binding pocket in carboxypeptidases with different substrate specificities. Residues are indicated following the RasMol color scheme that depicts amino acids accordingly to their properties.* [a]*Residue 207 is the major determinant*

of specificity for M14B carboxypeptidases. [b]Residue 255 is the major determinant of specificity for M14A carboxypeptidases. [c]Carboxypeptidase isolated from Thermoactinomyces vulgaris that is a model for broad substrate specificity.[d]M14D is the proposed classification for the M14 members that constitute the CCP subfamily. ***D)*** *Amino acid sequence alignment of the region around position 255 for CCPs and canonical bovine CPA. The positions known to participate in the binding of the substrate C-terminal residue are indicated.*

Structural modeling and experimental data shown in this chapter are in accordance with hCCP3 preferring acidic amino acids. Sequence alignments of the six human and mouse CCPs extend these conclusions to the entire murine and human CCP family (**Figures 3.10 C-D**). Thus, the structure of the active site of CCPs reveals that the entire family has a preference for cleaving acidic amino acids. The modeling further helped us determining the controversial identity of the specificity-determining residue corresponding to position 255 of bovine CPA in CCPs (Kalinina *et al.*, 2007; Rodriguez de la Vega *et al.*, 2007) as being an arginine (**Figures 3.10 C**).

DISCUSSION

Tubulin PTMs are increasingly considered to play a transcendent role in the rapid and local functional adaptation of MTs and their structural dynamics (Janke *et al.*, 2008). In this way, they regulate many cellular functions, such as cell cycle control, neuronal differentiation and intracellular trafficking. TTLLs and CCPs are key enzyme subfamilies involved in the opposite processes of glutamate/glycine addition and glutamate removal, respectively. The different members of the TTLL subfamily show high specialization in terms of substrate and reaction type preference (van Dijk *et al.*, 2007; Szyk *et al.*, 2011). Similarly, in the case of CCPs, functional diversification might have occurred through evolution, giving rise to interrelated enzymes but with specialized functions and substrate preferences. A phylogenetic analysis inferred that CCPs cluster in different clades with specialized roles in the assembly, trafficking and signaling in MTs (Rodríguez de la Vega Otazo *et al.*, 2013). CCP2 and CCP3 orthologs were included in a common phylogenetic clade and would be expected to show similar substrate specificity and play a common role in motile cilia. However, although CCP2

was proposed to detyrosinate α-tubulin, we here found that CCP3 acts as a deglutamylating enzyme, in accordance with the enzymatic activities described for CCP1, CCP4, CCP5 and CCP6 (Rogowski *et al.*, 2010). Additionally, hCCP3 substrate preference was experimentally demonstrated and further supported by a protein structural modeling analysis of the residues involved in substrate selection.

In this report, we showed that hCCP3 processes tubulin and generates Δ2-tubulin, a PTM that is enriched in brain tubulin, and particularly in differentiated neurons (Khawaja *et al.*, 1988; Paturle-Lafanechère *et al.*, 1994). In *C. elegans*, increased levels of axonal Δ2-tubulin have been associated with an increase in the number of growing axonal MTs and enhanced axon regrowth (Ghosh-Roy *et al.*, 2012). The Δ2-tubulin generation is in agreement with the hCCP3 structural model. In fact, all residues defining this region are conserved among human and mouse CCPs, a structural feature that explains their preference for substrates with long polyglutamate chains like polyglutamylated tubulin (Rogowski *et al.*, 2010; Berezniuk *et al.*, 2011; Wu *et al.*, 2012). Remarkably, the data on structural modeling analysis and sequence homology between CCP2 and CCP3 is consistent with CCP2 being also a deglutamylase. This hypothesis will be considered and studied in Chapter IV.

Since hCCP3 showed a preference for glutamate residues, we expected that it would be able to process tubulin polyglutamate side-chains, in analogy to other CCP members. Furthermore, hCCP3 action over long acidic tails can be expected from the structural analysis of CCP3 catalytic domain, which reveals a positively charged area around the active site entrance, defining binding pockets that point to an extended substrate specificity for acidic residues. However, no decrease in the polyE signal could be detected for hCCP3 using brain tubulin as a substrate. The polyE antibody recognizes glutamate chains of at least three residues (Shang et al., 2002), and brain tubulin possesses long glutamates side chains. We hypothesize that the activity of purified hCCP3 could be below the antibody sensitivity. Even more, a low activity generates the cleavage of only a few glutamates from tubulin polyglutamate side-chain, generating cleavage products that contain polyglutamic strains of more than three residues.

It has been previously demonstrated that CCP1 acts as a deglutamylating enzyme on the abundant and longer polyglutamate side-chains of brain MTs (Rogowski *et al.*, 2010). Our *in vitro* assay of CCP1 showed activity on brain tubulin, whereas CCP1 failed in showing its deglutamylating activity in HEK293T cell extract. This cell line presents scarce and shorter polyglutamate strains and, in average, cells are poorly polyglutamylated (Berezniuk *et al.*, 2012). Thus, the differential behavior of CCP1 between brain and HEK293T tubulin might be explained because of the low levels of highly polyglutamylated MTs in HEK293T cells and its precise allocation. In interphasic HEK293T cells, long polyglutamylated MTs are confined to the centrioles and axoneme of cilia, which are small structures precisely located in the cell (Janke and Bulinski, 2011).

Besides tubulin, it is highly probable that additional cellular substrates are C-terminally processed by CCP3 (**Figure 3.7 B**), as it has been already demonstrated for other CCPs (Rogowski *et al.*, 2010). Apart from brain tubulin, an additional substrate with a long glutamate stretch at its C-terminus was studied through mass spectrometry analysis to increase sensitivity. Proteomic analysis of CCP3 action on TRAD1 suggests that CCP3 can cleave only a few glutamates from TRAD1 C-terminus. When compared to other CCPs, we have observed an intrinsic low activity of CCP3 recombinant protein. This may explain the low processivity of CCP3 over TRAD1 C-terminal tail or why purified CCP3 fails to efficiently process polyglutamylated tubulin. Our results on long polyglutamate stretches are not conclusive so far. Additional research is needed to determine whether CCP3 can be considered an enzyme involved in the regulation of polyglutamylation; as well as elucidate the optimal conditions in which CCP3 trim long glutamate chains or which factors might prevent this CCP3 activity.

CCPs regulation is still an intriguing issue. Rodriguez de la Vega *et al*. showed that different CCPs display specific cellular distribution in the cell, suggesting that their regulation might rely on their localization (Rodríguez de la Vega Otazo *et al.*, 2013). Similarly, CCP3 through its binding to microtubular structures might regulate its localization and thus its function. We here used microtubule binding assays and confocal colocalization to show that CCP3 has the ability to interact with MTs. In

addition, spatio-temporal localization of CCPs seems to be highly regulated: CCP3 colocalization with tubulin is particularly visible at the midbody during cytokinesis (**Figure 3.3**), which is in agreement with the observed colocalization of CCP1, CCP2, CCP4, CCP5 and CCP6 with certain transient MT structures at certain cell cycle stages (Rodríguez de la Vega Otazo *et al.*, 2013).

Provided that CCP5 is the only CCP able to cleave the glutamylation branching point, a coordinated regulation with CCP1, CCP4 or CCP6 is required (Rogowski *et al.*, 2010). Signs of CCPs inter-regulation were experimentally observed in this work. CCP1 presents a shorter form (shortCCP1), previously observed by other authors (Wu et al., 2012), that might be generated posttranslationally. The observed decrease in shortCCP1 fragment levels upon hCCP3 overexpression, suggest that this form might be a functional unit that seems to functionally compete with hCCP3. An inter-regulation in the protein levels of the different CCP forms require unknown cellular mechanisms that would need further research for its elucidation. Pull-down assay not only corroborated the binding of hCCP3 to tubulin, but additionally permitted the identification of putative interactors (and possible regulators) of hCCP3.

Hsp90 has a wide spectrum of client proteins and has been seen to be recruited into microtubules driven by α-tubulin acetylation (Giustiniani *et al.*, 2009; Eckl and Richter, 2013). Therefore, among the chaperons identified we tried to look further into Hsp90β, the constitutively expressed Hsp90β in order to validate whether hCCP3 could be a customer of this chaperone, but the lack of specific CCP3 antibodies for endogenous detection in cell extracts enabled to get conclusive data. SKA1, another putative CCP3 interacting partner could give insight on the role of CCP3, in this case for its relation to the cytoskeleton. SKA1 is a protein required for kinetochore–microtubule attachments in cytokinesis that additionally could have a role in mitosis (Gaitanos *et al.*, 2009). SKA1 complex tracks depolymerizing microtubule ends and associates with both the microtubule lattice and curved protofilaments (Schmidt and Arthanari, 2012). The localization of hCCP3 in mitosis is consistent with SKA1 localization. Although further studies are required to fully confirm the association of SKA1 and CCP3, we might expeculate with two plausible scenarios: a direct SKA1-

hCCP3 interaction or an indirect interaction of hCCP3 with the same depolymerizing microtubules where SKA1 binds.

In summary, the CCP family seems to be integrated by carboxypeptidases with O-type substrate specificity based on its described deglutamylating activity (Lyons and Fricker, 2011). CCP3 would also present a lower processivity/intrinsic activity than the rest of CCPs. Differences in substrate affinity might explain the existence of a whole family of deglutamylating enzymes, with a conserved active site but highly diverse surrounding domains whose role remain unknown. The complete substrate repertoire of CCPs needs to be explored, as well as the regulatory mechanisms of these PTMs. Besides the already known relevance of these enzymes in neuroregeration and neurodegeneration, their newly described implication in mitosis and MTs point CCPs as targets for cancer therapy.

Chapter IV:
Functional characterization of mouse CCP2 and CCP3

CHAPTER IV: FUNCTIONAL CHARACTERIZATION OF MOUSE CCP2 AND CCP3

SUMMARY

The posttranslational modification of carboxy-terminal tails of tubulin plays an important role in the regulation of the microtubule cytoskeleton. Enzymes responsible for deglutamylating tubulin have been discovered within a novel family of mammalian cytosolic carboxypeptidases. The discovery of these enzymes also revealed the existence of a range of other substrates that are enzymatically deglutamylated. To date only four out of six mammalian cytosolic carboxypeptidases have been enzymatically characterized. Here we complete the functional characterization of this protein family by demonstrating that CCP2 and CCP3 are deglutamylases, with CCP3 being able to hydrolyze aspartic acids with similar efficiency. Deaspartylation is a novel posttranslational modification that could, in conjunction with deglutamylation, broaden the range of potential substrates that undergo carboxy-terminal processing. Additionally we show that CCP2 and CCP3 are highly regulated proteins confined to ciliated tissues. The report of two novel enzymes for carboxy-terminal protein modification provides novel insights into the broadness of this barely studied process.

RESULTS

1 Determination of CCP2 and CCP3 substrate specificities

In Chapter III, our alignments and structural modeling suggested that all human and mouse CCPs presents specificity towards acidic amino acids. This includes CCP2, the candidate for detyrosinating tubulin according to a recent report that attributed a detyrosinating activity to CCP2 in cells after knocking-down experiments (Sahab *et al.*, 2011). However unequivocal evidence for this activity was not provided. Furthermore,

considering that CCP2 and CCP3 are close paralogs (Rodríguez de la Vega Otazo *et al.*, 2013), we hypothesized that CCP2 may have similar substrate specificity and function to CCP3.

1.1 Prediction of substrate specificity for mouse CCP2

Likewise for hCCP3, we performed a structural model analysis to the homologous human CCP2 sequence. The identified catalytic and specificity determinant residues at the active site of hCCP3 correlate with hCCP2 model (**Figures3.9 C-D**). Moreover, the overlap of the structural models of hCCP3 and hCCP2 show that the main determinants of substrate binding are conserved in a comparable structure (**Figures 4.1 A**). This is consistent with hCCP3 and hCCP2 being deglutamylases.

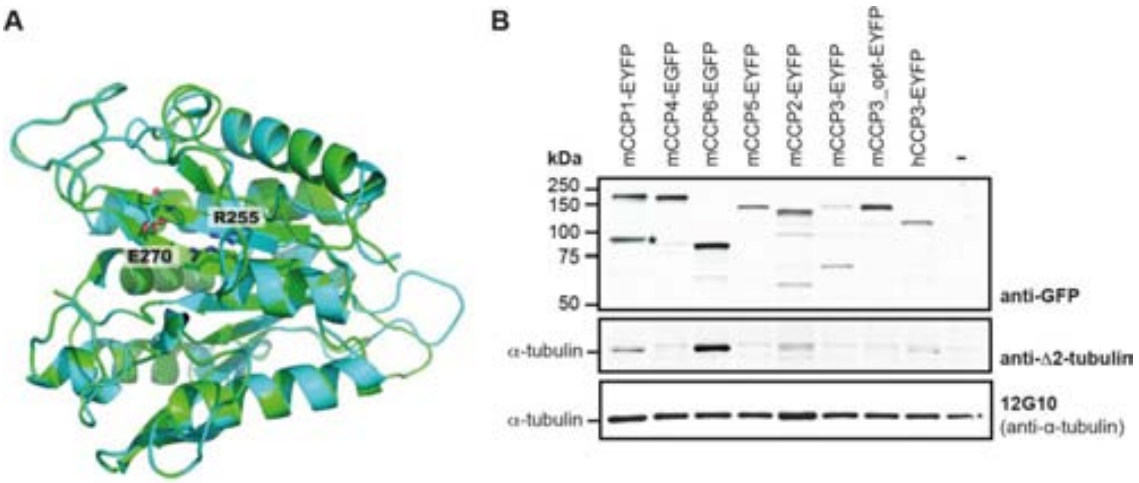

Figure 4.1. Structural model of human CCP2 and CCPs activity

A) *Overlapped model structures of hCCP2 (cyan) and hCCP3 (green) demonstrate the conserved positions in the active-site residues (key residues E270 and R255 are shown). The image of the structure was generated with PyMOL 1.3 overlapping the carboxypeptidase domain of hCCP2 model and hCCP3 model.* ***B)*** *Immunoblots of extracts of HEK293T cells, expressing YFP-tagged murine and human CCP proteins. Expression of YFP-CCPs was analyzed with anti-GFP, deglutamylating activity was visualized with anti-Δ2-tubulin labeling on endogenous α-tubulin. α-tubulin levels were controlled with 12G10 antibody. mCCP3_opt is a codon-optimized synthetic gene construct; hCCP3 is the human 72.6-kD isoform of CCP3 (Q8NEM8-2 Uniprot). *note the presence of a specific degradation product of mCCP1. (-) control without transfection.*

Deglutamylating activity for a human natural short CCP3 isoform was shown, and a similar function for hCCP2 was predicted. Previous experiments in our lab failed to associate a detyrosinating or deglutamylating function to CCP2. Similarly, the lab that first described mouse CCP1, CCP4, CCP5 and CCP6 as deglutamylases, could not show detyrosinating activity for CCP2 and CCP3 (personal communication C. Janke). This chapter, based on the results on hCCP3 and on its structural modelling, assesses the functional role of those phylogenetic-related CCPs.

1.1.1 Comparison of the activity for the different CCP family members

Deglutamylation can occur on the C-terminally exposed, gene-encoded glutamate residues of proteins, such as detyrosinated tubulin and myosin light-chain kinase (MLCK), or on posttranslationally added polyglutamate chains. This activity has been previously demonstrated for CCP1, CCP4 and CCP6, however no activity has so far been detected for CCP2 and CCP3 (Rogowski et al., 2010). One of the potential reasons for the absence of measurable activity of these two enzymes were their low expression levels as compared to the other CCP family members. To overcome this problem, we included a synthetic, codon-optimized cDNA of mouse CCP3 (Uniprot Q8CDP0-1), as well as the short human CCP3 isoform (Uniprot Q8NEM8-2) assayed in Chapter III. CCPs were expressed as YFP/GFP fusion proteins in HEK293T cells for 40 h.

After 40 h of expression, the cells were lysed and protein extracts analyzed by immunoblotting. As expected, CCP6 and CCP1 overexpression led to a marked increase in Δ2-tubulin, pointing them as the most active deglutamylases (Δ2-tubulin is barely detectable in these cells, thus increased levels indicate deglutamylating activity; **Figures 4.1 B**). A very weak signal of Δ2-tubulin was detected after overexpression of CCP2; but no clear Δ2-tubulin signal was seen after expression of full-length, codon-optimized murine CCP3. Instead, as expected from the results presented in Chapter III, human CCP3 generated a slight increase in the Δ2-tubulin signal (**Figures 4.1 B**). The simplest explanation to understand the behavior of the different CCP3 forms is that

the 72.6-kDa human CCP3 isoform we used was shorter than 116-kDa murine CCP3, and might thus be more active or better expressed in cells, analogous to what we previously observed for truncated glutamylase enzymes from the TTLL family (van Dijk *et al.*, 2007; Rogowski *et al.*, 2009).

1.2 CCP2 and CCP3 generate Δ2-tubulin in cells

1.2.1 Truncated forms of mouse CCP2 and CCP3 can generate Δ2-tubulin

Initially based on the size of hCCP3, a series of truncated forms of murine CCP2 and CCP3 were generated in order to determine the minimal active size of these enzymes (**Table 2.2**). Truncation was performed on the N-terminus and C-terminus of the enzymes keeping intact the CCP-conserved N-domain and carboxypeptidase domain (**Figures 4.2 A**). The YFP-tagged truncated forms were expressed in HEK293T cells, and their activity was assessed by immunoblot for Δ2-tubulin (**Figures 4.2 B**).

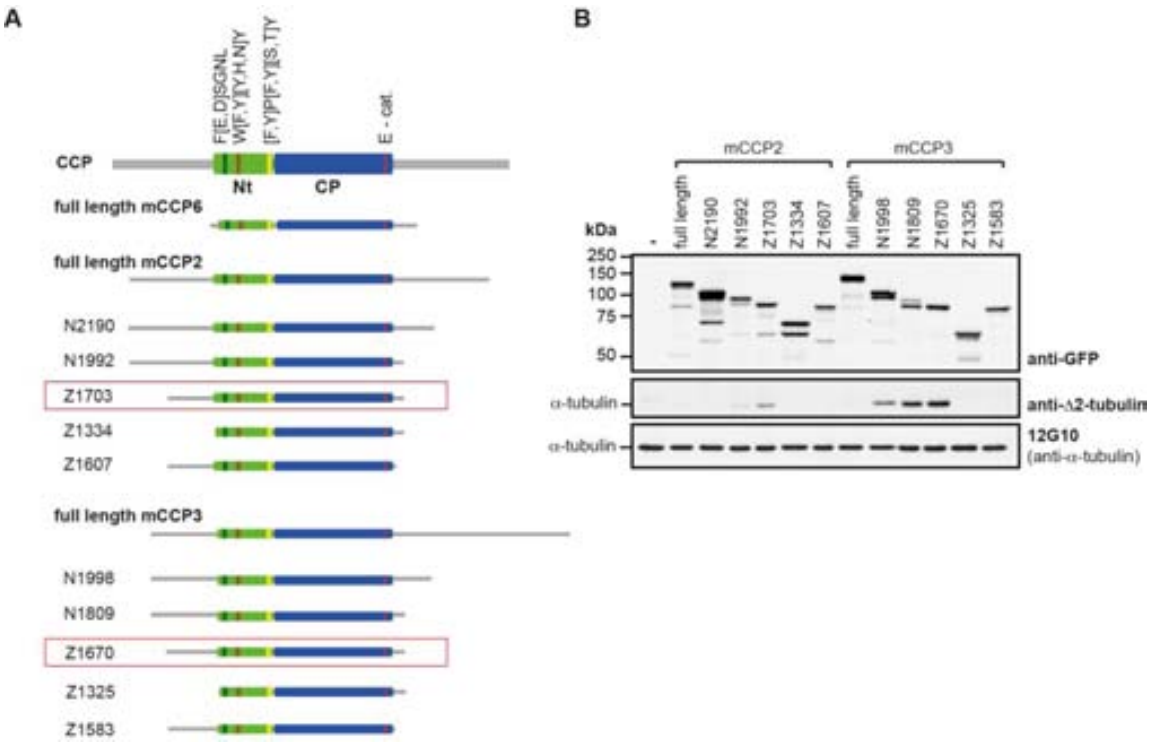

Figure 4.2. Sequence optimization of active mCCP2 and mCCP3

A) *Scheme of full-length of mCCP6, mCCP2, mCCP3 and several truncated forms of mCCP2 and mCCP3. The green boxes indicate the conserved N-domain (Nt) specific to CCPs, the blue box represents the conserved carboxypeptidase domain (CP; compare with* ***Figure 4.4 A****). The*

carboxypeptidase domain were delimitated with Superfamily 1.73 database (Gough *et al.*, 2001). *Gray lines represent non-conserved sequences that were partially truncated in this optimization assay.* ***B)*** *Immunoblot analysis of HEK293T cell extracts expressing different forms of YFP-mCCP2 and YFP-mCCP3 described in (A). The deglutamylase activity is monitored by the generation of Δ2-tubulin. 12G10, an anti-α-tubulin antibody, is used as a control of loading.*

Indeed, the truncated versions of both, murine CCP2 and CCP3 showed a clear Δ2-tubulin-generating activity, demonstrating that both could act as deglutamylating enzymes. The shortest and most active versions are CCP2_Z1703 and CCP3_Z1670, which were obtained by truncating non-conserved N- and C-terminal sequences, to obtain 65-kDa proteins that were similar in size and domain structure to the highly active deglutamylase CCP6 (**Figures 4.2A**). Note that to confirm that our truncated 65-kDa versions of mCCP2 and mCCP3 represent the shortest active version of these enzymes, further truncation of short sequences at their N- and the C-termini was performed, resulting in a decrease of the observed activity.

1.2.2 A short non-conserved C-terminal region is essential for CCP2/CCP3 activity

The fragment present in mCCP2_Z1703 and mCCP3_Z1670, absent in mCCP2_1607 and mCCP3_Z1583 appear to be essential for CCP2 and CCP3 activity (**Figures 4.2 A**). Consequently, this region was analyzed for secondary structure prediction and found to have a high probability to adopt a coiled-coil structure (**Figures 4.3**). Coiled-coil structures are known to participate in structural stabilization and oligomerization of proteins (Parry *et al.*, 2008). It is thus possible that the removal of these coiled-coil sequences from mCCP2 and mCCP3 resulted in partially misfolded enzyme altering the active site, and consequently in loss-of-activity. Alternatively, it could indicate that both enzymes need this short region for stabilizing or interacting with the substrate.

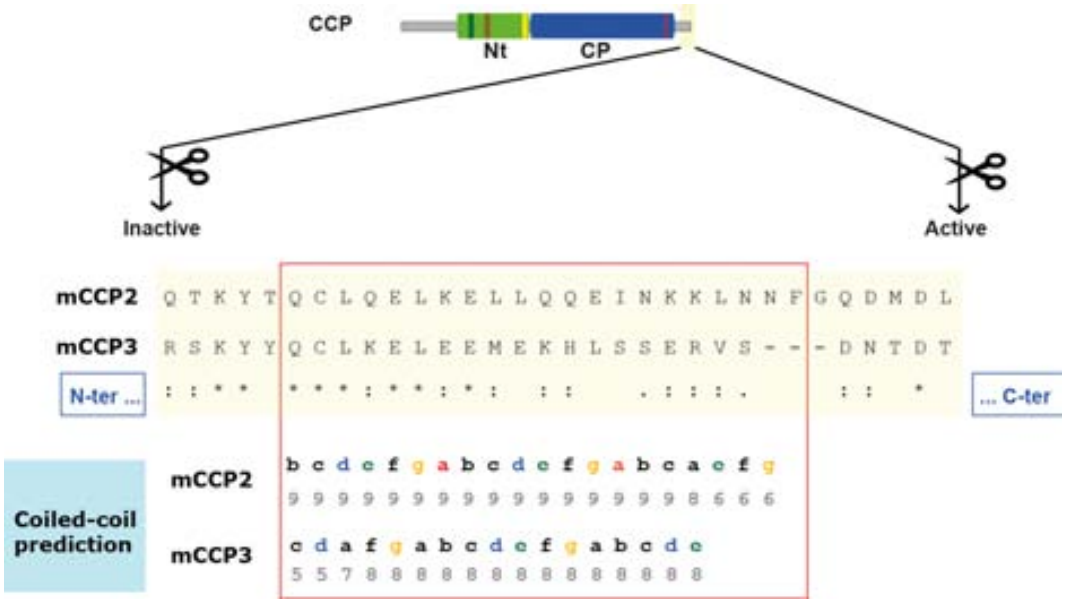

Figure 4.3. Secondary structure in the C-terminus of optimized CCP2 and CCP3
Secondary structure prediction of the C-terminal fragment of mCCP2_Z1703 and mCCP3_Z1670 performed with Coils server (Lupas *et al.*, 1991). *Note that in the absence of this sequence the protein is expressed but no activity is detected.*

1.3 Characterization of the truncated forms of mouse CCP2 and CCP3

1.3.1 Characterization of the deglutamylating activity of mCCP2 and mCCP3

To demonstrate that the observed Δ2-tubulin generation after CCP2 and CCP3 expression is directly catalyzed by their active carboxypeptidase (CP) domains, we generated enzymatically-dead versions by mutating the essential catalytic residues Glu593 in mouse CCP2, and Glu540 in mouse CCP3 (Glu270 in bovine CPA, and Glu1094 in mouse CCP1 (Wu *et al.*, 2012)). Enzymatically dead mutants of full-length and truncated versions of CCP2 and CCP3 (**Figure 4.4 A**) were expressed at similar levels as the active forms, but did not generate Δ2-tubulin (**Figure 4.4 B**). Strikingly, a very faint Δ2-tubulin band present in the control cells is now absent in the cells overexpressing the enzymatically dead enzymes (**Figure 4.4 B**), suggesting that these enzymes may possibly act as dominant negative competitors for endogenous enzymes. Immunocytochemical analysis of HEK293T cells expressing CCP2 and CCP3 further showed a specific Δ2-tubulin labeling associated with the MTs in YFP-positive cells (**Figure 4.4 C**).

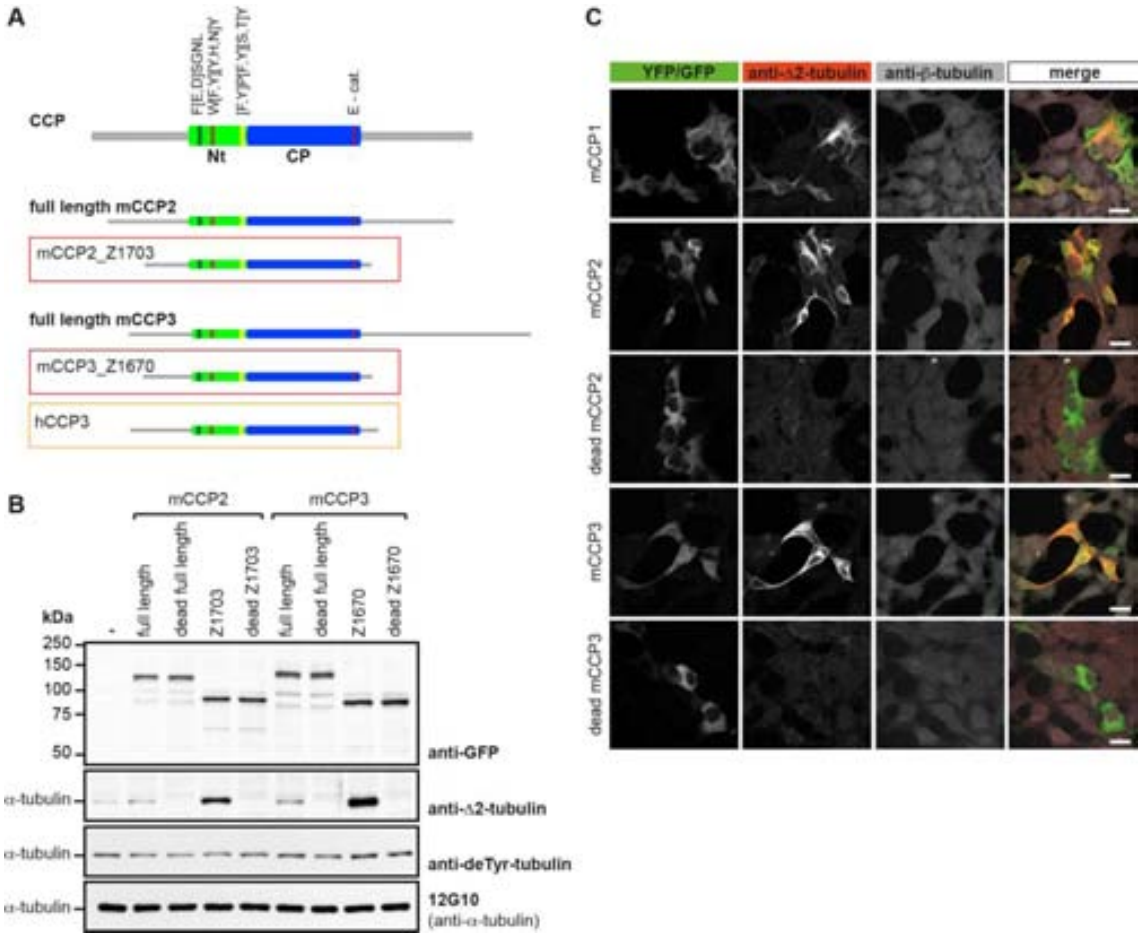

Figure 4.4. CCP2 and CCP3 generate Δ2-tubulin in HEK293T cells

A) *Scheme of a generic CCP; full-length and truncated forms of mCCP2 and mCCP3, and the 72.6-kDa hCCP3 isoform. The green boxes indicate the conserved N-domain (Nt) specific to CCPs, with FESGNL, WYYY and YPYTY as conserved motifs* (Rodriguez de la Vega *et al.*, 2007). *The blue box shows the conserved carboxypeptidase domain (CP) with the catalytic residue E270 (E-cat). Gray lines are non-conserved sequences that were partially truncated in the optimization. The shortest truncated versions that are still enzymatically active are mCCP2_Z1703 and mCCP3_Z1670 (red boxes). They are shown in comparison to the full-length versions and to hCCP3 (orange box).* ***B)*** *Immunoblot of cell extracts from HEK293T cells expressing YFP-tagged full-length mCCP2 and mCCP3, their optimized truncated forms (A) and enzymatically dead versions as controls. Δ2-tubulin was used as readout for deglutamylating activity. Detyrosination and deglutamylase activities were followed by generation of deTyr- and Δ2-tubulin. Active enzymes generate exclusively Δ2-tubulin.* ***C)*** *Immunocytochemistry of HEK293T cells transfected with active and inactive truncated YFP-tagged mCCP2 and mCCP3, as well as with GFP-mCCP1. After fixation of the cells with a protocol preserving microtubule structures* (Bell and Safiejko-Mroczka, 1995)*, Δ2-tubulin was detected. Images were collected on an inverted confocal microscope (Leica SP5) using a 63X objective at 25 °C and analyzed with LAF AS Lite 1.8.1 (Leica). Scale bar: 20 µm.*

These experiments demonstrate that the deglutamylating activities of CCP2 and CCP3 are mediated by their CP catalytic domain, leading to Δ2-tubulin generation.

1.3.2 CCP2 is not involved in detyrosinating tubulin

CCP2 was previously suggested to have a detyrosinating activity (Sahab *et al.*, 2011). Although comparison of active sites of CCPs with CPA, an enzyme that specifically hydrolyzes Tyr from C-terminal positions (Argarana *et al.*, 1980), strongly suggested that CCPs cannot catalyze Tyr hydrolysis (**Figure 4.1 A**), we still tested this possibility experimentally. We used the deTyr-tubulin antibody to specifically detect the generation of detyrosinated tubulin in HEK293T cell extracts overexpressing the optimized forms of CCP2 and CCP3. No detectable differences were observed in detyrosinated tubulin, while the increase of Δ2-tubulin signal clearly indicated the activity of the overexpressed enzymes (**Figure 4.4 B**). Thus, mCCP2 and mCCP3 are not involved in the detyrosination of tubulin, and the identity of these long-searched for enzymes (Argaraña *et al.*, 1978) still remains a conundrum.

2 Enzymatic specificities of CCP2 and CCP3

2.1 CCP2 and CCP3 can remove long polyglutamic chains

To further characterize if CCP2 and CCP3 can remove subsequent glutamate residues from longer stretches of glutamates, such as those generated by enzymatic polyglutamylation (Audebert *et al.*, 1993; van Dijk *et al.*, 2007), or genetically encoded as in the case of MLCK, C-terminally engineered versions of telokin were used. Telokin is a short version of MLCK, which is one of the few known substrates of CCP1 (Rogowski *et al.*, 2010). Truncated active versions of CCP2 and CCP3 were co-expressed in HEK293T cells together with different C-terminal variants of YFP-telokin. The deglutamylation (removal from long glutamate chains) was monitored using the polyE antibody in immunoblot analysis (Shang, 2002), and the final deglutamylation product (carrying only one glutamate) was detected with the anti-Δ2-tubulin antibody (**Figure**

4.5 A-B). Both, CCP2_Z1703 and CCP3_Z1670 were able to trim long (7-Glu) and shorter polyglutamate chains from the C-terminus of engineered telokin, as shown by decreased polyE signals and increased of Δ2-tubulin immunoreactivity (**Figure 4.5 C**). CCP1, known to shorten long glutamate chains, was used as positive control.

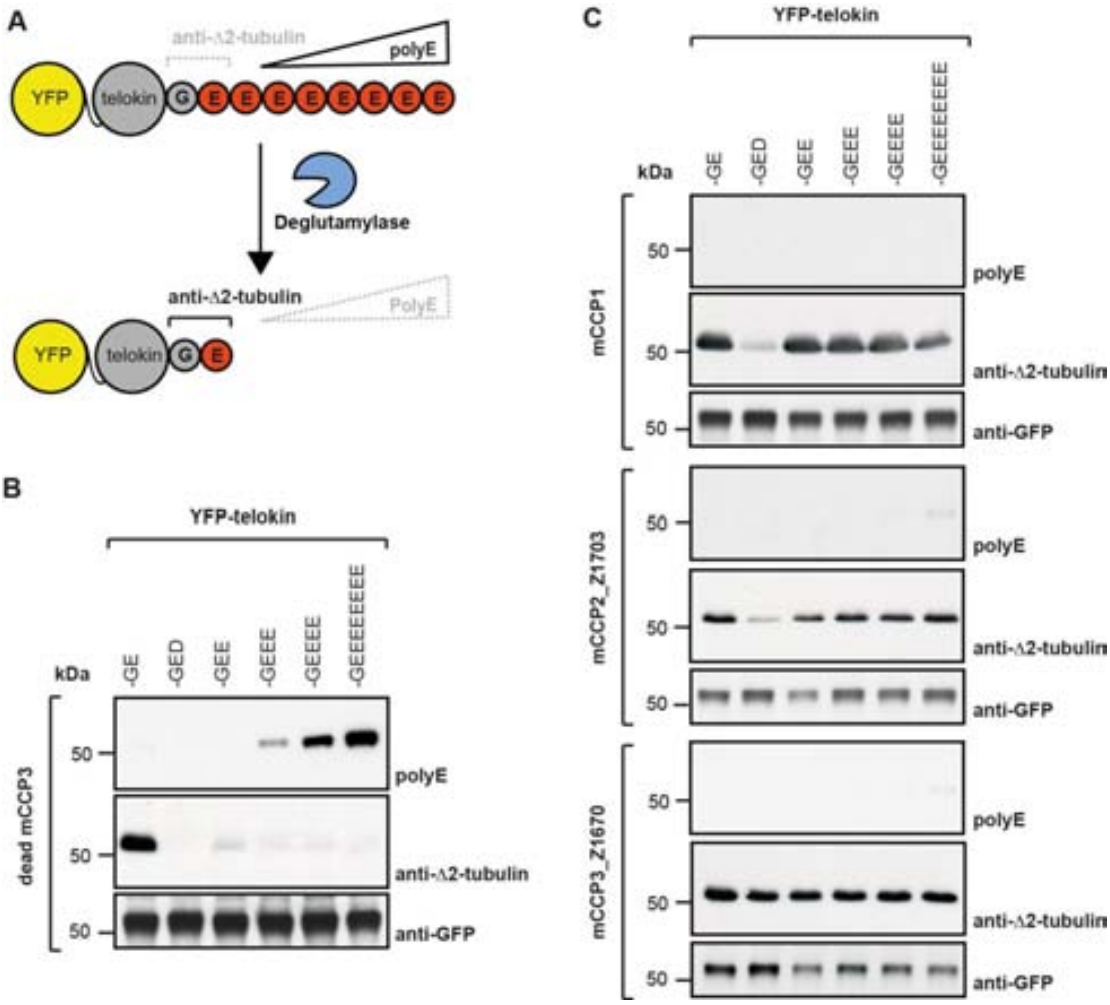

Figure 4.5. Substrate specificity of mCCP2 and mCCP3

A) *Schematic representation of the experimental setup. PolyE antibody recognizes telokin constructs with three or more consecutive C-terminal glutamate residues, while anti-Δ2-tubulin antibody detects specifically the C-terminal –GE epitope. C-terminal degradation is detected by generation of the Δ2-tubulin epitope on telokin* (Rogowski *et al.*, 2010). ***B)*** *Immunoblot analysis of HEK293T extracts after coexpression of YFP-deadCCP3 and YFP-telokin variants. This immunoblot shows how the polyE and anti-Δ2-tubulin antibodies detect the different telokin variants in absence of CCP activity.* ***C)*** *Immunoblot analysis of HEK293T extracts after coexpression of different YFP-CCPs and YFP-telokin variants. Activity is monitored as shown in (**A**). The activity of truncated mCCP2 and mCCP3 (**Figure 4.4 A**) is tested with telokin variants with different numbers of consecutive glutamate residues to test processivity, and with an*

aspartate residue to test specificity. The activities are compared to mCCP1, a well characterized deglutamylase (Rogowski *et al.*, 2010)*, and a dead version of mCCP3 as negative control. Note that only mCCP3 removes aspartate efficiently.*

2.2 CCPs can remove aspartic acids from protein C-termini

2.2.1 CCP3 has no preference for either aspartic or glutamic acids

According to the predictions from the molecular modeling, any negatively charged residue would be susceptible to be cleaved by CCPs, so aspartic acid could be considered as substrate. However, the previously tested CCP1, CCP4 and CCP6 where shown to exclusively process glutamate residues and no activity was observed on aspartate residues (Rogowski *et al.*, 2010). In order to test the specificity of CCP2 and CCP3, we co-expressed them with telokin variants exposing either one or two aspartic acids at their C-termini. CCP1 and CCP2 generated weak anti-Δ2-tubulin reactive bands at ~55 kDa when cleaving Asp, but a much stronger signal if telokin with C-terminal glutamate was expressed (**Figure 4.5 C**). Surprisingly, CCP3 converted both aspartate and glutamate-ending telokin variants to their Δ2-form with similar efficiency (**Figure 4.5 C**).

In order confirm whether aspartic acid residues had an inhibitory effect on the processivity of CCPs, we generated a telokin version ending with two aspartic acid residues and test this substrate in comparison with the ones previously assayed (**Figure 4.6 A)**. CCP3 converted the telokin ending with double aspartate into the anti-Δ2-form with the same efficientcy than the cleavage of one aspartate and one or more glutamic acid residues, while CCP1 and CCP2 discriminate aspartic from glutamic acids.

The weak Δ2-signal generated from Asp-telokin by CCP1 and CCP2 could be either related to a low-rate aspartate cleavage of the otherwise glutamate-specific enzymes, due to the strong overexpression, or represent endogenous Δ2-tubulin (**Figures 4.5 C** and **4.6 A**). In any case it is clear from this experiment that both, CCP1 and CCP2 preferentially hydrolyze glutamate from the C-terminus of proteins. In contrast, CCP3 has no enzymatic preference either for glutamic acids or for the

removal of C-terminal aspartate residues, which might be involved in the modification of a range of proteins.

2.2.2 Comparative analysis of C-terminal acidic tails in the genome

To check the potential impact of the novel enzymatic activity on the functional broadness of enzymatic C-terminal degradation of proteins on a proteome level, we compared the number of proteins with C-terminal poly-Glu stretches, which can be substrates of deglutamylases (Rogowski *et al.*, 2010), with the number of proteins with acidic C-terminal tails (in this case considering both Glu and Asp residues). We restricted our analysis to four very well annotated proteomes of *Homo sapiens*, *Mus musculus*, *Drosophila melanogaster* and *Caenorhabditis elegans* (**Figure 4.6 B**).

Three main conclusions can be drawn from the numbers we obtained. First, the presence of a deaspartylating activity (CCP3 and possibly other CCPs) strongly increases the number of proteins that could be C-terminally modified by the CCP family. Second, the number of proteins with acidic C-terminal stretches is much higher in the mouse and human as compared to *D. melanogaster* and *C. elegans*. This could indicate a greater need of this regulatory mechanism in more complex organisms, which is also underlined by the greater number of CCP genes in mouse and human as compared to *D. melanogaster* and *C. elegans*. Finally, it is not yet clear if deaspartylation activity is found in the latter two invertebrates, as clear homologs of CCP3 have so far not been identified. It thus appears that the discovery of a deaspartylating activity for CCP3 could have a marked impact on the functional reach of C-terminal degradation, and deliver essential evolutionary insight into the development of this PTM.

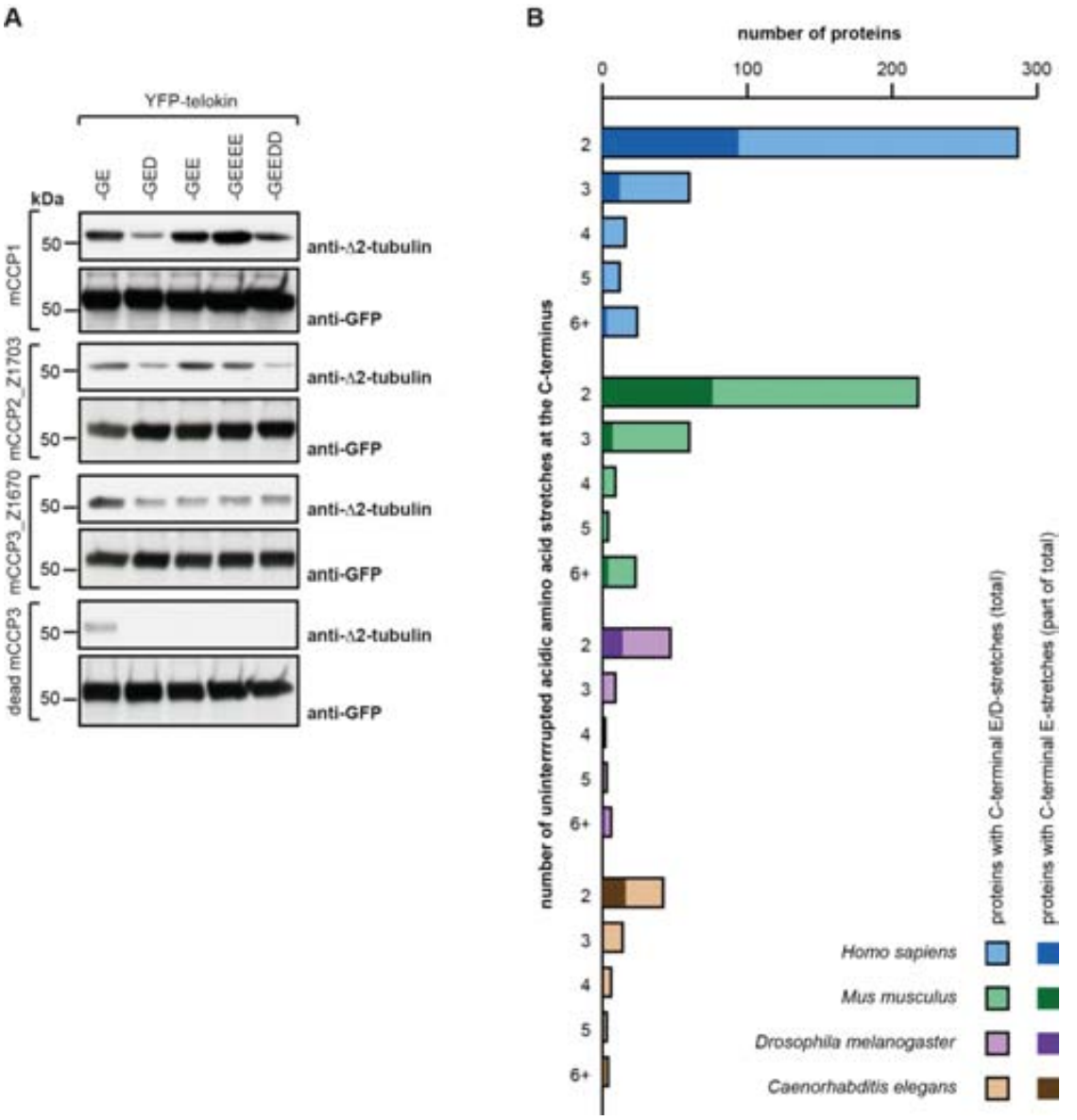

Figure 4.6. Insight into the deaspartylating activity of CCPs

A) *Coexpression of active or dead truncated forms of YFP-mCCP2 and YFP-mCCP3 together with YFP-telokin variants ending in different acidic tails to test their ability to release single of multiple Asp and/or Glu residues. Generation of the Δ2-tubulin epitope on telokin is used to monitor C-terminal degradation. mCCP1 is used as positive control for deglutamylation. Note that only mCCP3-Z1670 is efficiently removing single and consecutive Asp residues.* ***B)*** *Bioinformatic analysis of the number of proteins with uninterrupted C-terminal acid sequence stretches. Each column represents the total number of proteins per category (mixed Asp and Glu stretches), and the darker insets represent uninterrupted Glu-stretches.*

2.3 CCP2 and CCP3 are not deglycylases

Glycylation is a posttranslational modification similar to polyglutamylation, performed by members of the TTLL family (Rogowski *et al.*, 2009). So far, nothing is known about the enzymes responsible for shortening or removing this posttranslationally added glycine side-chains from tubulin. The unique deglycylase identified until present is an M20 peptidase family member in *Giardia duodenalis* (Lalle *et al.*, 2011). As this enzyme is deglycylating rather the 14-3-3 proteins, and as M20 peptidases are not found in the mammalian genome, other candidates were considered as potential deglycylases in mammals, with CCP2 and CCP3 among them. Glycylation is typically enriched on the axonemes of motile cilia and flagella (Redeker *et al.*, 1994). Thus, the presence of CCP2 and CCP3 genes in ciliated organisms (Rodríguez de la Vega Otazo *et al.*, 2013), and their strong expression in mouse tissues with motile cilia such as testis and trachea (**Figure 4.8 A**) provided a potential link to glycylation. While the structural model suggests that both enzymes are rather specific to acidic amino acids (**Figures 3.10** and **4.1 A**), we still wanted to obtain an additional experimental proof to confirm this notion. Our attempts to directly test deglycylase activity in cells with glycylated MTs, which could be generated by expression of glycylating enzymes, failed due to the toxicity of this treatment for the cells. Thus, we developed an alternative test for deglycylating activity, in which a modified telokin containing four Gly residues on the very C-terminus was co-expressed with the CCPs. This construct is specifically detected with the polyclonal antibody polyG, and removal of only one Gly residue would completely abolish detection (**Figure 4.7 A**). This construct was co-expressed together with CCP2_Z1703 or CCP3_Z1670, and a similar experiment was performed with a polyE antibody and a telokin with four Glu residues as positive control (**Figure 4.7 B**). While both CCP2_Z1703 and CCP3_Z1670 were perfectly able to remove C-terminal glutamates, the absence of changes in the polyG signals strongly suggest that C-terminally located Gly residues cannot be hydrolyzed by these enzymes. Thus, CCP2 and CCP3 would not carry an intrinsic deglycylase activity.

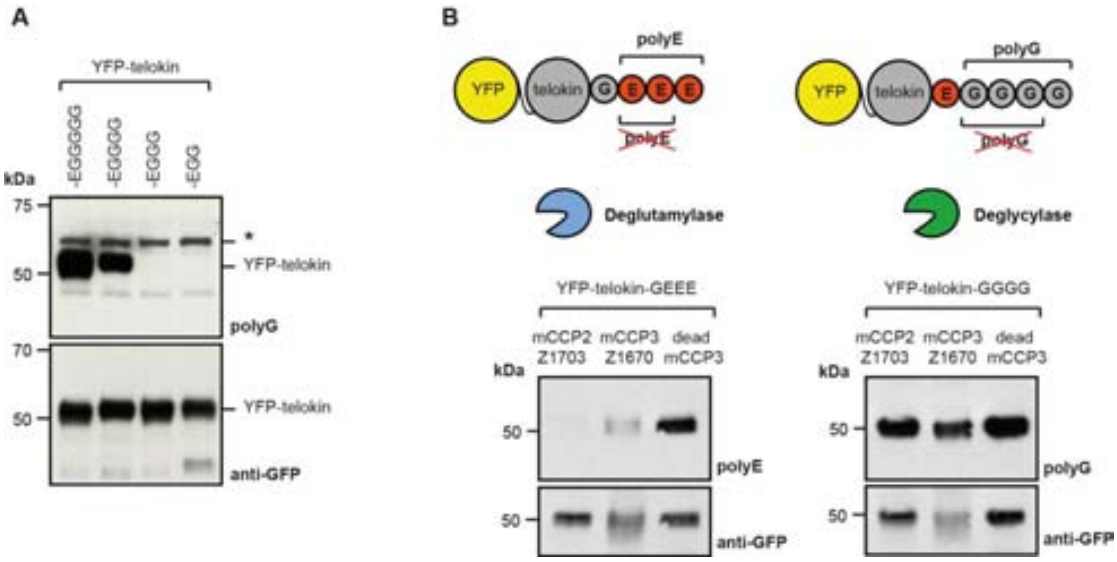

Figure 4.7. Test for deglycylating activity of mCCP2 and mCCP3.
A) *Epitope mapping of polyG antibody on artificial C-terminal tails of YFP-telokin with different numbers of Gly residues. Note that only poly-Gly chains of four and longer are recognized by this antibody. (*non-specific band recognized by the polyG antibody).* ***B)*** *Schematic representation of the experimental setup used to identify deglutamylation and deglycylation activities. YFP-telokin with 3-Glu tails (detected by the polyE antibody) or 4-Gly tails (detected with the polyG antibody) co-expressed with YFP-CCPs. The immunoblots show that truncated versions of YFP-mCCP2 and YFP-mCCP3 efficiently remove C-terminal Glu residues thus extinguishing the polyE signal. In contrast, no change in the polyG signal was detected.*

3 CCP2 and CCP3 have a potential role in cilia

3.1 CCP2 and CCP3 expression profiles in mouse tissues

Having demonstrated that all members of the CCP family are deglutamylating enzymes, we wanted to gain more insights into their specific functions on the whole-organism level. We thus quantified the relative expression levels of all six CCP family members by quantitative RT-PCR (qRT-PCR) with cDNA samples prepared from a representative range of organs. While qRT-PCR data are semi-quantitative, it was obvious that both CCP2 and CCP3 are expressed at relatively low levels in most organs (**Figure 4.8**, middle row), especially when compared to CCP1 (**Figure 4.8**, upper left). CCP4, in contrast, was barely detectable in a range of organs, suggesting a very specialized function in the subgroup of organs where it is expressed (**Figure 4.8**, upper right). CCP5 is higher expressed in testis more than any other tissue suggesting a role

in this male reproduction; while CCP6 has a similar profile to CCP1, being expressed in neuronal tissue (cortex, hippocampus, olfactory bulb) and testis.

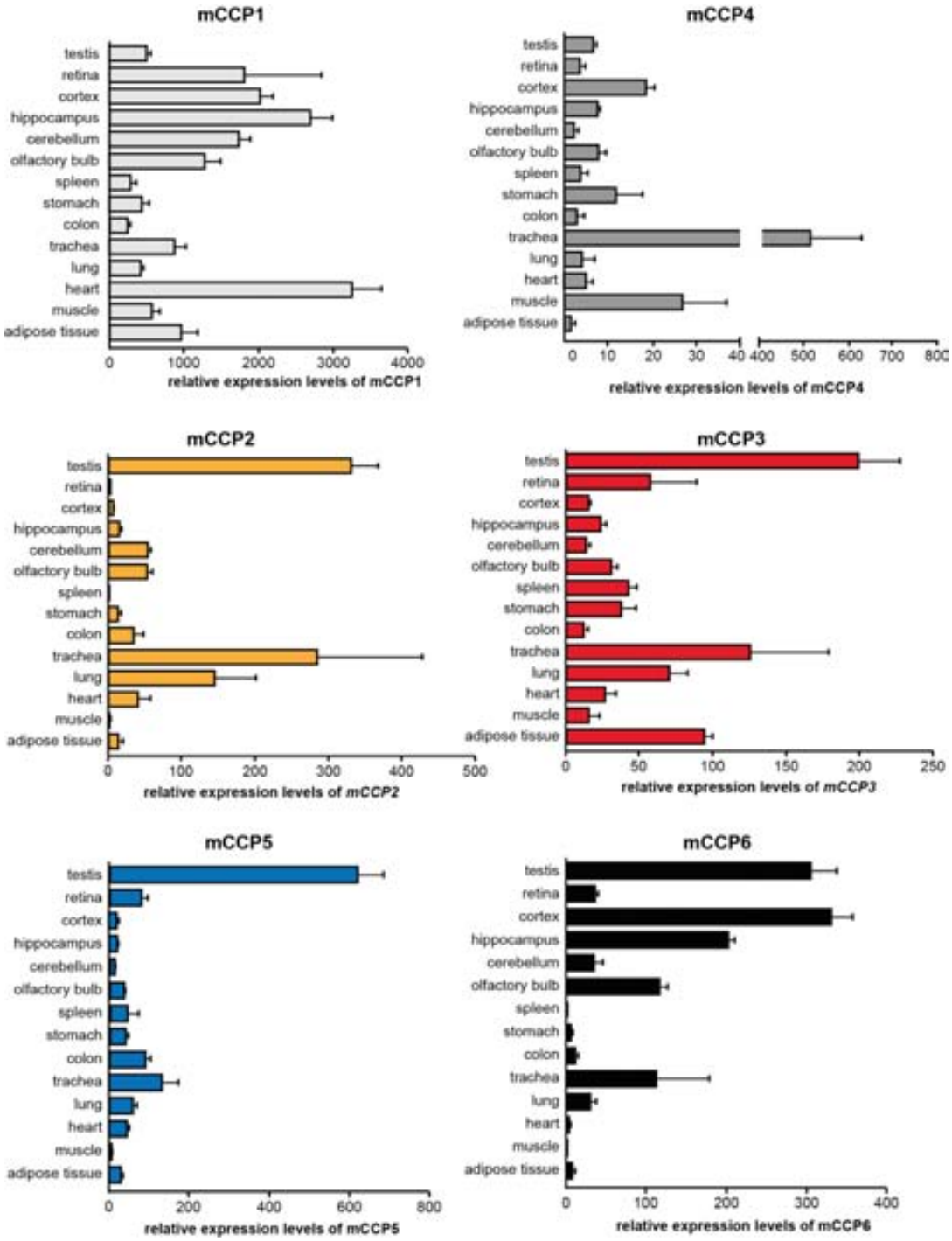

Figure 4.8. Analysis of mCCPs expression in mouse tissues

Relative expression levels of the six mouse CCPs in different organs of wild type mice as determined by qRT-PCR. Average values relative to the Tbp gene expression are represented, and error bars represent standard deviation of five independent experiments.

The expression profiles of CCP2 and CCP3 are highly similar; both enzymes are predominantly found in testis, trachea and lung, all tissues containing cells with motile cilia (**Figure 4.8**, middle row). In two tissues, the retina and adipose tissue, CCP3 was relatively strongly expressed while CCP2 was barely detected, in line with previous observations (Kalinina *et al.*, 2007).

Comparing the relative expression levels of the CCP enzymes as determined by qRT-PCR, it is clear that CCP1 is the deglutamylase with the highest expression levels and the broadest distribution in different tissues (**Figure 4.9 A**). While this does not allow judging the functional importance of those enzymes, it suggests that CCP1 catalyzes a large share of deglutamylation reactions. Indeed, the knockout model for CCP1, the Purkinje cell degeneration (*pcd*) mouse, shows severe defects related to tubulin hyperglutamylation in several organs (Rogowski *et al.*, 2010). In contrast, other CCP enzymes might have more specialized functions in specific cells, organelles or even on some selected MTs within cells.

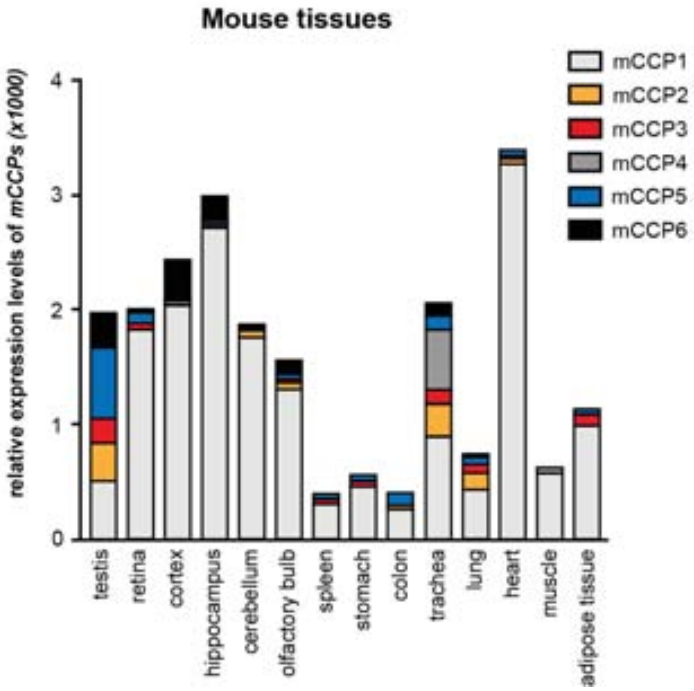

Figure 4.9. Expression of mCCP2 and mCCP3 in mouse tissues in cumulated view
*Cumulated view of the relative expression levels of all six CCP genes in different organs of 4-month-old wild type mice as determined by qRT-PCR (values from **Figure 4.8**). Average values relative to the Tbp gene expression are represented.*

3.2 CCP2 and CCP3 are upregulated during ciliogenesis

The elevated expression levels of CCP2 and CCP3 in ciliated tissues containing axonemes, such as testis, lung and trachea, suggest a potential role of these enzymes in the assembly or function of cilia. To investigate this link, we quantified the expression of all six CCPs during ciliogenesis in IMCD3 cells in culture by qRT-PCR at 0, 3 and 5 days after induction of ciliogenesis by serum starvation. Apart from CCP4, all other CCPs could be detected, but only CCP2 and CCP3 show a statistically significant increase of expression levels during ciliogenesis (**Figure 4.10**). Thus, several enzymes of the deglutamylase family are likely to be involved in ciliary outgrowth, maintenance and function. TTLLs have been shown to participate in cilia assembly and function through regulating the glutamylation levels (Bosch Grau *et al.*, 2013; Pathak *et al.*, 2014), but also the reverse enzymes, CCPs, might be involved in cilia. Among the six CCPs, CCP2 and CCP3 are likely to play highly specific role in these processes.

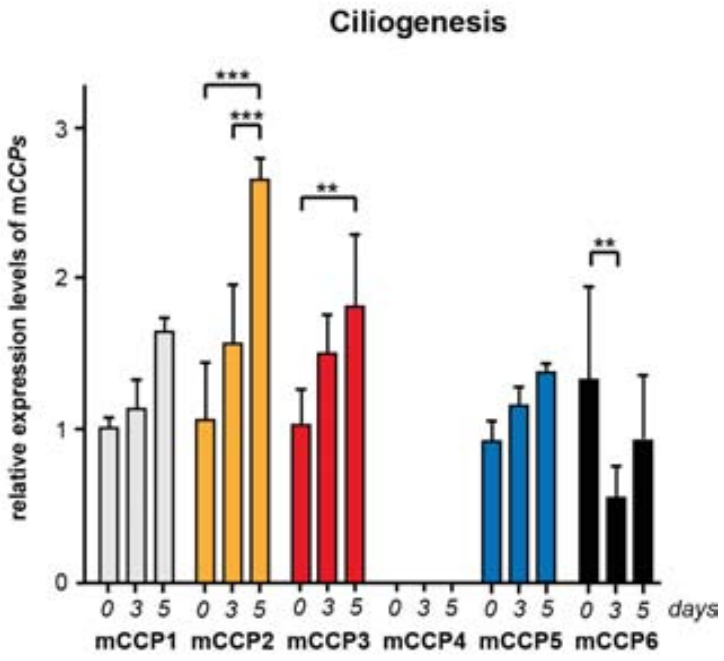

Figure 4.10. Expression of mCCPs during ciliogenesis

*qRT-PCR analysis of expression levels of all six CCP genes during ciliogenesis in cultured IMCD3 cells. Cells were serum-starved and analyzed at 0, 3 and 5 days after starvation. Mean values of expression levels relative to Tbp expression and relative to 0 day from 3 to 5 independent experiments are shown; error bars show standard deviation. Two-way ANOVA was used to determine significance levels (**p<0.01; ***p<0.001).*

4 CCP2 and CCP3 knockout mice display deficiencies in polyglutamylation

4.1 CCP2 KO and CCP3 KO mouse

4.1.1 Screening in mouse tissues in search of alteration in PTMs

In order to corroborate the deglutamylating activity of CCP2 and CCP3 *in vivo*, polyglutamylation levels were studied in the CCP2 and CCP3 KO mice. In a first screening a wide set of organs were evaluated for polyglutamylation and Δ2-tubulin immunoreactive bands and the total amount of tubulin (12G10) was used to evaluate protein loading. The purpose of this screening was to identified organs or tissues that could be affected as a result of the lack of CCP2 or CCP3.

In general, few changes in polyglutamylation or Δ2-tubulin were observed in both *Agbl2* (CCP2) and *Agbl3* (CCP3) KO mice compared to wild type (**Figure 4.11**). The only tissue showing indices of tubulin hyperpolyglutamylation was the testis from the *Agbl2* KO (**Figure 4.11 A**). On the other hand, a few non-tubulin proteins showed reactivity against the Δ2-tubulin or PolyE antibodies in tissues such as retina, kidney, stomach, colon or muscle in the mouse tissue analysis. In the KO mice but also in the wild type, the polyE antibody could distinguish a band of 130 kDa in stomach and retina and a band of 35 kDa in cortex. Also the Δ2-tubulin antibody detected bands at 130-KDa and 35 kDa (**Figure 4.11**). In the analysis of *Agbl3* KO tissues, it is relevant the differential immunoreactivity of a 130-kDa protein to the polyE antibody compared to the wild type (**Figure 4.11 A**). Particularly, this 130 kDa band resembles a previous observation in the *pcd* mouse, in which the 130-kDa substrate was identified as MLCK, of which the C-terminal glutamate stretch is detected with polyE (Rogowski *et al.*, 2010).

This screening over a wide range of tissues helped designing a strategy for focusing on putative affected tissues due to the lack of CCP2 or CCP3.

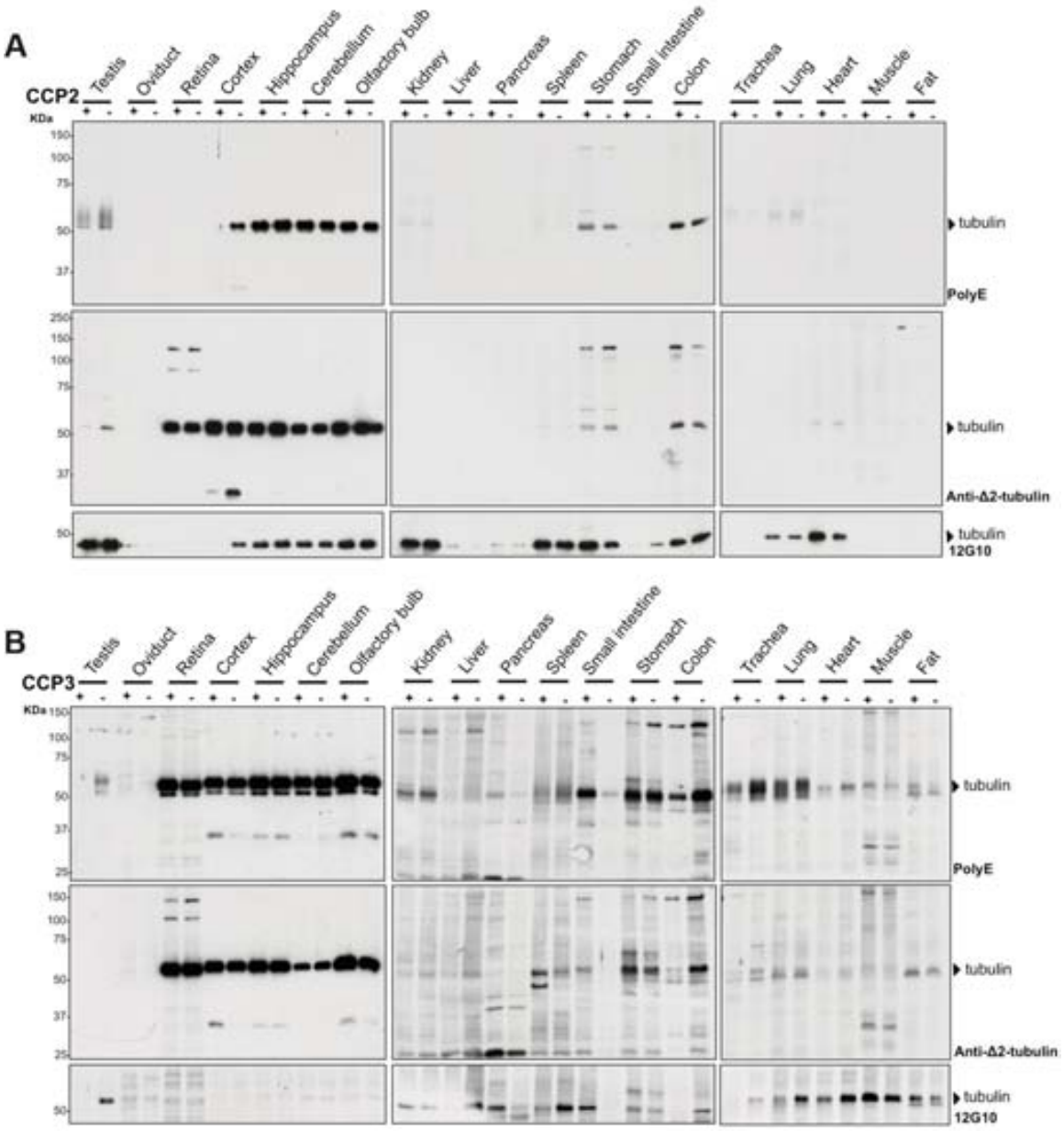

Figure 4.10. Screening for polyglutamylation and Δ2-tubulin in*Agbl2* and *Agbl3* KO mice
*Immunoblot screening of protein extracts from different organs of wild type (WT) and Agbl2 (**A**) or Agbl3 (**B**) KO mice, using the polyE and Δ2-tubulin antibodies. Total tubulin levels were detected with anti-α-tubulin antibody (12G10).*

4.1.2 Hyperpolyglutamylated substrate in *Agbl2*-KO and *Agbl3*-KO mice

In order to determine differences between the KOs and the WT mice, a more accurate analysis was performed in selected tissues. Tissue extracts of stomach, oviduct, testis, cerebellum and kidney were evaluated for their polyglutamylation levels and set in comparison between both KOs and its respective wild-type

littermates. Few variations were observed in the tubulin band but an increase in polyE immunoreactivity of a 130-kDa substrate (possibly MLCK) was observed in stomach of the *Agbl2*-KO mice, as well as in stomach and oviduct of the *Agbl3*-KO mice. These data show that in certain organs MLCK is predominantly modified by CCP2, CCP3 or by both enzymes (**Figure 4.11**), but so far no visible phenotype could be related to this change in deglutamylation in these mice.

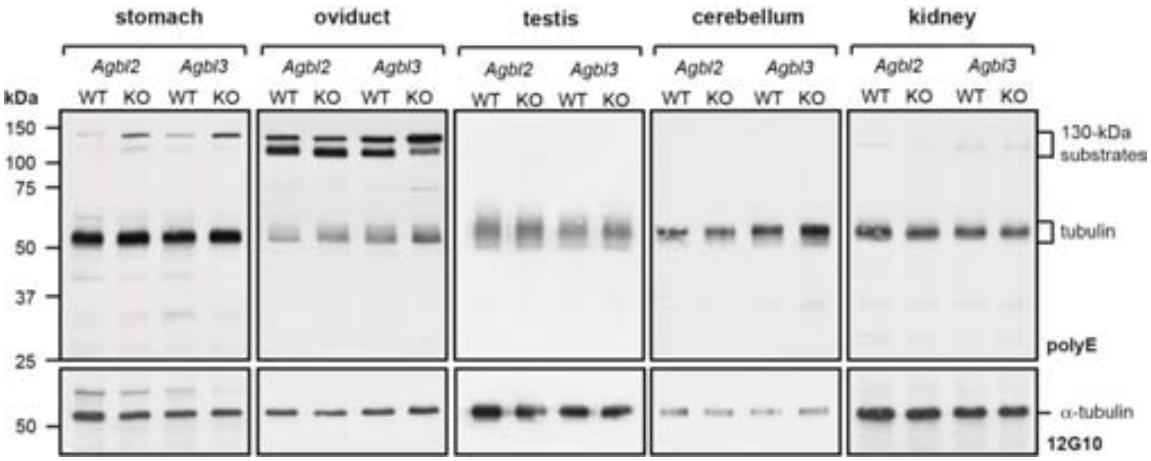

Figure 4.11. Polyglutamylation levels in *Agbl2* and *Agbl3* KO mice
Comparative immunoblot analysis of protein extracts from different organs of wild type (WT) and Agbl2 or Agbl3 KO mice with the polyE antibody. Total tubulin levels were detected with anti-α-tubulin antibody (12G10). Note that a 130-kDa substrate shows increased polyE immunoreactivity in stomach of Agbl2 or Agbl3 KO mice, and in oviduct of the Agbl3 KO mouse.

4.2 Polyglutamylation levels in the double CCP2/CCP3 KO mouse

The similar expression profiles of CCP2 and CCP3 determined by qRT-PCR and previously by *in situ* hybridization (Kalinina *et al.*, 2007) suggest some functional overlap of these two enzymes. As the individual knockout (KO) mouse models for CCP2 (*Agbl2*) and CCP3 (*Agbl3*) are both fertile, we generated double (*Agbl2*/*Agbl3*) KO mice. These mice were viable and displayed no obvious phenotypic alterations. To study the potential change in polyglutamylation levels on tubulin and other proteins, we dissected selected organs, prepared tissue extracts and analyzed them with the polyE antibody in immunoblot (**Figure 4.12 A**), similarly to the study we performed for

the individual KOs. Compared to wild type mice, tubulin polyglutamylation was increased in testes and sperm of the *Agbl2/Agbl3* double knockout mice (**Figure 4.12 B-C**). Apart from testes and sperm, no other organ showed detectable changes in tubulin polyglutamylation levels in *Agbl2/Agbl3* KO mice.

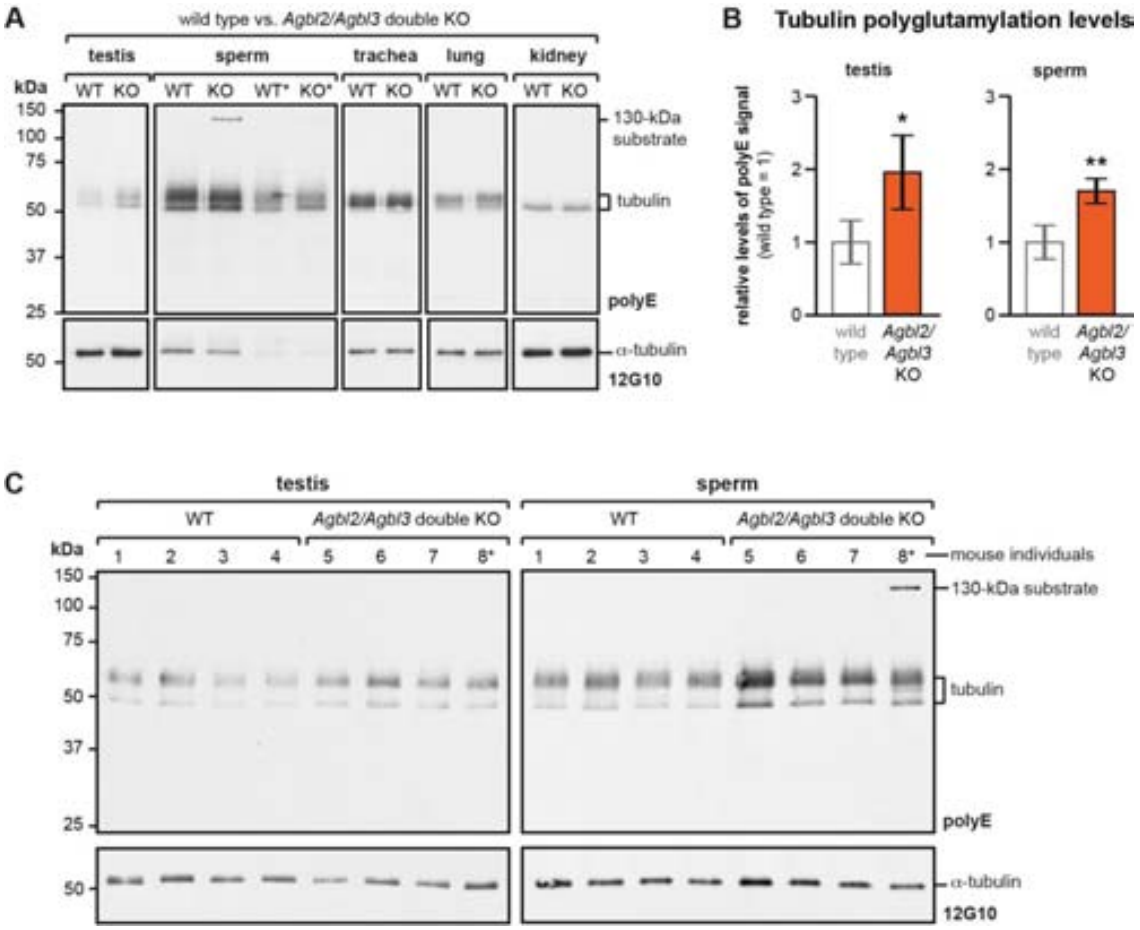

Figure 4.12. Analysis of the polyglutamylation levels in *Agbl2/Agbl3* double KO mice

***A**) Comparative immunoblot analysis of protein extracts from different organs of wild type (WT) and Agbl2/Agbl3 double KO mice with the polyE antibody. Total tubulin levels were detected with anti-α-tubulin antibody (12G10). **B**) Quantitative analysis of the polyE signal relative to the 12G10 signal Agbl2/Agbl3 double KO mice relative to WT. Four of each, WT and double KO mice were analyzed (**C**), and relative values were plotted (WT was set to 1); error bars show standard deviation. Student's t-test was used to determine significance levels (*p<0.05; **p<0.01). **C**) Immunoblots of testes and sperm extracts from four of each, WT and Agbl2/Agbl3 double KO mice (mice 1, 2, 3, 5, 6 and 7 were 4 months old; mice 4 and 8 were 5 weeks old). The polyE and 12G10 signals as represented here have been quantified using the software ImageJ, and polyE values have been adjusted to the total tubulin load detected with the antibody 12G10. *Note that the 130-kDa polyE-positive protein band is only detected in the 5-week-old mouse, but not in the older individuals.*

In addition to tubulin, polyE immunoreactivity of a 130-kDa protein was increased in sperm of a 5-week-old *Agbl2/Agbl3* KO mice, however this band was not anymore detected in the 4-month-old mice (**Figure 4.12 A**). To further study this substrate we analyzed the polyglutamylation levels of stomach samples of a set of eight individuals, four wild type and four *Agbl2/Agbl3* KO mice (**Figure 4.13 A**). Similar to the single knockout mice and to the sperm sample of the 5-week-old double KO mouse, a polyglutamylated 130-kDa protein was detected in stomach in the absence (knockout) of CCP2 and CCP3 (**Figure 4.13 B**).

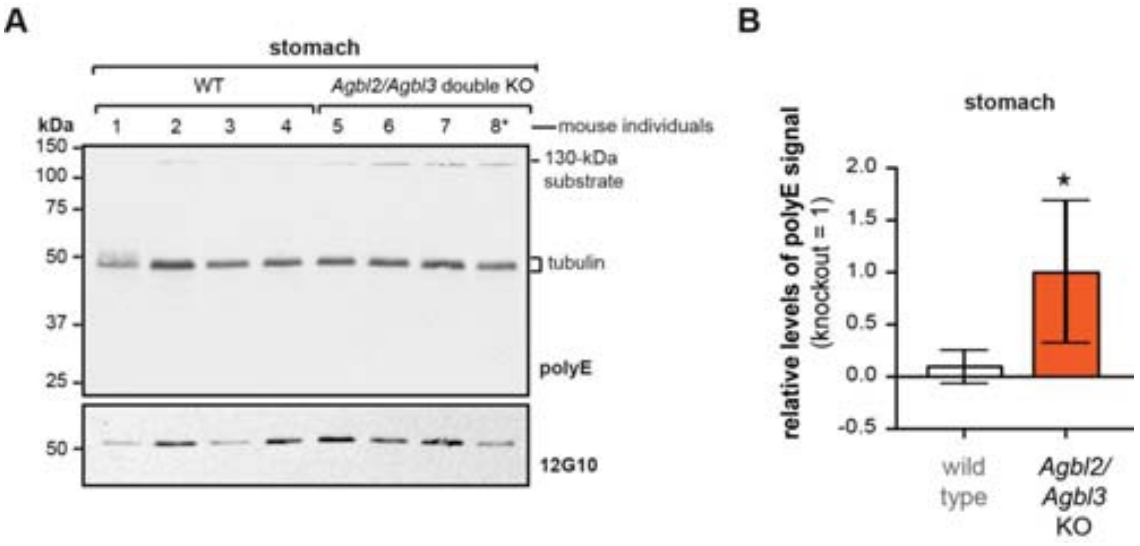

Figure 4.13. Polyglutamylation levels in stomach of *Agbl2/Agbl3* double-KO mice
***A**) Immunoblots of stomach protein extracts from four of each, WT and Agbl2/Agbl3 double KO mice (mice 1, 2, 3, 5, 6 and 7 were 4 months old; mice 4 and 8 were 5 weeks old). The polyE and 12G10 signals as represented here have been quantified using the software ImageJ, and polyE values have been adjusted to the total tubulin load detected with the antibody 12G10. *Note that the 130-kDa polyE-positive protein band is detected in the double knockout mice, but not in the wild type, independently from their ages. **B**) Quantitative analysis of the polyE signal relative to the 12G10 signal Agbl2/Agbl3 double KO mice relative to WT. Relative values were plotted (KO was set to 1); error bars show standard deviation. Student's t-test was used to determine significance levels (*p<0.05).*

The fact that this C-terminal tail is hardly detectable with polyE in wild type samples (sperm and stomach), while much stronger in the *Agbl2/Agbl3* KO mice

indicates that both enzymes are cooperatively involved in the deglutamylation of MLCK. But not only CCP2 and CCP3 are involved in this effect, since also CCP1 seems to show a complementarity activity (Rogowski *et al.*, 2010). The absence of CCP1, CCP2 or CCP3 causes independently a hyperpolyglutamylation of MLCK and also the lack of both CCP2 and CCP3 presents this effect. This shows that the CCPs can act on similar substrates and that there is still many questions open regarding the inter-regulation of the six CCP members.

DISCUSSION

Protein PTMs consisting in the ligation or hydrolysis of amino acids have recently been attributed an increasing range of functions, and the discovery of enzymes involved in polyglutamylation, polyglycylation or detyrosination/tyrosination have opened new opportunities for mechanistic and functional studies. Amino acid ligases for Glu, Gly or Tyr have been identified in the conserved TTLL family. Enzymes removing Glu residues from protein C-termini were found within the newly discovered CCP family (reviewed in Janke and Bulinski, 2011). Initially, these discoveries raised hopes that the remaining enzymes, such as detyrosinases or deglycylases, are also members of the CCP family (Sahab *et al.*, 2011). The goal of the present study was to unambiguously determine the enzymatic specificity of the remaining two members of the mammalian CCP family, CCP2 and CCP3.

The reason that CCP2 and CCP3 had not been analyzed with the same rigorousness as the other members of the family (Rogowski *et al.*, 2010) was mainly related to the difficulties in expressing these proteins, which hampered the development of enzymatic assays. The availability of the crystal structure of a CCP (Otero *et al.*, 2012) allowed us to generate a structural model of CCP2 and CCP3, on the base of which we predicted the acidic substrate specificity of these two enzymes. Guided by these predictions, and optimizing the coding sequences of CCP2 and CCP3 lead us to the demonstration that both enzymes are consistent with C-terminal deglutamylation activity on proteins, similar to the subfamily members CCP1, CCP4 and CCP6 (Rogowski *et al.*, 2010). At the level of MTs, CCP2 and CCP3 can generate Δ2-

tubulin, and their ability to shorten long Glu-chains also allows them to deglutamylate laterally polyglutamylated tubulin. Δ2-tubulin, as well as polyglutamylated forms of tubulin, are specifically accumulated on neuronal, centriolar, ciliary and flagellar MTs (Paturle-Lafanechère *et al.*, 1994; Ikegami and Sato, 2010; Vogel *et al.*, 2010; Bosch Grau *et al.*, 2013). Thus, the specific expression of CCP2 and CCP3 in ciliated tissues, as well as the increase of their expression levels during ciliogenesis suggest that they fulfill specific functions in the regulation of the two PTMs in these organelles. Indeed, we could show that the double knockout of both enzymes in mice shows significant changes in tubulin polyglutamylation in testes and sperm, which is coherent with the relatively high expression levels of CCP2 and CCP3 in testes. However similar changes could not be visualized in other ciliated tissues of these mice.

Our results show that CCP2 and CCP3 participate in the process of deglutamylation, however other enzymes, such as CCP1, CCP4 or CCP6, are also involved and might in most cases compensate for the absence of these two enzymes. It is thus perceivable that CCP2 and CCP3 play some highly regulated, specific roles in adjusting tubulin modifications locally or temporally in most cells and organs. This could be important for fine-tuning specific MT functions, but does not induce global changes visible on the level of the whole tubulin pool. The absence of strong phenotypic alterations in *Agbl2/Agbl3* double KO mice also points towards highly specified functions that might only be revealed under specific conditions, such as adaptation to evolutionary pressure, or diseases. A similar observation has been recently made for a member of the TTLL family (our unpublished work).

Analyzing the enzymatic activities of CCP3 further revealed that this particular enzyme can, besides Glu, also hydrolyze Asp residues from C-terminal positions. CCP3 seems to catalyze Glu and Asp removal with equal efficiency, while all other enzymes of the CCP family show only weak activity for Asp. It might thus be that Asp hydrolysis is an important function for CCPs, but apart from CCP3 other CCPs require specific co-factors or other regulatory events to efficiently catalyze this reaction. The biological impact of this novel enzymatic activity could be significant. In addition to modifying proteins with C-terminally exposed Glu residues, such as MLCK or telokin (Rogowski *et al.*, 2010), we now envisage differential C-terminal modification of a larger range of

potential substrates. The possibility to selectively remove the Glu and the Asp residues by different CCPs opens the possibility that this novel PTM has a broader impact on protein functions than initially expected from deglutamylation alone. Still, the absence of striking phenotypic alterations of the *Agbl3* (CCP3) knockout mouse indicates that these modifications can be redundantly performed, or have only fine-regulatory roles that remain to be discovered.

In summary, we have shown that all members of the murine CCP family are involved in protein deglutamylation, and we have further discovered a novel deaspartylating activity for CCP3. Our functional analyses suggest that CCP2 and CCP3 fulfill complementary functions in regulating protein glutamylation in ciliated cells and tissues. Strikingly, the deletion of both enzymes in mice did not impede key organism functions, which indicates that similar to other enzymes involved in this type of PTMs, the two CCPs might play roles in fine-tuning of protein functions. The analysis of the enzymatic activities of CCP2 and CCP3 now completes the repertoire of enzymes involved in ligation and removal of acidic amino acids on proteins. The discovery of a novel Asp-hydrolyzing activity further expands the complexity of this type of PTMs, broadens the range of potential substrates, and points towards novel functions of the CCP enzyme family.

Discussion and future perspectives

DISCUSSION AND FUTURE PERSPECTIVES

In this thesis, a first study on the uncharacterized CCP3 was performed. Taking advantage of its relatively short size (72.6 KDa) compared to the most studied of the CCPs (CCP1, with 116 KDa), expression and purification strategies were set up in order to obtain enough quantity of protein to biochemically characterize this enzyme. Previously in our research group, bacterial and yeast expression systems failed to produce soluble CCPs. In mammalian cells, CCP3 was expressed soluble but in low quantities. The first challenge was to optimize an expression system and a tag purification strategy, which permitted expressing detectable amounts of soluble protein, efficiently capture it for purification, and allowing to monitor the presence of the enzyme. After trials in different systems and vectors, this was finally solved with the HEK293F suspension cell system, an optimized pOPINFs vector (Berrow *et al.*, 2007) and a double tag (*Strep* and HA for purification and detection purposes, respectively). The amounts produced in the optimized system were still low for structural analysis with the additional difficulty that the enzyme seemed unstable upon purification.

The difficulties in expression and purification redirected the thesis to functional studies. As tubulin was on focus as a putative substrate candidate and we had access to a set of commercial antibodies to detect different tubulin PTMs, preliminary assays were performed and we could observe a promising generation of Δ2-tubulin. Meanwhile other members of the CCP family were characterized (Kimura *et al.*, 2010; Rogowski *et al.*, 2010) confirming a role of CCPs in tubulin PTMs, but CCP2 and CCP3 remained undefined in these publications, till CCP2 was proposed as tubulin detyrosinase (Sahab *et al.*, 2011). Although our research group failed to reproduce CCP2 function as detyrosinase, its low expression and activity could not show a deglutamylating activity neither.

At this point, structural modeling of the active site was performed and an acidic substrate preference was predicted pointing both CCP2 and CCP3 as deglutamylases. In an attempt to overpass the low activity limitation and based on the active form of

human CCP3, a protein engineering strategy was designed for mouse CCP2 and CCP3, which appeared inactive. This strategy consisted in several rounds of cloning, expression and comparatively test the newly generated forms till reaching the activity core of CCP2 and CCP3. In each step of truncation, protein alignment of CCPs helped defining non-homologous amino acid sequences. Finally, with the generation of two short active forms of CCP2 and CCP3, a complete activity specificity study was performed, showing that both CCP2 and CCP3 are deglutamylating carboxypeptidases, which remove the gene-encoded C-terminal glutamate from detyrosinated α-tubulin (deTyr-tubulin) to generate Δ2-tubulin.

During my stay in the laboratory of Dr. Janke in Institute Curie (Orsay, France), I participated in the elaboration of a set of artificial substrates (telokin C-terminal chimeras) that helped demonstrating the ability of CCP2 and CCP3 to trim long polyglutamate chains but not polyglycine stretches, and the additional deaspartylation capacity.

Finally, at Dr. Janke's team, the valuable tool of the CCP2 and CCP3 knockout mouse models were available to help resolving the question of the biological role of CCP2 and CCP3. A full screening of the tissue extracts of CCP2 and CCP3 revealed few alterations in the polyglutamylation levels compared to the CCP1 KO. Since no evident phenotypic alteration was observed, we generated the double CCP2/CCP3 knockout mouse line. Especially the latter one provided evidence of deglutamylating activity on tubulin *in vivo* and the existence of other polyglutamylated substrates of CCP2 and CCP3. With this work, the substrate specificity of the CCP family members was completed.

In this thesis, the question of the substrate specificity of the controversial CCP2 and CCP3 is elucidated, but several questions about these enzymes remain open to discussion. Not only CCP2 and CCP3, but few is known about CCPs regulation, the role *in vivo* of these enzymes or which is the potential of deaspartylation as a putative new PTM of proteins. In the next lines, an insight about some of these questions is proposed.

Who needs CCPs?

The amount of CCPs is highly variable among organisms. Human and mouse, each have six different CCP genes in their genome (Kalinina *et al.*, 2007; Rodriguez de la Vega *et al.*, 2007), whereas other organisms present both larger and smaller sets of CCPs (Rodríguez de la Vega Otazo *et al.*, 2013). Most Fungi lack CCP genes, *Plasmodium falciparum* and *Toxoplasma gondii* have one single CCP gene, and the multiciliated *Thetrahymena thermophila* and *Paramecium tetraurelia* possess 10 and 32 CCP paralogs, respectively (Rodríguez de la Vega Otazo *et al.*, 2013). This divergence in CCP numbers among organisms indicates changes in the role of CCPs along evolution that could have led to specialization at different levels. As polyglutamylation is necessary to control the beating behavior in motile cilia (Bosch Grau *et al.*, 2013), these unicellular motile organisms or pluricellular organisms with tissues displaying motile cilia might require more CCPs to ensure the proper beating coordination.

CCPs have a role in development. There are few studies on the role of CCPs in development. However, the levels of tubulin polyglutamylation and Δ2-tubulin vary during early developmental stages (Rogowski *et al.*, 2010). There are evidences of a role of CCP1 and CCP5, but not CCP2, during embryogenesis in zebrafish (Lyons *et al.*, 2013). Thus, some glutamylases and deglutamylases might work sequentially and coordinated to modulate tubulin glutamylation during development.

Why do mammals need six deglutamylases (from CCP1 to CCP6)?

CCPs are tissue specific. CCP1 plays a key role in neuronal cells as demonstrated by the CCP1 knockout mouse or *pcd* neurodegenerative phenotype (Fernandez-Gonzalez *et al.*, 2002; Rogowski *et al.*, 2010). Our expression analysis by qPCR further supports the role of CCP1 in neuronal tissues and also indicated that CCP6 presents a neuronal expression profile. CCP5, however, was lowly expressed in adult mouse brain but significantly in testis, indicating that neuronal cells need permanently basal levels of polyglutamylation. A plausible explanation is that once neuronal MTs are polyglutamylated, only shortening and extension of the glutamic acid length is needed but the branching point needs to keep stable. In this case, CCP5 would be poorly required while CCP1 (maybe assisted by other CCPs) would play the

main deglutamylating role. Surprisingly, mouse CCP4 appeared as trachea- and muscle-specific but its role has been poorly studied. CCP4 is a CCP1 paralog (Rodriguez de la Vega *et al.*, 2007; Rodríguez de la Vega Otazo *et al.*, 2013) with different tissue expression profile and levels, thus its function could completely differ from the rest of CCPs. CCP2 and CCP3 showed a clear correlation with ciliated tissues. Notably, the presence of CCPs in organisms correlates with the presence of cilia and basal bodies. In particular CCP2 and CCP3 correlate with organisms that present motile cilia (Rodríguez de la Vega Otazo *et al.*, 2013). In zebrafish, CCP2 expression is limited to the testis (Lyons *et al.*, 2013), that contains motile flagella. Likewise, in our quantitative analysis of CCP expression in mouse tissues, CCP2 and CCP3 were the only CCPs showing a clear correlation with tissues displaying motile cilia, including testis.

CCPs might prefer certain groups of MTs. The CCP tissue specificity could denote the preference of different CCPs to certain microtubular assemblies, such as neuronal axons, the mitotic spindle, the axoneme of cilia/flagella. For instance, typically ciliated tissues (*e.g.* trachea or kidney) will present a higher proportion of ciliated cells, consequently more groups of ciliarly MTs compared to other tissues. Therefore, it is likely that the expression of ciliary specific modifying enzymes is proportionally increased. What could define which groups of MTs are the target of CCPs is the length of the polyglutamate chain, the isotype of tubulin displaying the polyglutamylation. Higher affinity for longer glutamic acid strains has been shown for CCP1 on a synthetic substrate (Wu *et al.*, 2012). However, the affinity for polymerized tubulin seems not critical for their activity since, as we verified, these enzymes are active on depolymerized tubulin *in vitro* (Rogowski *et al.*, 2010; Berezniuk *et al.*, 2012).

The role of CCP extra domains

Some regulatory aspects internal to each CCP amino acidic sequence can be taken into consideration. CCPs differentially display extra domains, others than the catalytic domain, which may be relevant in the functional specialization of each member of the subfamily. In this way, it is possible that these extra domains determine still unknown interactions governing the specialization of each CCP into the different MT intracellular structures, tubulin isotypes or other substrates in the cell.

Which substrates do have CCPs preference for?

Tubulin as substrate of CCPs. Although α- and β-tubulin are structurally similar, TTLL members have a preference for one subunit of the heterodimer (*e.g*. TTLL5 and TTLL6 prefer α-tubulin while TTLL4 and TTLL7 favor β-tubulin); and are specific for initiation or elongation reaction (TTLL4 and TTLL5 initiate whereas TTLL6 and TTLL11 elongate the polyglutamic chain). Among the deglutamylases, only CCP5 is able to cleave the branching point, thus reversing the initiation reaction of TTLL4 or TTLL5, but shows no specificity for α- or β-tubulin. CCP1 is also described to cleave glutamic acids from both α- or β-tubulins (Berezniuk *et al.*, 2012), but there is no data on CCP2, CCP3, CCP4, and CCP6 so far. A drawback of those studies comes from the substrate used for the assays, since porcine brain tubulin almost completely lacks polyglutamylation on β-tubulin. Tubulin treated with TTLL4 and TTLL5 or brain tubulin from young animals (*e.g.* cow, pig, mouse) display β-tubulin polyglutamylation, thus they are more appropriate substrates. Alternatively, the study of tubulin in the several CCP knockout mouse tissues and cells will help revealing their tubulin selectivity properties.

The non-tubulin substrates. So far, tubulin has been proposed as the main substrate of TTLLs and CCPs. However other nuclear and cytoplasmic substrates are known, such as the nucleosome assembly proteins (NAPs) for TTLL4, or MLCK and telokin for CCP1 (Van Dijk *et al.*, 2008; Rogowski *et al.*, 2010), CCP2 and CCP3 in this work. Recent proteomic studies on CCP1 revealed a set of acidic-tailed proteins that can be modified by CCP1 (Tanco *et. al.,* manuscript submitted to MCP). Moreover, CCP1 is translocated to and from the nucleus, proving again its versatile localization, which is consistent with having access to nuclear substrates (Valero *et al.*, 2006; Thakar *et al.*, 2013).

Disruption of the polyglutamylation equilibrium. The effects of altering the enzymatic machinery of TTLLs and CCPs can not only generate changes in the MT-based organelles but also in other proteins, particularly nuclear proteins. Thus, the phenotype of the *pcd* mouse can be due to hyperglutamylation of tubulin and other proteins. To assess this, a conditional knockout system to tissues where few CCPs are expressed or, alternatively, a system where the endogenous tubulin is substituted by a non PTM-modifiable one should be elaborated. Alternatively, proteomic screening for

the substrates and biochemical studies on the alteration in acidic proteins could give information of the process. Main chain and lateral polyglutamylation could constitute a reversible and general posttranslational modification system, which has the advantage of not only functioning as an *on/off* message but also as a gradual signal depending on the length of the polyglutamate stretch.

Which functions do CCPs have in cilia?

Role of CCPs in ciliopathies. Polyglutamylation participates in regulating cilia/flagella motility (Suryavanshi *et al.*, 2010) and in controlling the beating behavior of the flagella (Ikegami and Setou, 2010; Bosch Grau *et al.*, 2013). Consistent with this role, functional and localization studies have revealed that TTLLs and CCPs are required in cilia and basal bodies (van Dijk *et al.*, 2007; Ikegami and Sato, 2010; O'Hagan *et al.*, 2011; Pathak *et al.*, 2014). The lack of the initiating glutamylase TTLL1 causes disfunction of the respiratory cilia and sperm motility, but no other PCD symptoms such as *situs inversus* or severe hydrocephalus are observed (Ikegami and Setou, 2010). Also the lack of TTLL5 causes male infertility (Lee *et al.*, 2013) and retinal dystrophy of the cone receptors (Sergouniotis *et al.*, 2014). Surprisingly, the CCP1 knockout (*pcd*) mouse also suffers from male infertility (Handel and Dawson, 1981; Fernandez-Gonzalez *et al.*, 2002; Kim *et al.*, 2011). Thus both the hyperpolyglutamylation and the hypopolyglutamylation lead to male infertility affectation characterized in both cases by reduced counts and immotile spermatozoa. In terms of sperm morphology, *pcd* mouse sperm cells present structural abnormalities of the head and/or the tail (Handel and Dawson, 1981), whereas *Ttll1* KO mouse sperm affectation is manifested mostly in the tail with missing or shortened flagella and thickened midpieces (Ikegami and Sato, 2010; Vogel *et al.*, 2010) and *Ttll5* KO sperm lack one MT doublet and have the sperm head dislocated from their tails.

Given that these mouse models have immotile axonemes, the link between polyglutamylation may be difficult to assess. Sperm from the double *Agbl2/Agbl3* KO are motile though display slight changes in polyglutamylation. Sperm motility studies of this (mildly hyperpolyglutamylated) mouse model can bring a better understanding

compared to strong hyperpolyglutamylated phenotypes of which parameters of cilia/flagella motility are regulated by polyglutamylation.

Which is the biological function of CCP2 and CCP3?

The synergy of CCPs. Surprisingly, knockout mice of at least three CCPs (CCP1, CCP2 and CCP3) and also the double CCP2/3 KO display hyperpolyglutamylated MLCK in the stomach. This could indicate that the three CCPs are somehow redundant but still all needed for the same function. TTLLs were isolated from a complex of tubulin ligases (Janke *et al.*, 2005b). CCPs could likewise be in a complex, although when performing pull-down experiments with CCP3, we could not identify other CCPs. Further studies on the regulation of these enzymes will be needed to understand the precise cellular function and their interrelation.

Towards the effect of sperm hyperpolyglutamylation. Focusing on microtubules, CCP2/3 double KO showed increased levels of polyglutamylation in testis and sperm tubulin but these mice were fertile. Considering the slightly hyperpolyglutamylated sperm of the KO compared to wild type sperm, we can expect a range of polyglutamylated levels that ensures a proper mobility, thus fertility. Slight changes in polyglutamylation might modify the beating pattern but not sufficiently to disrupt their activity. Defining the beating parameters of hyperpolyglutamylated axoneme could bring a better understanding of the role of poluglutamylation in motile cilia.

Evidences arise showing that PTMs and tubulin isoforms vary from motile to immotile sperm (asthenozoospermia). A recent study described the lack of α-tubulin acetylation in asthenozoospermia, and associated this to higher levels of TUBA4A (non acetylable tubulin and with an intrinsically detyrosinated C-terminal) and reduced TUBA3C (testis-specific and acetylable) as compared to normal spermatozoa (Bhagwat *et al.*, 2014). Further studies on tubulin isotypes and PTMs may lead to great advances in the field of fertility in the understanding of ciliopathies applied in sperm cells but also in developing therapies that could correct the deficiencies.

Is deaspartylation a novel posttranslational modification?

The deaspartylating activity in the proteomic context.

This thesis first describes the ability of CCP1, CCP2 and particularly CCP3 to cleave aspartic acids apart from glutamic acid residues. In the proteome of complex organisms, the acidic C-terminus of proteins contain stretches of [Asp] or [Asp,Glu]. The presence of an aspartic acid between two Glu-stretches may slow down the advance of CCP1 and CCP2. However, the introduction of CCP3 in this context could efficiently overpass this limitation. An example of an acidic tail with Asp intercalated between Glu stretches is the family of High mobility binding proteins, where certain members have Asp intercalated in a polyglutamylated tail (Tanco *et al.*). **Polyaspartylated C-terminal tails exist.** An extreme case is the presence of a long polyaspartylated tail in a calcium regulator protein named calcequestrin-1 (C-terminal: -NTEDDDDDDDDDDDDDDDD). Probably the acidic properties of this protein are needed, so having an Asp instead of a Glu stretch protects it from CCP-degradation. In the hypothetic condition where this acidic tail needs to be processed, CCP3 might be the required protease for this task.

Concluding remarks

CONCLUDING REMARKS

1. Structural models of CCP2 and CCP3 carboxypeptidase domains have been built and predict an extended positively charged area at the entrance of the active site, consistent with recognition and specificity for acidic residues of protein substrates.

2. Recombinant human CCP3 copurify with microtubules, as well as tubulin copurify with the recombinant hCCP3 evidencing their interaction. Moreover, endogenous human CCP3 localize to the midbody during cytokinesis.

3. Mouse CCP2 and mouse and human CCP3 are active metallocarboxypeptidases, which can be inactivated by mutating the catalytic Glu270 equivalent residue. Mouse CCP2 and CCP3 are able to generate Δ2-tubulin in HEK cells but lack detyrosinating activity. Thus the CCP subfamily is entirely integrated by deglutamylating enzymes.

4. CCP2 and CCP3 truncated forms reveal that the core domain of these proteins presents the maximal activity and corresponds in size to CCP6, the shortest CCP paralog in mouse and human proteome.

5. Truncated forms of CCP2 and CCP3 are able to trim the long polyglutamylated C-terminal from telokin until generating its Δ2-form, while they show no activity towards the same substrate displaying other residues and a polyglycylated C-terminal tail.

6. Expression of *Agbl2* and *Agbl3* genes in adult wild type mice correlate with tissues displaying motile cilia, and both genes are induced during ciliogenesis in IMCD3 cells showing a role of those enzymes in cilia or cilia-related structures.

7. *Agbl2*/*Agbl3* knockout mice sperm and testis show significant differences in the tubulin polyglutamylation levels compared to wild type mice.

8. *Agbl2*/*Agbl3* knockout mice display a hyperpolyglutamylated substrate (MLCK) at 4-week age that is absent at 3-month age, thus the hyperglutamylation of MLCK may be dependent on the developmental stage.

9. Testis and sperm microtubules of *Agbl2*/*Agbl3* double knockout mice exhibit significant hyperpolyglutamylation compared to wild type mice but the mice were still fertile. This mouse model showed no strong phenotype compared to wild type and no ataxic or infertile phenotypes compared to the *pcd* mouse.

10. CCP2, CCP3 and CCP1 can cleave aspartic acid residues besides glutamic acids. CCP1 and CCP2 have preference for glutamic acid residues while CCP3 show no preference for either Asp/Glu cleavage. This shows a potentially new deaspartylation activity.

Bibliography

BIBLIOGRAPHY

Afzelius, B. A. (1976). A human syndrome caused by immotile cilia. Science *193*, 317–319.

Akhmanova, A., and Steinmetz, M. O. (2008). Tracking the ends: a dynamic protein network controls the fate of microtubule tips. Nat. Rev. Mol. Cell Biol. *9*, 309–322.

Allan, V. J., Thompson, H. M., and McNiven, M. A. (2002). Motoring around the Golgi. Nat. Cell Biol. *4*, E236–42.

Alushin, G. M., Lander, G. C., Kellogg, E. H., Zhang, R., Baker, D., and Nogales, E. (2014). High-Resolution Microtubule Structures Reveal the Structural Transitions in αβ-Tubulin upon GTP Hydrolysis. Cell *157*, 1117–1129.

Arce, C. A., and Barra, H. S. (1983). Association of tubulinyl-tyrosine carboxypeptidase with microtubules. FEBS Lett. *157*, 75–78.

Argarana, C. E., Barra, H. S., and Caputto, R. (1980). Tubulinyl-tyrosine Carboxypeptidase from Chicken Brain: Properties and Partial Purification. J. Neurochem. *34*, 114–118.

Argaraña, C., Barra, H., and Caputto, R. (1978). Release of tyrosine from tubulinyl- tyrosine by brain extract. Separation of a carboxypeptidase from tubulin-tyrosine ligase. Mol. Cell. Biochem. *19*, 17–21.

Arolas, J. L., Popowicz, G. M., Lorenzo, J., Sommerhoff, C. P., Huber, R., Aviles, F. X., and Holak, T. A. (2005). The three-dimensional structures of tick carboxypeptidase inhibitor in complex with A/B carboxypeptidases reveal a novel double-headed binding mode. J. Mol. Biol. *350*, 489–498.

Arolas, J. L., Vendrell, J., Aviles, F. X., and Fricker, L. D. (2007). Metallocarboxypeptidases: emerging drug targets in biomedicine. Curr. Pharm. Des. *13*, 347–364.

Audebert, S., Desbruyères, E., Gruszczynski, C., Koulakoff, A., Gros, F., Denoulet, P., and Eddé, B. (1993). Reversible polyglutamylation of alpha- and beta-tubulin and microtubule dynamics in mouse brain neurons. Mol. Biol. Cell *4*, 615–626.

Ayaz, P., Ye, X., Huddleston, P., Brautigam, C. A., and Rice, L. M. (2012). A TOG:αβ-tubulin complex structure reveals conformation-based mechanisms for a microtubule polymerase. Science *337*, 857–860.

Azimzadeh, J., and Marshall, W. F. (2010). Building the centriole. Curr. Biol. *20*, R816–25.

Bahi-Buisson, N. *et al.* (2014). The wide spectrum of tubulinopathies: what are the key features for the diagnosis? Brain *137*, 1676–1700.

Baird, F. J., and Bennett, C. L. (2013). Microtubule defects and neurodegeneration. J. Genet. Syndr. Gene Ther. *4*, 203.

Bajzar, L., Manuel, R., and Nesheim, M. (1995). Purification and characterization of TAFI, a thrombin-activable fibrinolysis inhibitor. J. Biol. Chem. *270*, 14477–14484.

Baltanas, F. C., Casafont, I., Lafarga, V., Weruaga, E., Alonso, J. R., Berciano, M. T., and Lafarga, M. (2011). Purkinje cell degeneration in pcd mice reveals large-scale chromatin reorganization and gene silencing linked to defective DNA repair. J. Biol. Chem. *286*, 28287–28302.

Barbato, A. *et al.* (2009). Primary ciliary dyskinesia: a consensus statement on diagnostic and treatment approaches in children. Eur. Respir. J. *34*, 1264–1276.

Barrett, A. J. (2000). Proteases. In: Current Protocols in Protein Science, John Wiley & Sons, Inc., 21.1.1–21.1.12.

Barrett, A., and Mc Donald, J. (1986). Nomenclature: protease, proteinase and peptidase. Biochem. J. *237*, 935.

Beaudouin, J., Gerlich, D., Daigle, N., Eils, R., and Ellenberg, J. (2002). Nuclear Envelope Breakdown proceeds by Microtubule-Induced Tearing of the Lamina. Cell *108*, 83–96.

Bell, P. J., and Safiejko-Mroczka, B. (1995). Improved methods for preserving macromolecular structures and visualizing them by fluorescence and scanning electron microscopy. Scanning Microsc. *9*, 843–57; discussion 858–60.

Berezniuk, I., Lyons, P. J., Sironi, J. J., Xiao, H., Setou, M., Angeletti, R. H., Ikegami, K., and Fricker, L. D. (2013a). Cytosolic carboxypeptidase 5 removes α- and γ-linked glutamates from tubulin. J. Biol. Chem. *288*, 30445–30453.

Berezniuk, I., Sironi, J. J., Wardman, J., Pasek, R. C., Berbari, N. F., Yoder, B. K., and Fricker, L. D. (2013b). Quantitative peptidomics of Purkinje cell degeneration mice. PLoS One *8*, e60981.

Berezniuk, I., Vu, H. T., Lyons, P. J., Sironi, J. J., Xiao, H., Burd, B., Setou, M., Angeletti, R. H., Ikegami, K., and Fricker, L. D. (2011). Cytosolic carboxypeptidase 1 is involved in processing of alpha-tubulin and beta-tubulin. J. Biol. Chem.

Berezniuk, I., Vu, H. T., Lyons, P. J., Sironi, J. J., Xiao, H., Burd, B., Setou, M., Angeletti, R. H., Ikegami, K., and Fricker, L. D. (2012). Cytosolic carboxypeptidase 1 is involved in processing α- and β-tubulin. J. Biol. Chem. *287*, 6503–6517.

Berrow, N. S., Alderton, D., Sainsbury, S., Nettleship, J., Assenberg, R., Rahman, N., Stuart, D. I., and Owens, R. J. (2007). A versatile ligation-independent cloning method suitable for high-throughput expression screening applications. Nucleic Acids Res. *35*, e45.

Bettencourt-Dias, M., Hildebrandt, F., Pellman, D., Woods, G., and Godinho, S. A. (2011). Centrosomes and cilia in human disease. Trends Genet. *27*, 307–315.

Bhagwat, S., Dalvi, V., Chandrasekhar, D., Matthew, T., Acharya, K., Gajbhiye, R., Kulkarni, V., Sonawane, S., Ghosalkar, M., and Parte, P. (2014). Acetylated α-tubulin is reduced in individuals with poor sperm motility. Fertil. Steril. *101*, 95–104.e3.

Blum, M., Feistel, K., Thumberger, T., and Schweickert, A. (2014). The evolution and conservation of left-right patterning mechanisms. Co. Biol. *141*, 1603–1613.

Bonnet, C., Boucher, D., Lazereg, S., Pedrotti, B., Islam, K., Denoulet, P., and Larcher, J. C. (2001). Differential binding regulation of microtubule-associated proteins MAP1A, MAP1B, and MAP2 by tubulin polyglutamylation. J. Biol. Chem. *276*, 12839–12848.

Bornens, M. (2012). The centrosome in cells and organisms. Science *335*, 422–426.

Bosch Grau, M., Gonzalez Curto, G., Rocha, C., Magiera, M. M., Marques Sousa, P., Giordano, T., Spassky, N., and Janke, C. (2013). Tubulin glycylases and glutamylases have distinct functions in stabilization and motility of ependymal cilia. J. Cell Biol. *202*, 441–451.

Bosson, A., Soleilhac, J.-M., Valiron, O., Job, D., Andrieux, A., and Moutin, M.-J. (2012). Cap-Gly proteins at microtubule plus ends: is EB1 detyrosination involved? PLoS One *7*, e33490.

Bowie, J. U., Ltcy, R., and Eisenberg, D. (1990). A method to identify protein sequences that fold into a known three-dimensional stucture. Science *253*, 164–170.

Bré, M. H., Redeker, V., Vinh, J., Rossier, J., and Levilliers, N. (1998). Tubulin polyglycylation: differential posttranslational modification of dynamic cytoplasmic and stable axonemal microtubules in paramecium. Mol. Biol. Cell *9*, 2655–2665.

De Castro, E., Sigrist, C. J. A., Gattiker, A., Bulliard, V., Langendijk-Genevaux, P. S., Gasteiger, E., Bairoch, A., and Hulo, N. (2006). ScanProsite: detection of PROSITE signature matches and ProRule-associated functional and structural residues in proteins. Nucleic Acids Res. *34*, W362–365.

Cawley, N. X., Wetsel, W. C., Murthy, S. R. K., Park, J. J., Pacak, K., and Loh, Y. P. (2012). New roles of carboxypeptidase E in endocrine and neural function and cancer. Endocr. Rev. *33*, 216–253.

Cha, J., and Auld, D. S. (1997). Site-directed mutagenesis of the active site glutamate in human matrilysin: investigation of its role in catalysis. Biochemistry *36*, 16019–16024.

Chakrabarti, L., Eng, J., Ivanov, N., Garden, G. A., and La Spada, A. R. (2009). Autophagy activation and enhanced mitophagy characterize the Purkinje cells of pcd mice prior to neuronal death. Mol. Brain *2*, 24.

Chakrabarti, L., and Zahra, R. (2010). Mitochondrial dysfunction in NnaD mutant flies and Purkinje cell degeneration mice reveals a role for Nna proteins in neuronal bioenergetics. Neuron *66*, 835–847.

Chang, P., Giddings, T. H., Winey, M., and Stearns, T. (2003). Epsilon-tubulin is required for centriole duplication and microtubule organization. Nat. Cell Biol. *5*, 71–76.

Chang, P., and Stearns, T. (2000). Delta-tubulin and epsilon-tubulin: two new human centrosomal tubulins reveal new aspects of centrosome structure and function. Nat. Cell Biol. *2*, 30–35.

Christianson, D. W., and Lipscomb, W. N. (1986). X-ray crystallographic investigation of substrate binding to carboxypeptidase A at subzero temperature. Proc. Natl. Acad. Sci. U. S. A. *83*, 7568–7572.

Chu, C.-W., Hou, F., Zhang, J., Phu, L., Loktev, A. V, Kirkpatrick, D. S., Jackson, P. K., Zhao, Y., and Zou, H. (2011). A novel acetylation of β-tubulin by San modulates microtubule polymerization via down-regulating tubulin incorporation. Mol. Biol. Cell *22*, 448–456.

Conacci-Sorrell, M., Ngouenet, C., and Eisenman, R. N. (2010). Myc-nick: a cytoplasmic cleavage product of Myc that promotes alpha-tubulin acetylation and cell differentiation. Cell *142*, 480–493.

Contín, M. A., Purro, S. A., Bisig, C. G., Barra, H. S., and Arce, C. A. (2003). Inhibitors of protein phosphatase 1 and 2A decrease the level of tubulin carboxypeptidase activity associated with microtubules. Eur. J. Biochem. *270*, 4921–4929.

Contín, M. A., Sironi, J. J., Barra, H. S., and Arce, C. A. (1999). Association of tubulin carboxypeptidase with microtubules in living cells. Biochem. J. *339*, 463–471.

Creppe, C. *et al.* (2009). Elongator controls the migration and differentiation of cortical neurons through acetylation of alpha-tubulin. Cell *136*, 551–564.

Cushion, T. D. *et al.* (2013). Overlapping cortical malformations and mutations in TUBB2B and TUBA1A. Brain *136*, 536–548.

Das, V., Kanakkanthara, A., Chan, A., and Miller, J. H. (2014). Potential role of tubulin tyrosine ligase-like enzymes in tumorigenesis and cancer cell resistance. Cancer Lett. *350*, 1–4.

Devault, A., and Nault, C. (1988). Expression of neutral endopeptidase (enkephalinase) in heterologous COS-1 cells. Characterization of the recombinant enzyme and evidence for a glutamic acid. J. Biol. Chem. *263*, 4033–4040.

Devel, L., Czarny, B., Beau, F., Georgiadis, D., Stura, E., and Dive, V. (2010). Third generation of matrix metalloprotease inhibitors: Gain in selectivity by targeting the depth of the S1' cavity. Biochimie *92*, 1501–1508.

Van Dijk, J., Miro, J., and Strub, J. (2008). Polyglutamylation is a post-translational modification with a broad range of substrates. J. Biol. Chem. *283*, 3915–3922.

Van Dijk, J., Rogowski, K., Miro, J., Lacroix, B., Eddé, B., and Janke, C. (2007). A targeted multienzyme mechanism for selective microtubule polyglutamylation. Mol. Cell *26*, 437–448.

Driscoll, M., and Gerstbrein, B. (2003). Dying for a cause: invertebrate genetics takes on human neurodegeneration. Nat. Rev. Genet. *4*, 181–194.

Dutcher, S. K., and Trabuco, E. C. (1998). The UNI3 gene is required for assembly of basal bodies of Chlamydomonas and encodes delta-tubulin, a new member of the tubulin superfamily. Mol. Biol. Cell *9*, 1293–1308.

Eckl, J. M., and Richter, K. (2013). Functions of the Hsp90 chaperone system: lifting client proteins to new heights. Int. J. Biochem. Mol. Biol. *4*, 157–165.

Eddé, B., Rossier, J., Le Caer, J. P., Desbruyères, E., Gros, F., and Denoulet, P. (1990). Posttranslational glutamylation of alpha-tubulin. Science *247*, 83–85.

Elad, N., Abramovitch, S., Sabanay, H., and Medalia, O. (2011). Microtubule organization in the final stages of cytokinesis as revealed by cryo-electron tomography. J. Cell Sci. *124*, 207–215.

Emoto, K., Masugi, Y., Yamazaki, K., Effendi, K., Tsujikawa, H., Tanabe, M., Kitagawa, Y., and Sakamoto, M. (2014). Presence of primary cilia in cancer cells correlates with prognosis of pancreatic ductal adenocarcinoma. Hum. Pathol. *45*, 817–825.

Erck, C. *et al.* (2005). A vital role of tubulin-tyrosine-ligase for neuronal organization. Proc. Natl. Acad. Sci. U. S. A. *102*, 7853–7858.

Escalier, D. (2006). Knockout mouse models of sperm flagellum anomalies. Hum. Reprod. Update *12*, 449–461.

Etienne-Manneville, S. (2004). Actin and microtubules in cell motility: which one is in control? Traffic *5*, 470–477.

Feng, Y., and Walsh, C. A. (2001). Protein-protein interactions, cytoskeletal regulation and neuronal migration. Nat. Rev. Neurosci. *2*, 408–416.

Fernández, D., Boix, E., Pallarès, I., Avilés, F. X., and Vendrell, J. (2010a). Analysis of a new crystal form of procarboxypeptidase B: further insights into the catalytic mechanism. Biopolymers *93*, 178–185.

Fernández, D., Pallarès, I., Covaleda, G., Avilés, F. X., and Vendrell, J. (2013). Metallocarboxypeptidases and their inhibitors: recent developments in biomedically relevant protein and organic ligands. Curr. Med. Chem. *20*, 1595–1608.

Fernández, D., Pallarès, I., Vendrell, J., and Avilés, F. X. (2010b). Progress in metallocarboxypeptidases and their small molecular weight inhibitors. Biochimie *92*, 1484–1500.

Fernández, D., Testero, S., Vendrell, J., Avilés, F. X., and Mobashery, S. (2010). The X-Ray Structure of Carboxypeptidase A Inhibited by a Thiirane Mechanism-Based Inhibitor. Chem Biol Drug Des. *75*, 29–34.

Fernandez-Gonzalez, A., La Spada, A. R., Treadaway, J., Higdon, J. C., Harris, B. S., Sidman, R. L., Morgan, J. I., and Zuo, J. (2002). Purkinje cell degeneration (pcd) phenotypes caused by mutations in the axotomy-induced gene, Nna1. Science *295*, 1904–1906.

Foley, J. H., Kim, P. Y., Mutch, N. J., and Gils, a (2013). Insights into thrombin activatable fibrinolysis inhibitor function and regulation. J. Thromb. Haemost. *11 Suppl 1*, 306–315.

De Forges, H., Bouissou, A., and Perez, F. (2012). Interplay between microtubule dynamics and intracellular organization. Int. J. Biochem. Cell Biol. *44*, 266–274.

Fourest-Lieuvin, A. (2006). Purification of tubulin from limited volumes of cultured cells. Protein Expr. Purif. *45*, 183–190.

Fry, A., Leaper, M., and Bayliss, R. (2014). The primary cilium: Guardian of organ development and homeostasis. Organogenesis *10*, 62–68.

Gaitanos, T. N., Santamaria, A., Jeyaprakash, A. A., Wang, B., Conti, E., and Nigg, E. A. (2009). Stable kinetochore-microtubule interactions depend on the Ska complex and its new component Ska3/C13Orf3. EMBO J. *28*, 1442–1452.

García-Sáez, I., Reverter, D., Vendrell, J., Avilés, F. X., and Coll, M. (1997). The three-dimensional structure of human procarboxypeptidase A2. Deciphering the basis of the inhibition, activation and intrinsic activity of the zymogen. EMBO J. *16*, 6906–6913.

George, A. J., Thomas, W. G., and Hannan, R. D. (2010). The renin-angiotensin system and cancer: old dog, new tricks. Nat. Rev. Cancer *10*, 745–759.

Ghosh-Roy, A., Goncharov, A., Jin, Y., and Chisholm, A. D. (2012). Kinesin-13 and tubulin posttranslational modifications regulate microtubule growth in axon regeneration. Dev. Cell *23*, 716–728.

Giustiniani, J., Daire, V., Cantaloube, I., Durand, G., Poüs, C., Perdiz, D., and Baillet, A. (2009). Tubulin acetylation favors Hsp90 recruitment to microtubules and stimulates the signaling function of the Hsp90 clients Akt/PKB and p53. Cell. Signal. *21*, 529–539.

Gogonea, C. B., Gogonea, V., Ali, Y. M., Merz, K. M., and Siddiqui, S. S. (1999). Computational prediction of the three-dimensional structures for the Caenorhabditis elegans tubulin family. J. Mol. Graph. Model. *17*, 90–100, 126–130.

Gomis-Rüth, F. X. (2008). Structure and mechanism of metallocarboxypeptidases. Crit. Rev. Biochem. Mol. Biol. *43*, 319–345.

Gough, J., Karplus, K., Hughey, R., and Chothia, C. (2001). Assignment of homology to genome sequences using a library of hidden Markov models that represent all proteins of known structure. J. Mol. Biol. *313*, 903–919.

Guang, C., Phillips, R. D., Jiang, B., and Milani, F. (2012). Three key proteases--angiotensin-I-converting enzyme (ACE), ACE2 and renin--within and beyond the renin-angiotensin system. Arch. Cardiovasc. Dis. *105*, 373–385.

Gundersen, G. G., Kalnoski, M. H., and Bulinski, J. C. (1984). Distinct populations of microtubules: tyrosinated and nontyrosinated alpha tubulin are distributed differently in vivo. Cell *38*, 779–789.

Guo, J., Walss-Bass, C., and Ludueña, R. F. (2010). The beta isotypes of tubulin in neuronal differentiation. Cytoskeleton (Hoboken). *67*, 431–441.

Guttula, S. V., Allam, A., and Gumpeny, R. S. (2012). Analyzing microarray data of Alzheimer's using cluster analysis to identify the biomarker genes. Int. J. Alzheimers. Dis. *2012*, 649456.

Hallak, M., Rodriguez, J., Barra, H., and Caputto, R. (1977). Release of tyrosine from tyrosinated tubulin. Some common factors that affect this process and the assembly of tubulin. FEBS Lett. *73*, 147–150.

Handel, M. A., and Dawson, M. (1981). Effects on spermiogenesis in the mouse of a male sterile neurological mutation, Purkinje cell degeneration. Gamete Res. *4*, 185–192.

Harris, A., Morgan, J. I., Pecot, M., Soumare, A., Osborne, A., and Soares, H. D. (2000). Regenerating motor neurons express Nna1, a novel ATP/GTP-binding protein related to zinc carboxypeptidases. Mol. Cell. Neurosci. *16*, 578–596.

Hassounah, N. B., Bunch, T. A., and McDermott, K. M. (2012). Molecular pathways: the role of primary cilia in cancer progression and therapeutics with a focus on Hedgehog signaling. Clin. Cancer Res. *18*, 2429–2435.

Helenius, J., Brouhard, G., Kalaidzidis, Y., Diez, S., and Howard, J. (2006). The depolymerizing kinesin MCAK uses lattice diffusion to rapidly target microtubule ends. Nature *441*, 115–119.

Howard, J., and Hyman, A. A. (2003). Dynamics and mechanics of the microtubule plus end. Nature *422*, 753–758.

Howard, J., and Hyman, A. A. (2009). Growth, fluctuation and switching at microtubule plus ends. Nat. Rev. Mol. Cell Biol. *10*, 569–574.

Hubbert, C., Guardiola, A., Shao, R., Kawaguchi, Y., Ito, A., Nixon, A., Yoshida, M., Wang, X.-F., and Yao, T.-P. (2002). HDAC6 is a microtubule-associated deacetylase. Nature *417*, 455–458.

Ikegami, K. *et al.* (2007). Loss of alpha-tubulin polyglutamylation in ROSA22 mice is associated with abnormal targeting of KIF1A and modulated synaptic function. Proc. Natl. Acad. Sci. U. S. A. *104*, 3213–3218.

Ikegami, K., Horigome, D., and Mukai, M. (2008). TTLL10 is a protein polyglycylase that can modify nucleosome assembly protein 1. FEBS Lett. *582*, 1129–1134.

Ikegami, K., Mukai, M., Tsuchida, J., Heier, R. L., Macgregor, G. R., and Setou, M. (2006). TTLL7 is a mammalian β-tubulin polyglutamylase required for growth of MAP2-positive neurites. J. Biol. Chem. *281*, 30707–30716.

Ikegami, K., and Sato, S. (2010). Tubulin polyglutamylation is essential for airway ciliary function through the regulation of beating asymmetry. Proc. Natl. Acad. Sci. U. S. A. *107*, 10490–10495.

Ikegami, K., and Setou, M. (2009). TTLL10 can perform tubulin glycylation when co-expressed with TTLL8. FEBS Lett. *583*, 1957–1963.

Ikegami, K., and Setou, M. (2010). Unique Post-Translational Modifications in Specialized Microtubule Architecture Detyrosination / Tyrosination. Cell Struct. Funct. *22*, 15–22.

Janke, C. *et al.* (2005a). Tubulin polyglutamylase enzymes are members of the TTL domain protein family. Science *308*, 1758–1762.

Janke, C. (2014). The tubulin code: Molecular components, readout mechanisms, and functions. J. Cell Biol. *206*, 461–472.

Janke, C., and Bulinski, J. C. (2011). Post-translational regulation of the microtubule cytoskeleton: mechanisms and functions. Nat. Rev. Mol. Cell Biol. *12*, 773–786.

Janke, C., Rogowski, K., and van Dijk, J. (2008). Polyglutamylation: a fine-regulator of protein function? "Protein Modifications: beyond the usual suspects" review series. EMBO Rep. *9*, 636–641.

Janke, C., Rogowski, K., Wloga, D., and Regnard, C. (2005b). Tubulin Polyglutamylase Enzymes Are Members of the TTL Domain Protein Family. Science *1758*.

Joshi, H. C., Palacios, M. J., McNamara, L., and Cleveland, D. W. (1992). γ-Tubulin is a centrosomal protein required for cell cycle-dependent microtubule nucleation. Nature *356*, 80–83.

Kalinina, E., Biswas, R., Berezniuk, I., Hermoso, A., Aviles, F. X., and Fricker, L. D. (2007). A novel subfamily of mouse cytosolic carboxypeptidases. FASEB J. *21*, 836–850.

Källberg, M., Wang, H., Wang, S., Peng, J., Wang, Z., Lu, H., and Xu, J. (2012). Template-based protein structure modeling using the RaptorX web server. Nat. Protoc. *7*, 1511–1522.

Kapitein, L. C., Schlager, M. A., Kuijpers, M., Wulf, P. S., van Spronsen, M., MacKintosh, F. C., and Hoogenraad, C. C. (2010). Mixed microtubules steer dynein-driven cargo transport into dendrites. Curr. Biol. *20*, 290–299.

Kashiwaya, K., Nakagawa, H., and Hosokawa, M. (2010). Involvement of the Tubulin Tyrosine Ligase-Like Family Member 4 Polyglutamylase in PELP1 Polyglutamylation and Chromatin Remodeling in Pancreatic Cancer Cells. Cancer Res. *70*, 4024–4033.

Kassell, B., and Kay, J. (1973). Zymogens of proteolytic enzymes. Science *180*, 1022–1027.

Kaul, N., Soppina, V., and Verhey, K. J. (2014). Effects of α-Tubulin K40 Acetylation and Detyrosination on Kinesin-1 Motility in a Purified System. Biophys. J. *106*, 2636–2643.

Kavallaris, M. (2010). Microtubules and resistance to tubulin-binding agents. Nat. Rev. Cancer *10*, 194–204.

Keil, C., Maskos, K., Than, M., Hoopes, J. T., Huber, R., Tan, F., Deddish, P. A., Erdös, E. G., Skidgel, R. A., and Bode, W. (2007). Crystal structure of the human carboxypeptidase N (kininase I) catalytic domain. J. Mol. Biol. *366*, 504–516.

Khawaja, S., Gundersen, G., and Bulinski, J. (1988). Enhanced stability of microtubules enriched in detyrosinated tubulin is not a direct function of detyrosination level. J. Cell Biol. *106*, 141–149.

Khodiyar, V. K. *et al.* (2007). A revised nomenclature for the human and rodent alpha-tubulin gene family. Genomics *90*, 285–289.

Kilshtain-Vardi, A., Glick, M., Greenblatt, H. M., Goldblum, A., and Shoham, G. (2003). Refined structure of bovine carboxypeptidase A at 1.25 A resolution. Acta Crystallogr. D. Biol. Crystallogr. *D59*, 323–333.

Kim, N., Xiao, R., Choi, H., Jo, H., Kim, J.-H., Uhm, S.-J., and Park, C. (2011). Abnormal sperm development in pcd 3J-/- mice: the importance of Agtpbp1 in spermatogenesis. Mol. Cells *31*, 39–48.

Kim, S., and Tsiokas, L. (2011). Cilia and cell cycle re-entry: More than a coincidence. Cell Cycle *10*, 2683–2690.

Kimura, Y., Kurabe, N., Ikegami, K., Tsutsumi, K., Konishi, Y., Kaplan, O. I., Kunitomo, H., Iino, Y., Blacque, O. E., and Setou, M. (2010). Identification of tubulin deglutamylase among Caenorhabditis elegans and mammalian cytosolic carboxypeptidases (CCPs). J. Biol. Chem. *285*, 22936–22941.

Ko, J., Park, H., Heo, L., and Seok, C. (2012). GalaxyWEB server for protein structure prediction and refinement. Nucleic Acids Res. *40*, W294–7.

Koning, R. I., Zovko, S., Bárcena, M., Oostergetel, G. T., Koerten, H. K., Galjart, N., Koster, A. J., and Mieke Mommaas, a (2008). Cryo electron tomography of vitrified fibroblasts: microtubule plus ends in situ. J. Struct. Biol. *161*, 459–468.

Konishi, Y., and Setou, M. (2009). Tubulin tyrosination navigates the kinesin-1 motor domain to axons. Nat. Neurosci. *12*, 559–567.

Kumar, N., and Flavin, M. (1981). Preferential action of a brain detyrosinolating carboxypeptidase on polymerized tubulin. J. Biol. Chem. *256*, 7678–7686.

L'Hernault, S. W., and Rosenbaum, J. L. (1985). Chlamydomonas alpha-tubulin is posttranslationally modified by acetylation on the epsilon-amino group of a lysine. Biochemistry *24*, 473–478.

Lacroix, B., Bourdages, K. G., Dorn, J. F., Ihara, S., Sherwood, D. R., Maddox, P. S., and Maddox, A. S. (2014). In Situ Imaging in C. elegans Reveals Developmental Regulation of Microtubule Dynamics. Dev. Cell *29*, 203–216.

Lacroix, B., van Dijk, J., Gold, N. D., Guizetti, J., Aldrian-Herrada, G., Rogowski, K., Gerlich, D. W., and Janke, C. (2010). Tubulin polyglutamylation stimulates spastin-mediated microtubule severing. J. Cell Biol. *189*, 945–954.

Lafanechère, L., Courtay-Cahen, C., Kawakami, T., Jacrot, M., Rüdiger, M., Wehland, J., Job, D., and Margolis, R. L. (1998). Suppression of tubulin tyrosine ligase during tumor growth. J. Cell Sci. *111*, 171–181.

Lafanechère, L., and Job, D. (2000). The third tubulin pool. Neurochem. Res. *25*, 11–18.

Lalle, M., Camerini, S., Cecchetti, S., Blasetti Fantauzzi, C., Crescenzi, M., and Pozio, E. (2011). Giardia duodenalis 14-3-3 protein is polyglycylated by a tubulin tyrosine ligase-like member and deglycylated by two metallocarboxypeptidases. J. Biol. Chem. *286*, 4471–4484.

Landis, S. C., and Mullen, R. J. (1978). The development and degeneration of Purkinje cells in pcd mutant mice. J. Comp. Neurol. *177*, 125–143.

Lange, P. F., and Overall, C. M. (2013). Protein TAILS: when termini tell tales of proteolysis and function. Curr. Opin. Chem. Biol. *17*, 73–82.

Laskowski, R. A. (2001). PDBsum: summaries and analyses of PDB structures. Nucleic Acids Res. *29*, 221–222.

Lee, G.-S. *et al.* (2013). Disruption of Ttll5/stamp gene (tubulin tyrosine ligase-like protein 5/SRC-1 and TIF2-associated modulatory protein gene) in male mice causes sperm malformation and infertility. J. Biol. Chem. *288*, 15167–15180.

Lee, J. E., and Gleeson, J. G. (2011). Cilia in the nervous system: linking cilia function and neurodevelopmental disorders. Curr. Opin. Neurol. *24*, 98–105.

Lee, L. (2013). Riding the wave of ependymal cilia: genetic susceptibility to hydrocephalus in primary ciliary dyskinesia. J. Neurosci. Res. *91*, 1117–1132.

Leigh, M. W., Pittman, J. E., Carson, J. L., Ferkol, T. W., Dell, S. D., Davis, S. D., Knowles, M. R., and Zariwala, M. A. (2009). Clinical and genetic aspects of primary ciliary dyskinesia/Kartagener syndrome. Genet. Med. *11*, 473–487.

Lindemann, C. B., and Lesich, K. a (2010). Flagellar and ciliary beating: the proven and the possible. J. Cell Sci. *123*, 519–528.

Lobo, L. J., Zariwala, M. a, and Noone, P. G. (2014). Primary ciliary dyskinesia. QJM, [Epub].

Lodish, H. F. (2008). Molecular Cell Biology, W. H. Freeman and Company.

Lucas, J. S., Burgess, A., Mitchison, H. M., Moya, E., Williamson, M., and Hogg, C. (2014). Diagnosis and management of primary ciliary dyskinesia. Arch. Dis. Child., [Epub].

Ludueña, R., and Banerjee, A. (2008). The isotypes of tubulin: distribution and functional significance. In: The Role of Microtubules in Cell Biology, Neurobiology, and Oncology, ed. T. Fojo, Totowa NJ: Humana Press, 123–175.

Lupas, A., Dyke, M. Van, and Stock, J. (1991). Predicting coiled coils from protein sequences. Science *252*, 1162–1164.

Luthy, R., Bowie, J. U., and Eisenberg, D. (1992). Assessment of protein models with three-dimensional profiles. Nature *356*, 83–85.

Lyons, P. J., and Fricker, L. D. (2010). Substrate specificity of human carboxypeptidase A6. J. Biol. Chem. *285*, 38234–38242.

Lyons, P. J., and Fricker, L. D. (2011). Carboxypeptidase O is a glycosylphosphatidylinositol-anchored intestinal peptidase with acidic amino acid specificity. J. Biol. Chem. *286*, 39023–39032.

Lyons, P. J., Sapio, M. R., and Fricker, L. D. (2013). Zebrafish cytosolic carboxypeptidases 1 and 5 are essential for embryonic development. J. Biol. Chem. *288*, 30454–30462.

Magiera, M. M., and Janke, C. (2014). Post-translational modifications of tubulin. Curr. Biol. *24*, R351–4.

Margolis, R. L., and Wilson, L. (1978). Opposite end assembly and disassembly of microtubules at steady state in vitro. Cell *13*, 1–8.

Mariño, G., Niso-Santano, M., Baehrecke, E. H., and Kroemer, G. (2014). Self-consumption: the interplay of autophagy and apoptosis. Nat. Rev. Mol. Cell Biol. *15*, 81–94.

Maurer, S. P., Fourniol, F. J., Bohner, G., Moores, C. A., and Surrey, T. (2012). EBs recognize a nucleotide-dependent structural cap at growing microtubule ends. Cell *149*, 371–382.

McCarty, S. M., and Percival, S. L. (2013). Proteases and delayed wound healing. Adv. Wound Care *2*, 438–447.

McKean, P. G., Vaughan, S., and Gull, K. (2001). The extended tubulin superfamily. J. Cell Sci. *114*, 2723–2733.

Mi, H., Muruganujan, A., and Thomas, P. D. (2013). PANTHER in 2013: modeling the evolution of gene function, and other gene attributes, in the context of phylogenetic trees. Nucleic Acids Res. *41*, D377–86.

Michaud, E. J., and Yoder, B. K. (2006). The primary cilium in cell signaling and cancer. Cancer Res. *66*, 6463–6467.

Miller, L. M., Xiao, H., Burd, B., Horwitz, S. B., Angeletti, R. H., and Verdier-Pinard, P. (2010). Methods in tubulin proteomics., Elsevier.

Mitchison, T. J. (2014). The engine of microtubule dynamics comes into focus. Cell *157*, 1008–1010.

Mitchison, T., and Kirschner, M. (1984). Dynamic instability of microtubule growth. Nature *13*, 1–8.

Molla-Herman, A. *et al.* (2010). The ciliary pocket: an endocytic membrane domain at the base of primary and motile cilia. J. Cell Sci. *123*, 1785–1795.

Moore, D. J. *et al.* (2013). Mutations in ZMYND10, a gene essential for proper axonemal assembly of inner and outer dynein arms in humans and flies, cause primary ciliary dyskinesia. Am. J. Hum. Genet. *93*, 346–356.

Mullen, R. J., Eicher, E. M., and Sidman, R. L. (1976). Purkinje cell degeneration, a new neurological mutation in the mouse. Proc. Natl. Acad. Sci. U. S. A. *73*, 208–212.

Nandadasa, S., Foulcer, S., and Apte, S. S. (2014). The multiple, complex roles of versican and its proteolytic turnover by ADAMTS proteases during embryogenesis. Matrix Biol. *35*, 34–41.

Nava, P., Kamekura, R., and Nusrat, A. (2013). Cleavage of transmembrane junction proteins and their role in regulating epithelial homeostasis. Tissue Barriers *1*, e24783.

Nogales, E., and Ramey, V. H. (2009). Structure-function insights into the yeast Dam1 kinetochore complex. J. Cell Sci. *122*, 3831–3836.

Nogales, E., Wolf, S., and Downing, K. (1998). Structure of the αβ tubulin dimer by electron crystallography. Nature *391*, 199–204.

North, B. J., Marshall, B. L., Borra, M. T., Denu, J. M., Verdin, E., and Francisco, S. (2003). The human Sir2 ortholog, SIRT2, is an NAD+-dependent tubulin deacetylase. Mol. Cell *11*, 437–444.

O'Hagan, R., Piasecki, B. P., Silva, M., Phirke, P., Nguyen, K. C. Q., Hall, D. H., Swoboda, P., and Barr, M. M. (2011). The tubulin deglutamylase CCPP-1 regulates the function and stability of sensory cilia in C. elegans. Curr. Biol. *21*, 1685–1694.

Oakley, B. R. (2000). An abundance of tubulins. Trends Cell Biol. *10*, 537–542.

Oakley, C., and Oakley, B. (1989). Identification of γ-tubulin, a new member of the tubulin superfamily encoded by mipA gene of Aspergillus nidulans. Nature *338*, 662–664.

Ohkawa, N., Sugisaki, S., Tokunaga, E., Fujitani, K., Hayasaka, T., Setou, M., and Inokuchi, K. (2008). N-acetyltransferase ARD1-NAT1 regulates neuronal dendritic development. Genes Cells *13*, 1171–1183.

Okada, Y., Takeda, S., Tanaka, Y., Izpisúa Belmonte, J.-C., and Hirokawa, N. (2005). Mechanism of nodal flow: a conserved symmetry breaking event in left-right axis determination. Cell *121*, 633–644.

Otero, A., Rodríguez de la Vega, M., Tanco, S., Lorenzo, J., Avilés, F. X., and Reverter, D. (2012). The novel structure of a cytosolic M14 metallocarboxypeptidase (CCP) from Pseudomonas aeruginosa: a model for mammalian CCPs. FASEB J. *26*, 3754–3764.

Pan, J., Seeger-Nukpezah, T., and Golemis, E. (2013). The role of cilium in normal and abnormal cell cycles: emphasis on renal cystic pathologies. Cell. Mol. Life Sci. *70*, 1849–1874.

Parry, D. a D., Fraser, R. D. B., and Squire, J. M. (2008). Fifty years of coiled-coils and alpha-helical bundles: a close relationship between sequence and structure. J. Struct. Biol. *163*, 258–269.

Pathak, N., Austin, C. A., and Drummond, I. A. (2011). Tubulin tyrosine ligase-like genes ttll3 and ttll6 maintain zebrafish cilia structure and motility. J. Biol. Chem. *286*, 11685–11695.

Pathak, N., Austin-Tse, C. A., Liu, Y., Vasilyev, A., and Drummond, I. A. (2014). Cytoplasmic carboxypeptidase 5 regulates tubulin glutamylation and zebrafish cilia formation and function. Mol. Biol. Cell *25*, 1836–1844.

Paturle-Lafanechère, L., Eddé, B., Denoulet, P., Dorsselaer, A. Van, Mazargui, H., Le Caer, J. P., Wehland, J., Job, D., Van Dorsselaer, A., and Mazarguil, H. (1991). Characterization of a major brain tubulin variant which cannot be tyrosinated. Biochemistry *30*, 10523–10528.

Paturle-Lafanechère, L., Manier, M., Trigault, N., Pirollet, F., Mazarguil, H., and Job, D. (1994). Accumulation of delta 2-tubulin, a major tubulin variant that cannot be tyrosinated, in neuronal tissues and in stable microtubule assemblies. J. Cell Sci. *107*, 1529–1543.

Pejler, G., Abrink, M., Ringvall, M., and Wernersson, S. (2007). Mast cell proteases. Adv. Immunol. *95*, 167–255.

Peris, L. *et al.* (2006). Tubulin tyrosination is a major factor affecting the recruitment of CAP-Gly proteins at microtubule plus ends. J. Cell Biol. *174*, 839–849.

Peris, L., Wagenbach, M., Lafanechère, L., Brocard, J., Moore, A. T., Kozielski, F., Job, D., Wordeman, L., and Andrieux, A. (2009). Motor-dependent microtubule disassembly driven by tubulin tyrosination. J. Cell Biol. *185*, 1159–1166.

Pilhofer, M., Ladinsky, M. S., McDowall, A. W., Petroni, G., and Jensen, G. J. (2011). Microtubules in bacteria: Ancient tubulins build a five-protofilament homolog of the eukaryotic cytoskeleton. PLoS Biol. *9*, e1001213.

Pilling, A., and Horiuchi, D. (2006). Kinesin-1 and Dynein are the primary motors for fast transport of mitochondria in Drosophila motor axons. Mol. Biol. Cell *17*, 2057–2068.

Piperno, G., and Fuller, M. T. (1985). Monoclonal antibodies specific for an acetylated form of alpha-tubulin recognize the antigen in cilia and flagella from a variety of organisms. J. Cell Biol. *101*, 2085–2094.

Poirier, K. *et al.* (2010). Mutations in the neuronal ß-tubulin subunit TUBB3 result in malformation of cortical development and neuronal migration defects. Hum. Mol. Genet. *19*, 4462–4473.

Poole, C. A., Flint, M. H., and Beaumont, B. W. (1985). Analysis of the morphology and function of primary cilia in connective tissues: a cellular cybernetic probe? Cell Motil. *5*, 175–193.

Prota, A. E. *et al.* (2013). Structural basis of tubulin tyrosination by tubulin tyrosine ligase. J. Cell Biol. *200*, 259–270.

Puente, X. S., Gutiérrez-Fernández, A., Ordóñez, G. R., Hillier, L. W., and López-Otín, C. (2005). Comparative genomic analysis of human and chimpanzee proteases. Genomics *86*, 638–647.

Puente, X. S., Sánchez, L. M., Overall, C. M., and López-Otín, C. (2003). Human and mouse proteases: a comparative genomic approach. Nat. Rev. Genet. *4*, 544–558.

Quinones, G. B., Danowski, B. A., Devaraj, A., Singh, V., and Ligon, L. A. (2011). The posttranslational modification of tubulin undergoes a switch from detyrosination to acetylation as epithelial cells become polarized. Mol. Biol. Cell *22*, 1045–1057.

Ramamurthy, V., and Cayouette, M. (2009). Development and disease of the photoreceptor cilium. Clin. Genet. *76*, 137–145.

Rawlings, N. D., and Barrett, A. J. (1993). Evolutionary families of peptidases. Biochem. J. *290*, 205–218.

Rawlings, N. D., Barrett, A. J., and Bateman, A. (2012). MEROPS: the database of proteolytic enzymes, their substrates and inhibitors. Nucleic Acids Res. *40*, D343–50.

Rawlings, N. D., and Salvesen, G. (2013). Handbook of proteolytic enzymes, Oxford: Elsevier Academic Press.

Rawlings, N., Morton, F., and Barrett, A. (2006). MEROPS: the peptidase database. Nucleic Acids Res. *28*, 323–325.

Raybin, D., and Flavin, M. (1977). Modification of tubulin by tyrosylation in cells and extracts and its effect on assembly in vitro. J. Cell Biol. *73*, 492–504.

Redeker, V., Levilliers, N., Schmitter, J. M., Le Caer, J. P., Rossier, J., Adoutte, A., and Bré, M. H. (1994). Polyglycylation of tubulin: a posttranslational modification in axonemal microtubules. Science *266*, 1688–1691.

Regnard, C., Desbruyères, E., Denoulet, P., and Eddé, B. (1999). Tubulin polyglutamylase: isozymic variants and regulation during the cell cycle in HeLa cells. J. Cell Sci. *112 (Pt 2*, 4281–4289.

Riazuddin, S. A., Vasanth, S., Katsanis, N., and Gottsch, J. D. (2013). Mutations in AGBL1 cause dominant late-onset Fuchs corneal dystrophy and alter protein-protein interaction with TCF4. Am. J. Hum. Genet. *93*, 758–764.

Rios, R. M., and Bornens, M. (2003). The Golgi apparatus at the cell centre. Curr. Opin. Cell Biol. *15*, 60–66.

Robert, A., Margall-Ducos, G., Guidotti, J.-E., Bregerie, O., Celati, C., Brechot, C., and Desdouets, C. (2007). The intraflagellar transport component IFT88/polaris is a centrosomal protein regulating G1-S transition in non-ciliated cells. J. Cell Sci. *120*, 628–637.

Rodriguez de la Vega, M., Sevilla, R. G., Hermoso, A., Lorenzo, J., Tanco, S., Diez, A., Fricker, L. D., Bautista, J. M., and Avilés, F. X. (2007). Nna1-like proteins are active metallocarboxypeptidases of a new and diverse M14 subfamily. FASEB J. *20*, 851–865.

Rodríguez de la Vega Otazo, M., Lorenzo, J., Tort, O., Avilés, F. X., and Bautista, J. M. (2013). Functional segregation and emerging role of cilia-related cytosolic carboxypeptidases (CCPs). FASEB J. *27*, 424–431.

Rogowski, K. *et al.* (2009). Evolutionary divergence of enzymatic mechanisms for posttranslational polyglycylation. Cell *137*, 1076–1087.

Rogowski, K. *et al.* (2010). A family of protein-deglutamylating enzymes associated with neurodegeneration. Cell *143*, 564–578.

Romaniello, R., Arrigoni, F., Cavallini, A., Tenderini, E., Baschirotto, C., Triulzi, F., Bassi, M.-T., and Borgatti, R. (2014). Brain malformations and mutations in α- and β-tubulin genes: a review of the literature and description of two new cases. Dev. Med. Child Neurol. *56*, 354–360.

Ross, P. L., Cheng, I., Liu, X., Cicek, M. S., Carroll, P. R., Casey, G., and Witte, J. S. (2009). Carboxypeptidase 4 gene variants and early-onset intermediate-to-high risk prostate cancer. BMC Cancer *9*, 69.

Roy, A., Kucukural, A., and Zhang, Y. (2010). I-TASSER: a unified platform for automated protein structure and function prediction. Nat. Protoc. *5*, 725–738.

Ruat, M., Roudaut, H., Ferent, J., and Traiffort, E. (2012). Hedgehog trafficking, cilia and brain functions. Differentiation. *83*, S97–104.

Rüdiger, M., Wehland, J., and Weber, K. (1994). The carboxy-terminal peptide of detyrosinated alpha tubulin provides a minimal system to study the substrate specificity of tubulin-tyrosine ligase. Eur. J. Biochem. *220*, 309–320.

Ruiz, F., Krzywicka, A., Klotz, C., Keller, A., Cohen, J., Koll, F., Balavoine, G., and Beisson, J. (2000). The SM19 gene, required for duplication of basal bodies in Paramecium, encodes a novel tubulin, eta-tubulin. Curr. Biol. *10*, 1451–1454.

Sahab, Z. J., Hall, M. D., Me Sung, Y., Dakshanamurthy, S., Ji, Y., Kumar, D., and Byers, S. W. (2011). Tumor suppressor RARRES1 interacts with cytoplasmic carboxypeptidase AGBL2 to regulate the α-tubulin tyrosination cycle. Cancer Res. *71*, 1219–1228.

Sapio, M. R., and Fricker, L. D. (2014). Carboxypeptidases in disease: Insights from peptidomic studies. Proteomics. Clin. Appl. *8*, 327–337.

Satir, P., and Christensen, S. T. (2007). Overview of structure and function of mammalian cilia. Annu. Rev. Physiol. *69*, 377–400.

Schechter, I., and Berger, A. (1967). On the size of the active site in proteases. I. Papain. Biochem. Biophys. Res. Commun. *27*, 157–162.

Schmidt, J., and Arthanari, H. (2012). The kinetochore-bound Ska1 complex tracks depolymerizing microtubules and binds to curved protofilaments. Dev. Cell *23*, 968–980.

Schneider, L., Clement, C. A., Teilmann, S. C., Pazour, G. J., Hoffmann, E. K., Satir, P., and Christensen, S. T. (2005). PDGFRαα signaling is regulated through the primary cilium in fibroblasts. Curr. Biol. *15*, 1861–1866.

Scholey, J. M. (2008). Intraflagellar transport motors in cilia: moving along the cell's antenna. J. Cell Biol. *180*, 23–29.

Schröder, H. C., Wehland, J., and Weber, K. (1985). Purification of brain tubulin-tyrosine ligase by biochemical and immunological methods. J. Cell Biol. *100*, 276–281.

Sergouniotis, P. I. *et al.* (2014). Biallelic variants in TTLL5, encoding a tubulin glutamylase, cause retinal dystrophy. Am. J. Hum. Genet. *94*, 760–769.

Sève, P., Reiman, T., Isaac, S., Trillet-Lenoir, V., Lafanéchère, L., Sawyer, M., and Dumontet, C. (2008). Protein abundance of class III beta-tubulin but not Delta2-alpha-tubulin or tau is related to paclitaxel response in carcinomas of unknown primary site. Anticancer Res. *28*, 1161–1167.

Shang, Y. (2002). Tetrahymena thermophila contains a conventional gamma-tubulin that is differentially required for the maintenance of different microtubule-organizing centers. J. Cell Biol. *158*, 1195–1206.

Shpak, M., Goldberg, M. M., and Cowperthwaite, M. C. (2014). Cilia gene expression patterns in cancer. Cancer Genomics Proteomics *11*, 13–24.

Sippl, M. J. (1993). Recognition of errors in three-dimensional structures of proteins. Proteins *17*, 355–362.

Sirajuddin, M., Rice, L. M., and Vale, R. D. (2014). Regulation of microtubule motors by tubulin isotypes and post-translational modifications. Nat. Cell Biol. *16*, 335–344.

Song, Y., Kirkpatrick, L. L., Schilling, A. B., Helseth, D. L., Chabot, N., Keillor, J. W., Johnson, G. V. W., and Brady, S. T. (2013). Transglutaminase and polyamination of tubulin: posttranslational modification for stabilizing axonal microtubules. Neuron *78*, 109–123.

Stanchi, F., Corso, V., Scannapieco, P., Ievolella, C., Negrisolo, E., Tiso, N., Lanfranchi, G., and Valle, G. (2000). TUBA8: A new tissue-specific isoform of alpha-tubulin that is highly conserved in human and mouse. Biochem. Biophys. Res. Commun. *270*, 1111–1118.

Steigemann, P., and Gerlich, D. W. (2009). Cytokinetic abscission : cellular dynamics at the midbody. Trends Cell Biol. *19*, 606–616.

Strömqvist, M., Hansson, L., Andersson, J.-O., Johansson, T., Edlund, M., Enoksson, M., Goossens, F., Scharpé, S., and Hendriks, D. (2004). Properties of recombinant human plasma procarboxypeptidase U produced in mammalian and insect cells. Clin. Chim. Acta *347*, 49–59.

Suryavanshi, S. *et al.* (2010). Tubulin glutamylation regulates ciliary motility by altering inner dynein arm activity. Curr. Biol. *20*, 435–440.

Szyk, A., Deaconescu, A. M., Piszczek, G., and Roll-Mecak, A. (2011). Tubulin tyrosine ligase structure reveals adaptation of an ancient fold to bind and modify tubulin. Nat. Struct. Mol. Biol. *18*, 1250–1258.

Szyk, A., Deaconescu, A. M., Spector, J., Goodman, B., Valenstein, M. L., Ziolkowska, N. E., Kormendi, V., Grigorieff, N., and Roll-Mecak, A. (2014). Molecular Basis for Age-Dependent Microtubule Acetylation by Tubulin Acetyltransferase. Cell *157*, 1405–1415.

Tam, E. M., Wu, Y. I., Butler, G. S., Stack, M. S., and Overall, C. M. (2002). Collagen binding properties of the membrane type-1 matrix metalloproteinase (MT1-MMP) hemopexin C domain. The ectodomain of the 44-kDa autocatalytic product of MT1-MMP inhibits cell invasion by disrupting native type I collagen cleavage. J. Biol. Chem. *277*, 39005–39014.

Tanaka, T. U. (2010). Kinetochore-microtubule interactions: steps towards bi-orientation. EMBO J. *29*, 4070–4082.

Tanco, S., Tort, O., Demol, H., and Aviles, F. X. C-terminomics screen for natural substrates of cytosolic carboxypeptidase 1 reveals processing of acidic protein C-termini. Submitt. to Mol. Cell. Proteomics.

Tanco, S., Zhang, X., Morano, C., Avilés, F. X., Lorenzo, J., and Fricker, L. D. (2010). Characterization of the substrate specificity of human carboxypeptidase A4 and implications for a role in extracellular peptide processing. J. Biol. Chem. *285*, 18385–18396.

Thakar, K., Karaca, S., Port, S. A., Urlaub, H., and Kehlenbach, R. H. (2013). Identification of CRM1-dependent Nuclear Export Cargos Using Quantitative Mass Spectrometry. Mol. Cell. Proteomics *12*, 664–678.

Thompson, W. C. (1977). Post-translational addition of tyrosine to alpha tubulin in vivo intact brain and in myogenic cells in culture. FEBS Lett. *80*, 9–13.

Tischfield, M. A. *et al.* (2010). Human TUBB3 mutations perturb microtubule dynamics, kinesin interactions, and axon guidance. Cell *140*, 74–87.

Tischfield, M. A., and Engle, E. C. (2010). Distinct alpha- and beta-tubulin isotypes are required for the positioning, differentiation and survival of neurons: new support for the “multi-tubulin” hypothesis. Biosci. Rep. *30*, 319–330.

Turk, B. (2006). Targeting proteases : successes, failures and future prospects. Nat. Rev. Drug Discov. *5*, 785–800.

Turk, B., Turk, D., and Turk, V. (2012). Protease signalling : the cutting edge. EMBO J. *31*, 1630–1643.

Tuszynski, J. A., Carpenter, E. J., Huzil, J. T., Malinski, W., Luchko, T., and Luduena, R. F. (2006). The evolution of the structure of tubulin and its potential consequences for the role and function of microtubules in cells and embryos. Int. J. Dev. Biol. *50*, 341–358.

Van der Vaart, B., Akhmanova, A., and Straube, A. (2009). Regulation of microtubule dynamic instability. Biochem. Soc. Trans. *37*, 1007–1013.

Valero, J., Berciano, M. T., Weruaga, E., Lafarga, M., and Alonso, J. R. (2006). Pre-neurodegeneration of mitral cells in the pcd mutant mouse is associated with DNA damage, transcriptional repression, and reorganization of nuclear speckles and Cajal bodies. Mol. Cell. Neurosci. *33*, 283–295.

Valiron, O., Caudron, N., and Job, D. (2001). Microtubule dynamics. Cell. Mol. Life Sci. *58*, 2069–2084.

Vaughan, S., Attwood, T., and Navarro, M. (2000). New tubulins in protozoal parasites. Curr. Biol. *10*, R258–59.

Vendrell, J., Querol, E., and Avilés, F. X. (2000). Metallocarboxypeptidases and their protein inhibitors. Structure, function and biomedical properties. Biochim. Biophys. Acta *1477*, 284–298.

Verhey, K., and Gaertig, J. (2007). The tubulin code. Cell Cycle *6*, 2152–2160.

Vinh, J., Langridge, J. I., Bré, M. H., Levilliers, N., Redeker, V., Loyaux, D., and Rossier, J. (1999). Structural characterization by tandem mass spectrometry of the posttranslational polyglycylation of tubulin. Biochemistry *38*, 3133–3139.

Vogel, P., Hansen, G., Fontenot, G., and Read, R. (2010). Tubulin tyrosine ligase-like 1 deficiency results in chronic rhinosinusitis and abnormal development of spermatid flagella in mice. Vet. Pathol. *47*, 703–712.

Wang, Z., and Sheetz, M. P. (2000). The C-terminus of tubulin increases cytoplasmic dynein and kinesin processivity. Biophys. J. *78*, 1955–1964.

Webster, D. R., Modesti, N. M., and Bulinski, J. C. (1992). Regulation of cytoplasmic tubulin carboxypeptidase activity during neural and muscle differentiation: characterization using a microtubule-based assay. Biochemistry *31*, 5849–5856.

Wehenkel, A., and Janke, C. (2014). Towards elucidating the tubulin code. Nat. Cell Biol. *16*, 303–305.

Wehland, J., and Weber, K. (1987). Turnover of the carboxy-terminal tyrosine of alpha-tubulin and means of reaching elevated levels of detyrosination in living cells. J. Cell Sci. *88*, 185–203.

Wei, S., Segura, S., Vendrell, J., Aviles, F. X., Lanoue, E., Day, R., Feng, Y., and Fricker, L. D. (2002). Identification and characterization of three members of the human metallocarboxypeptidase gene family. J. Biol. Chem. *277*, 14954–14964.

Wheatley, D. N. (1971). Cilia in cell-cultured fibroblasts. 3. Relationship between mitotic activity and cilium frequency in mouse 3T6 fibroblasts. J. Anat. *110*, 367–382.

Whipple, R., Cheung, A., and Martin, S. (2007). Detyrosinated microtubule protrusions in suspended mammary epithelial cells promote reattachment. Exp. Cell Res. *313*, 1326–1336.

Wiederstein, M., and Sippl, M. J. (2007). ProSA-web: interactive web service for the recognition of errors in three-dimensional structures of proteins. Nucleic Acids Res. *35*, W407–10.

Willemse, J., and Heylen, E. (2009). Carboxypeptidase U (TAFIa): a new drug target for fibrinolytic therapy? J. Thromb. Haemost. *7*, 1962–1971.

Wloga, D., Dave, D., Meagley, J., Rogowski, K., Jerka-Dziadosz, M., and Gaertig, J. (2010). Hyperglutamylation of tubulin can either stabilize or destabilize microtubules in the same cell. Eukaryot. Cell *9*, 184–193.

Wloga, D., and Gaertig, J. (2010). Post-translational modifications of microtubules. J. Cell Sci. *124*, 3447–3455.

Wu, H.-Y., Wang, T., Li, L., Correia, K., and Morgan, J. I. (2012). A structural and functional analysis of Nna1 in Purkinje cell degeneration (pcd) mice. FASEB J. *26*, 4468–4480.

Wynshaw-Boris, A. (2009). Elongator bridges tubulin acetylation and neuronal migration. Cell *136*, 393–394.

Yoo, S., Niekerk, E. van, Merianda, T., and Twiss, J. (2010). Dynamics of axonal mRNA transport and implications for peripheral nerve regeneration. Exp. Neurol. *223*, 19–27.

Young, R. W. (1967). The renewal of photoreceptor cell outer segments. J. Cell Biol. *33*, 61–72.

Zhang, H., Ren, Y., Pang, D., and Liu, C. (2014). Clinical implications of AGBL2 expression and its inhibitor latexin in breast cancer. World J. Surg. Oncol. *12*, 142.

Zhang, Y. (2008). I-TASSER server for protein 3D structure prediction. BMC Bioinformatics *9*, 40.

Zhao, X., Onteru, S. K., Dittmer, K. E., Parton, K., Blair, H. T., Rothschild, M. F., and Garrick, D. J. (2012). A missense mutation in AGTPBP1 was identified in sheep with a lower motor neuron disease. Heredity (Edinb). *109*, 156–162.

Annexes

ANNEX I

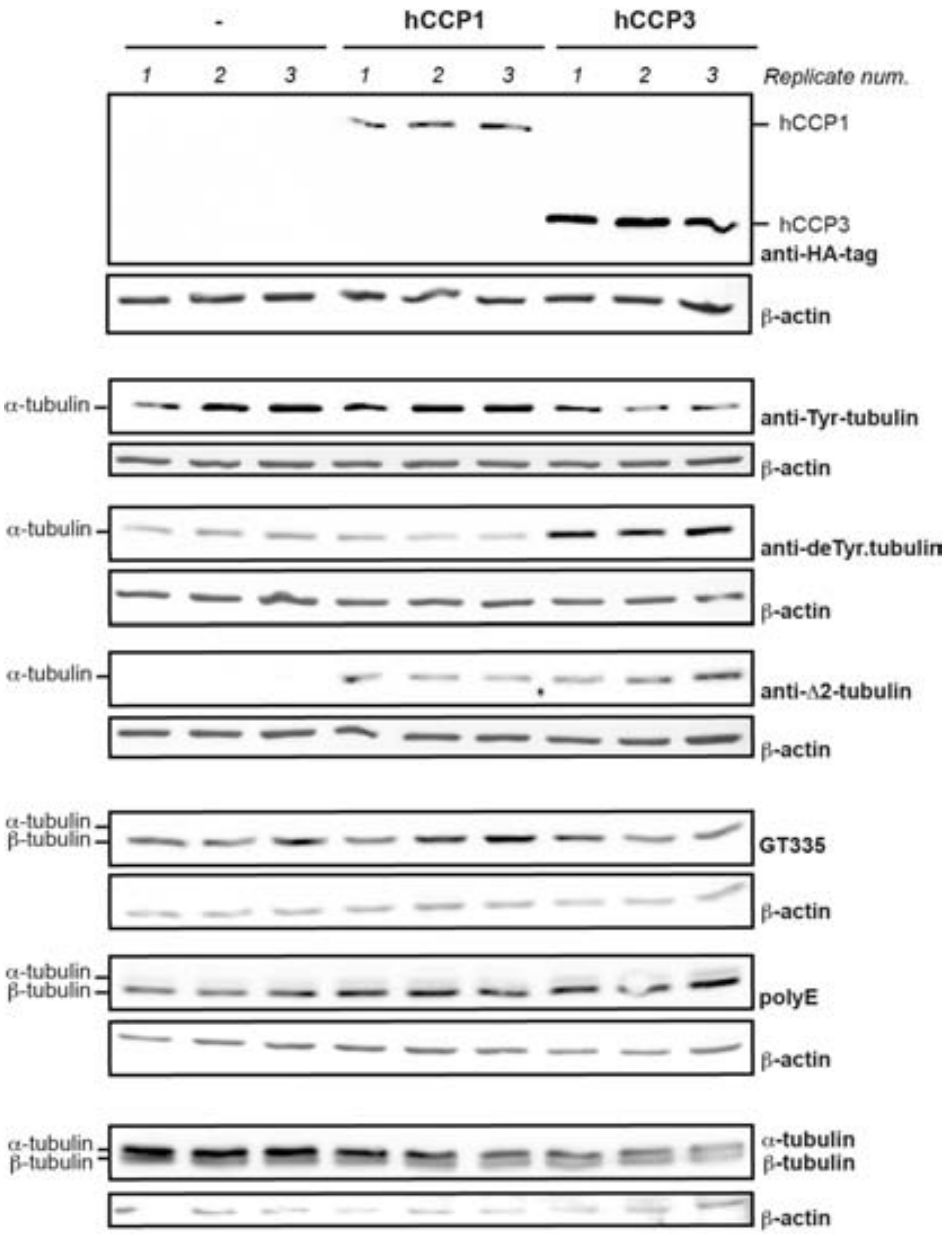

Figure S2. Δ2-tubulin generation in HEK 293T cells over-expressing CCP3.

Western blots for cell extracts of CCP3 and CCP1 over-expression compared to control cells. Cells were recovered after 72 h over-expressing HA-tagged versions of CCP3 and CCP1. Samples were analyzed for α- and β-tubulins and diverse tubulin PTMs levels. An increase in Δ2-tubulin was detected for both CCP3 and CCP1 cell extracts when compared with control cells.